2007-07-19

Buckling-Restrained Braced Frame Connection Design and Testing

Bradly B. Coy
Brigham Young University - Provo

BUCKLING-RESTRAINED BRACED FRAME CONNECTION DESIGN AND TESTING

by

Bradly B. Coy

A thesis submitted to the faculty of

Brigham Young University

in partial fulfillment of the requirements for the degree of

Master of Science

Department of Civil and Environmental Engineering

Brigham Young University

August 2007

BRIGHAM YOUNG UNIVERSITY

GRADUATE COMMITTEE APPROVAL

of a thesis submitted by

Bradly B. Coy

This thesis has been read by each member of the following graduate committee and by majority vote has been found to be satisfactory.

Date	Paul W. Richards, Chair
Date	Richard J. Balling
Date	Fernando S. Fonseca

BRIGHAM YOUNG UNIVERSITY

As chair of the candidate's graduate committee, I have read the thesis of Bradly B. Coy in its final form and have found that (1) its format, citations, and bibliographical style are consistent and acceptable and fulfill university and department style requirements; (2) its illustrative materials including figures, tables, and charts are in place; and (3) the final manuscript is satisfactory to the graduate committee and is ready for submission to the university library.

Date

Paul W. Richards
Chair, Graduate Committee

Accepted for the Department

E. James Nelson
Graduate Coordinator

Accepted for the College

Alan R. Parkinson
Dean, Ira A. Fulton College
of Engineering and Technology

ABSTRACT

BUCKLING-RESTRAINED BRACED FRAME CONNECTION DESIGN AND TESTING

Bradly B. Coy

Department of Civil and Environmental Engineering

Master of Science

As typically designed, the beam-column-brace connections of buckling-restrained braced steel frames have undesirable failure modes that compromise the integrity and performance of the frames and are costly to repair. To decrease the time and resources needed to repair the frames following an earthquake, a new connection design was developed that attempts to confine yielding to replaceable frame components. The design incorporates a gap in the beam beyond the edge of the beam-gusset weld that acts as a hinge and reduces moment forces transferred to the connection; it is bridged by splice plates that are bolted to the beam top flanges. The splice plates and buckling-restrained braces are the only frame components that are expected to yield.

To investigate the performance of the proposed connection design, a prototype bay was designed and two test specimens were fabricated and tested. Each specimen represented a corner of the prototype braced bay and consisted of a beam, column, gusset

plate, brace core extension assembly, splice plates, and lateral bracing angles. Both standard design procedures and newly developed criteria were used to design the connection.

In preparation for testing, a method was developed for estimating the hysteretic response of a buckling-restrained brace. By using this method to program an actuator, the specimens could be tested without using actual braces, resulting in a significant reduction in testing cost.

Testing was conducted using two 600 kip actuators; the first followed a static loading protocol with a maximum design drift of 6.5%, and the second replicated the prototype BRB's response. The tests yielded promising results: both specimens withstood the maximum displacements and avoided yielding in the beams, columns, and gusset plates; yielding did occur in the splice plates and BRB core extension assembly, as anticipated.

Possible limitations in the design may arise under the presence of increased shear loads, concrete floor slabs, or out-of-plane loading. Additional testing is recommended.

ACKNOWLEDGMENTS

I wish to express gratitude for all of those who helped me along the way, in particular: Dr. Paul W. Richards for his guidance, direction, the project, everything; Dr. Richard J. Balling and Dr. Fernando S. Fonseca for their support and suggestions as members of my graduate committee; SME Fabricators and CoreBrace (especially Mark Daniels and Andy Hinchman) for donating the specimens and providing resources, data, and support; Dave Anderson and the Structures Lab crew for manual and technical assistance during the specimen instrumentation and testing; the BYU Civil Engineering Department (especially Janice Sorenson) for facilitating my transition into the thesis track; Mason Walters, Larry Fahnestock, and Adam Christopulos for performing research on similar projects and providing me with images of their work; my parents for their help and concern; and most of all, Meredith for her love, support, and encouragement.

TABLE OF CONTENTS

LIST OF TABLES

LIST OF FIGURES

1 Introduction

The Buckling-Restrained Braced Frame (BRBF) is a relatively new type of Concentrically Braced Frame (CBF) that incorporates the use of buckling-restrained braces (BRBs) as its principal bracing members. In this chapter, the components and performance of BRBs are explained, current BRBF research is discussed, and a proposed connection design is introduced.

1.1 Buckling-Restrained Braces

BRBs are made up of three principal components: a steel core coated in an "unbonding" substance, concrete, and an outer tube (see Figure 1-1). The steel core plays the primary role of the brace by providing the necessary resistance to any applied axial forces. The core is encased in a concrete-filled sleeve that prohibits buckling under compression loads; this enables the brace to take advantage of the compressive strength of steel (1). Beyond the edges of the sleeve, the core extends and transitions into a configuration that allows for bolting to gusset plates (see Figure 1-2).

To preclude bonding between the concrete and steel core, an "un-bonding" material is applied to the steel; this enables the BRB axial forces to be restricted to the steel core. Due to the importance of this additional material, buckling-restrained braces are often referred to as "unbonded braces" (1).

The principal advantage of BRBs is their ability to yield in compression as well as in tension (2). In comparison, a typical brace, such as a steel tube (HSS) or I-beam wide flange section (WF), is weaker in compression due to its tendency to buckle. Because BRBs resist buckling, they exhibit a symmetric hysteretic behavior that is more stable than a typical buckling brace (see Figure 1-3) (1).

Another advantage of BRBs is that yielding is confined to the steel core. By limiting yielding to the core, there is an increased control of performance. The strength, stiffness, and ductility of a BRB can be optimized since its core cross-sectional area, yield stress, and yield length can each be independently specified (1). The result is a brace that can be tailored to meet specific project needs. Such independence is not the case in traditional brace design, where the choice is between discrete sections (e.g. HSS or WF sections).

An important design consideration for a BRB is the transition segment located between the steel core and core extension (see Figure 1-2). During tensile yielding, the inner core will lengthen and a portion of the enclosed core will be exposed. Early brace failure may occur if this exposed portion buckles. The transition segment is designed to eliminate buckling by adding stiffeners to the core material; it is intended to be the only portion of the enclosed core that will exit the sleeve upon tensile deformation.

1.2 BRBF Experimental Results

Initial buckling-restrained braced frame testing focused on BRBs and results provided a solid understanding of BRB properties (1, 3, and 4). The more recent concern has been how BRBs perform within the BRBF system. Accordingly, efforts have shifted,

and more recent tests have been performed on BRBF subassemblies (5, 6, 7, 9, 12, 14, and 15).

In a recent sub-assemblage test performed by W. A. Lopez et. al. (5) (see Figure 1-4), the ultimate failures occurred near the connection at 2.5% inter-story drift and included yielding and buckling of the gusset plates, flexural yielding of the beam and column, flange fracture of the beam, and shear yielding of the column (see Figure 1-5).

Another recent test was conducted by A. Christopulos (6) (see Figure 1-6), and failures occurred at 2.5% inter-story drift and included fracture of the gusset-to-beam weld, flexural yielding and buckling of the beam, flexural yielding and buckling of the column, flange fracture of the beam, and shear yielding of the column (see Figure 1-7).

While the performance of the BRBs was satisfactory in both tests, the overall frame performance was not. Each failure involved vital elements to the structural integrity of the frame and would require significant and expensive repairs following a major earthquake. These and other tests indicate one main limitation of BRBFs: ultimate failures occur near the connections. Thus, for better system performance, connection designs that limit beam, column, and gusset plate damage must be utilized.

1.3 Pin Connection with Web Splice

Many of the connection failures are hypothesized to result from the connection's rigidity (6). A possible way to reduce connection rigidity while maintaining strength is to incorporate a connection hinge. L. A. Fahnestock et. al. (7) tested a new connection design (see Figures 1-8 and 1-9) that included a hinge in the form two T-shaped members, one on each side of the beam web. The gap was on the order of inches and was

located just beyond the edge of the gusset plate. A large scale test was performed on these connections by employing them in a planar BRBF four stories high and a single bay wide (see Figure 1-10).

The test frame was subjected to a pseudo-dynamic earthquake simulation loading protocol for a total of four tests. The connections performed as expected and had only minor yielding at bolt holes. The remaining components of the connection region remained damage-free. Global performance did not experience strength or stiffness degradation. The general conclusion was that a non-conventional connection detail that minimizes connection moment and allows rotation should exhibit excellent performance and sustain only minor yielding at very large story drifts. Furthermore, properly detailed BRBFs may withstand the largest anticipated seismic input and still maintain their structural integrity (7).

1.4 Pin Connection with Flange Splice

Walters, et. al. (8) proposed another connection design that incorporates a hinge in the beam just beyond the gusset plate; the hinge is the result of a gap in the beam, with the gap being bridged by splice plates on both the webs and flanges (see Figure 1-11). The plates connected to the top flange are designed to transfer axial loads, while the other plates with slotted bolt holes provide stability, resist buckling, and contribute to shear strength.

There are various consequences of transferring the full axial load through the top plates. Since the beam flange is bolted to the plates, it must be designed to carry the full axial load. Because the beam-plate connection is in close proximity to the beam-column-

brace connection, it is probable that the beam forces will remain in the top flange. The result is that the working point, which is concentric to the beam and column forces, shifts up from the centroid of the beam to the centroid of the top flange. To avoid eccentricity in the connection, the orientation of the BRB must also shift, which requires the use of different gusset plate geometries for the upper and lower connections (see Figure 1-12).

One potential advantage of the design proposed by Walters et. al. (8) is that the axial forces would be transferred across the gap at a point closer to the overlaying concrete slab. If a couple forms between the connection plates and concrete, then it may have a small enough moment arm for its effects to be negligible. A larger moment arm has a greater possibility of diminishing the hinging capability of the gap and increasing the damage to the connection, both of which are counterproductive to design objectives.

1.5 Proposed Connection

A modified version of the design proposed by Walters, et. al. (8) was developed with the intent to make the connection more economical. The main modification was to remove the splice plates located on the web and bottom flange of the beam (see Figure 1-13). Two concerns arose from the removal of the plates: out-of-plane buckling and shear transfer. To prevent out-of-plane buckling, angles were placed on both sides of the web and oversized holes were drilled in the angles to avoid inhibiting the full range of motion of the hinge. To resolve the shear transfer concern, the top splice plates were designed to resist the shear forces; the concrete slab may also be designed to help resist shear.

In addition, the top flanges were not tapered because the benefit was considered small compared to the additional labor it would require. Furthermore, the splice plate

bolts were designed to be fully tensioned because the additional strength gained was deemed more important than the benefit of reduced clamping effects.

In summary, the modified connection design seeks to best satisfy the objective of developing a safe, economical, and easy to assemble BRBF connection that under a substantial amount of drift would confine yielding to the BRB and splice plates, which are the most cost and time effective components to repair or replace.

1.6 Additional Concerns Relating to BRBFs

Buckling-restrained braced frame gusset plates are often unable to withstand the flexural forces transferred to them as the bay rotates. They are susceptible to buckling, and it has been determined that stiffeners along the free edges of a gusset plate are effective in preventing buckling (9). On gusset plate edges where buckling was a concern, the proposed design includes stiffeners.

Hinging of the BRB is another concern. As the frame experiences drift and the connection rotates, yielding and hinge formation has been observed near the extended core section (6). Under large tensile loads, the rectangular core plate can exit one end of the sleeve and hinge against the weak axis of its reduced cross section. Depending on the orientation of the core section, the hinging can be either in-plane or out-of-plane. Although uncontrolled hinging is undesirable, in-plane hinging may be beneficial insomuch as it reduces the moment demand on the gusset plates. Possible methods to ensure in-plane hinging is controlled involve connecting the BRB to the gusset plate using a pin or designing a predefined and unobtrusive hinge point in the core extension when the BRB is bolted.

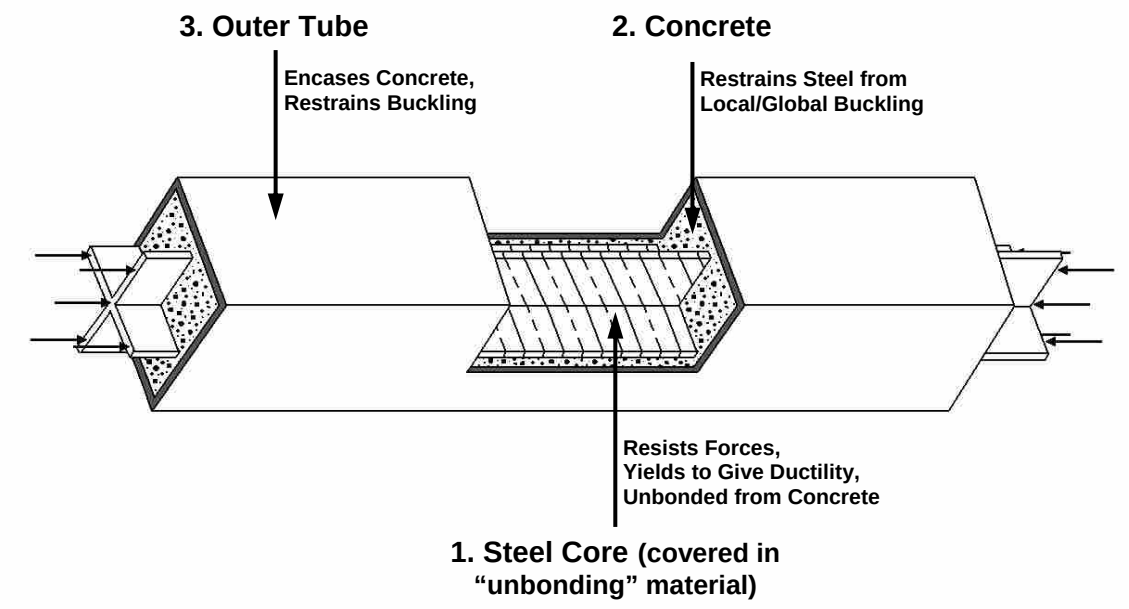

Figure 1-1 Principal BRB Components (with middle section cut away)

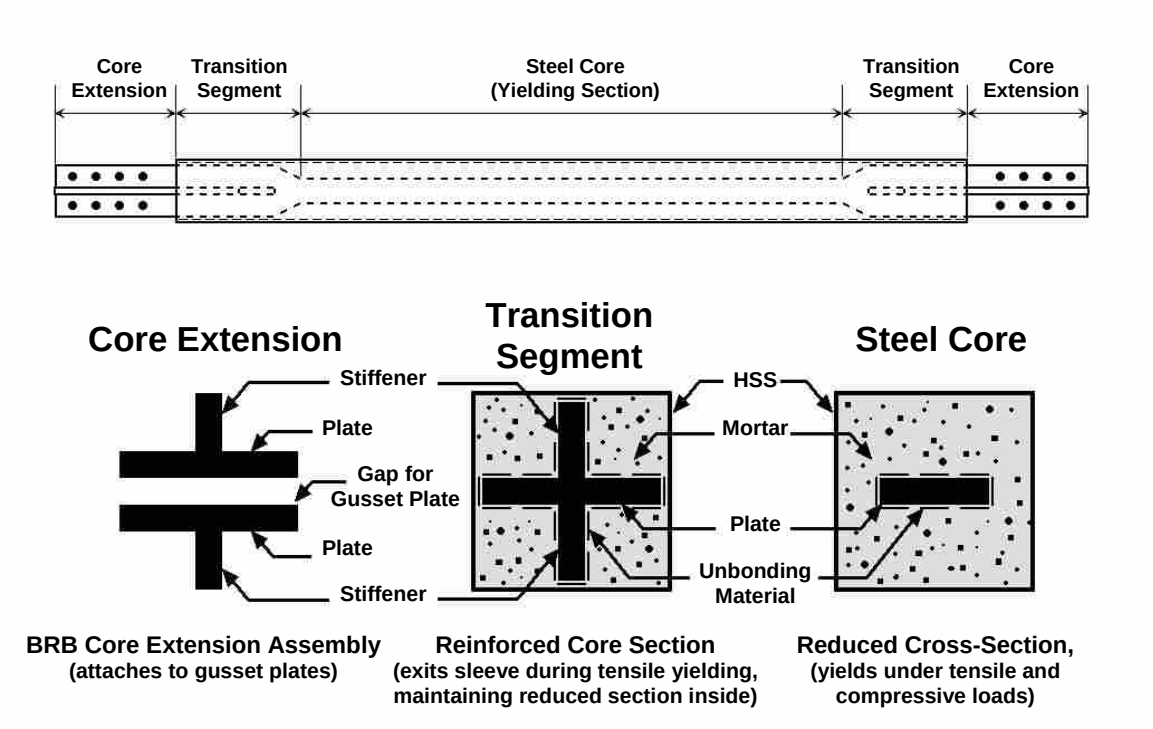

Figure 1-2 Cross-Section Diagrams for a BRB's Principal Segments

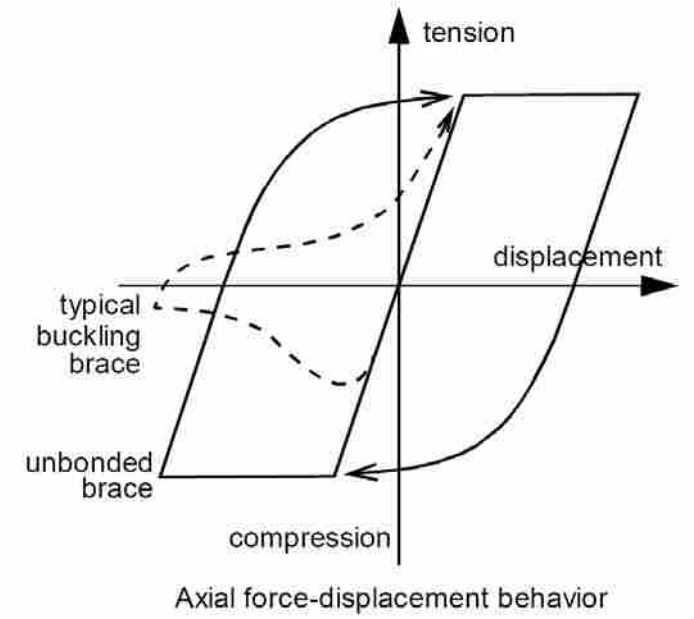

Figure 1-3 Buckling-Restrained Brace Hysteretic Behavior (1)

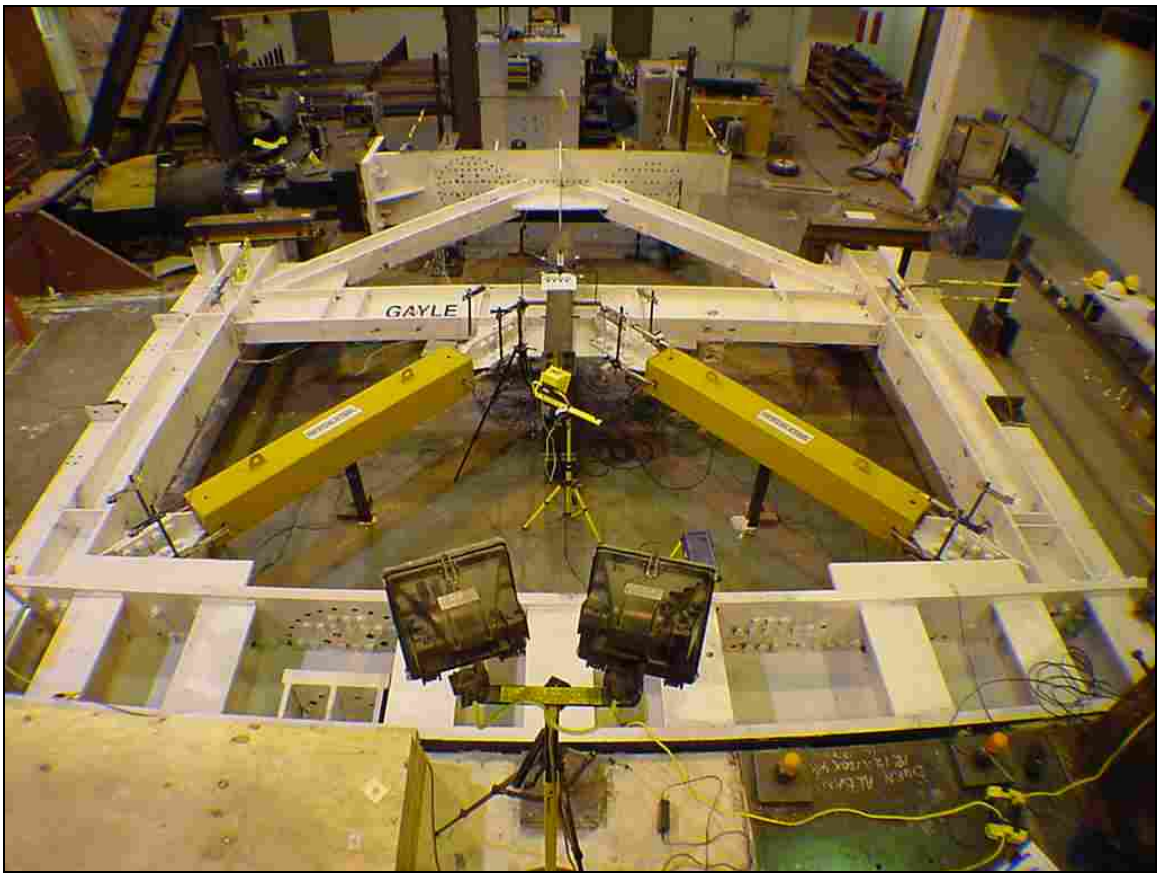

Figure 1-4 W. A. Lopez et. al. Sub-Assemblage Test Setup (5)

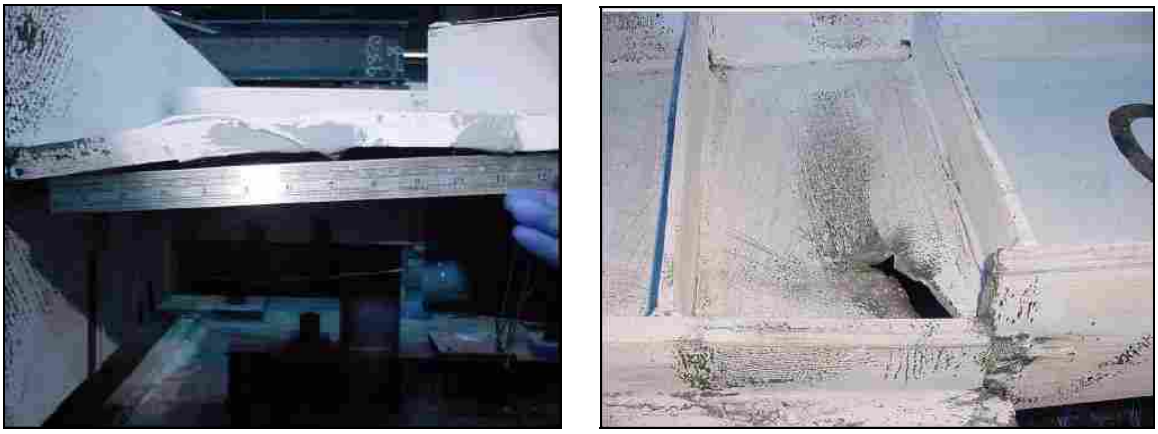

(a) Buckling of Gusset Plate **(b) Fracture of Beam Flange**

Figure 1-5 W. A. Lopez et. al. Sub-Assemblage Test Failures (2.5 % Drift) (5)

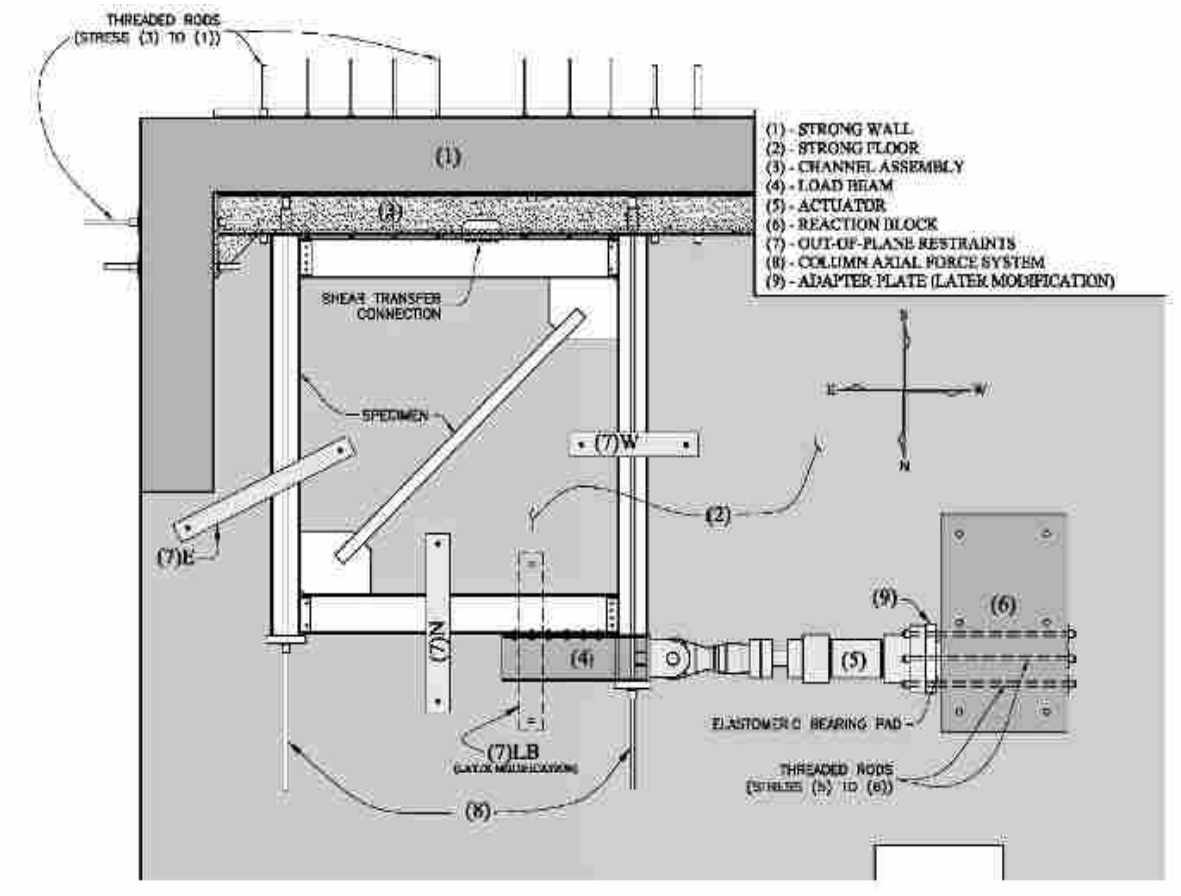

Figure 1-6 A. Christopolus Sub-Assemblage Test Setup (6)

(a) Fracture of Gusset-to-Beam Weld

(b) Yielding and Buckling of Beam

(c) Fracture of Beam

(d) Yielding and Warping of Column

Figure 1-7 A. Christopolus Sub-Assemblage Test Failures (2.5 % Drift) (6)

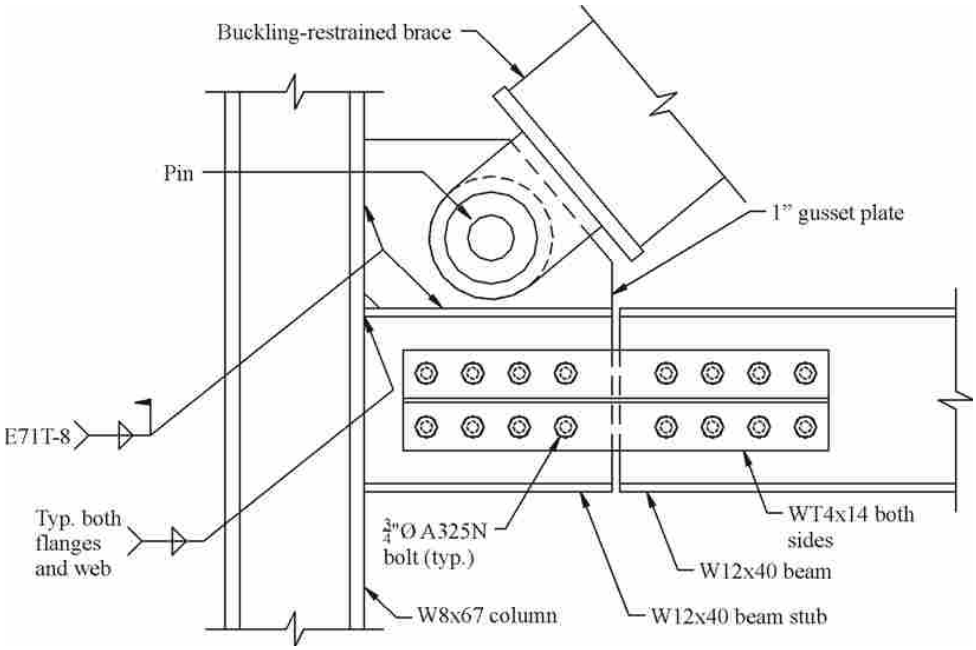

(a) Schematic

(b) Close-up View

Figure 1-8 Lehigh Test Connection Design: Pin Connection with Web Splice (7)

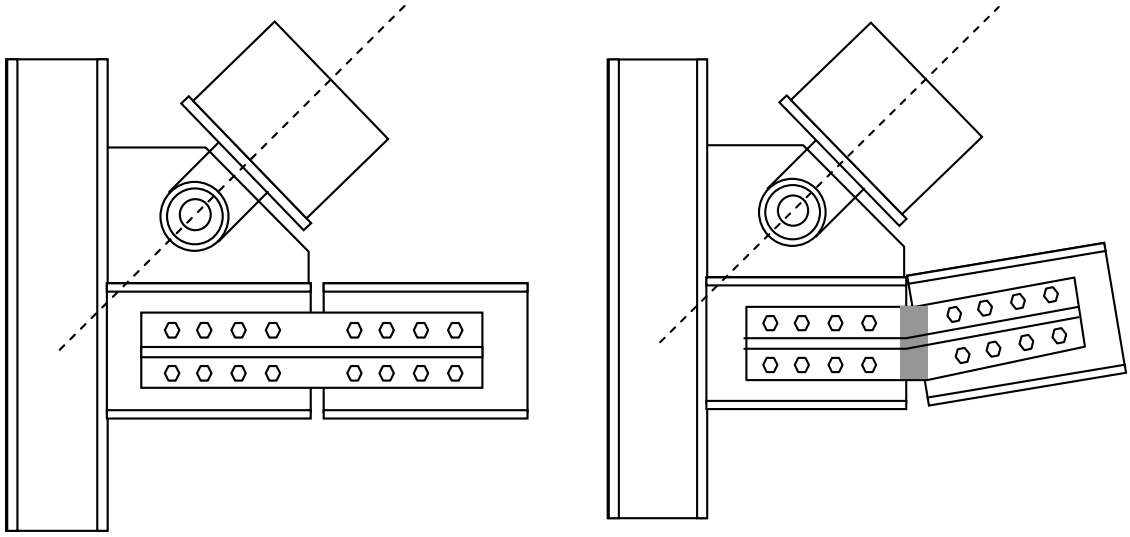

(a) Initial Condition **(b) Deformed Condition**

Figure 1-9 Lehigh Test Connection Response to Loading (7)

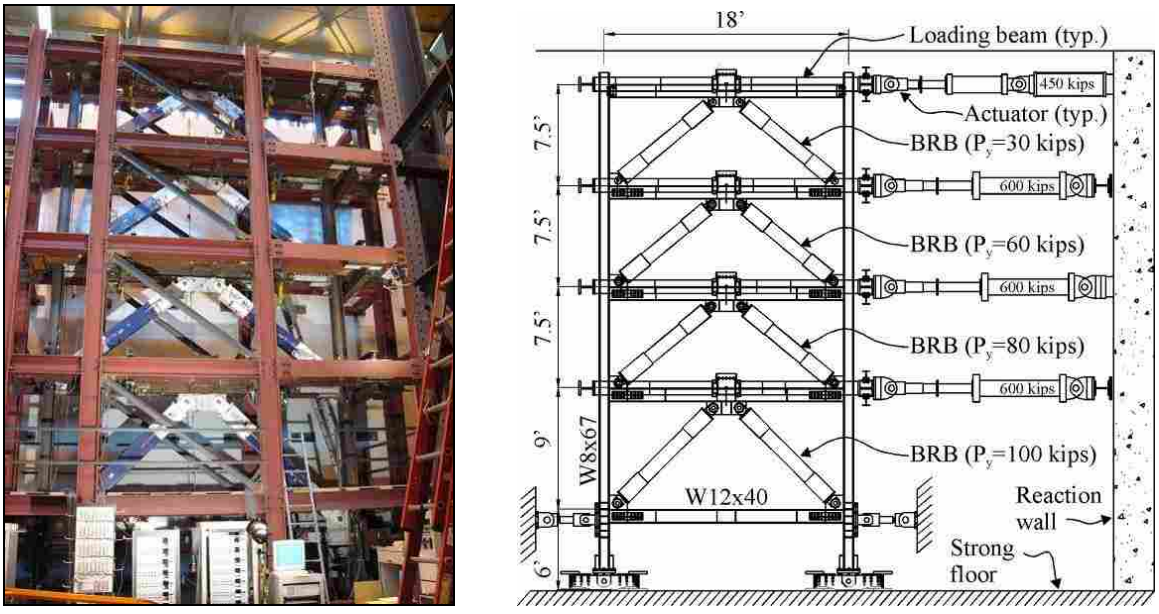

(a) Image **(b) Schematic**

Figure 1-10 Lehigh Test Frame (7)

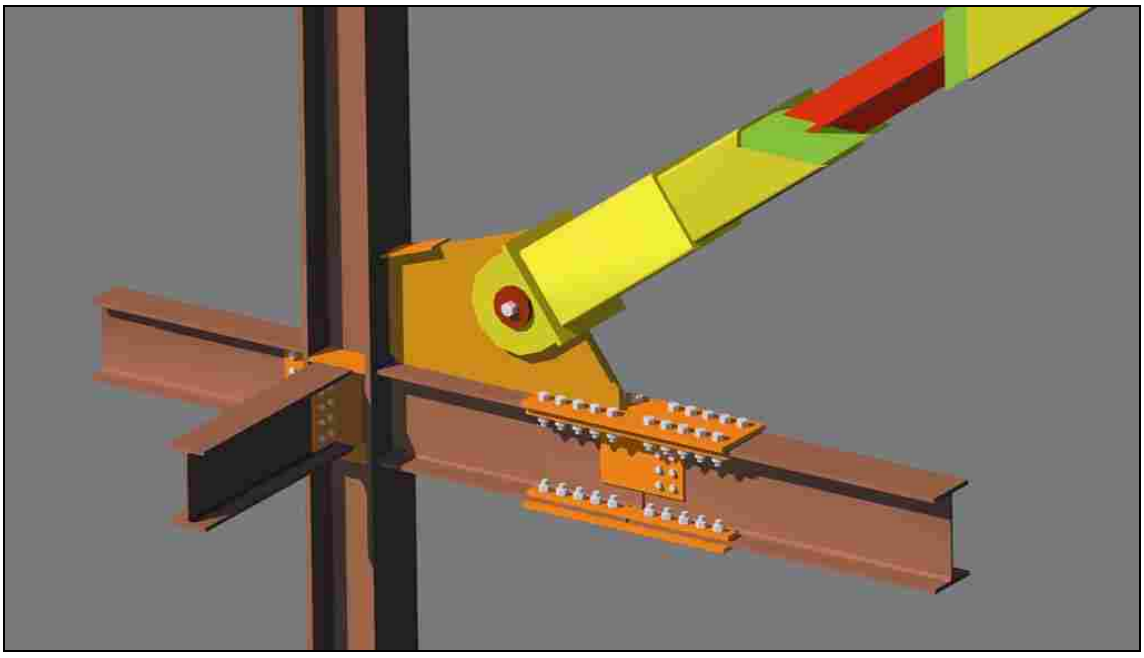

Figure 1-11 Proposed Connection: Utilizing a Hinge in the Beam (8)

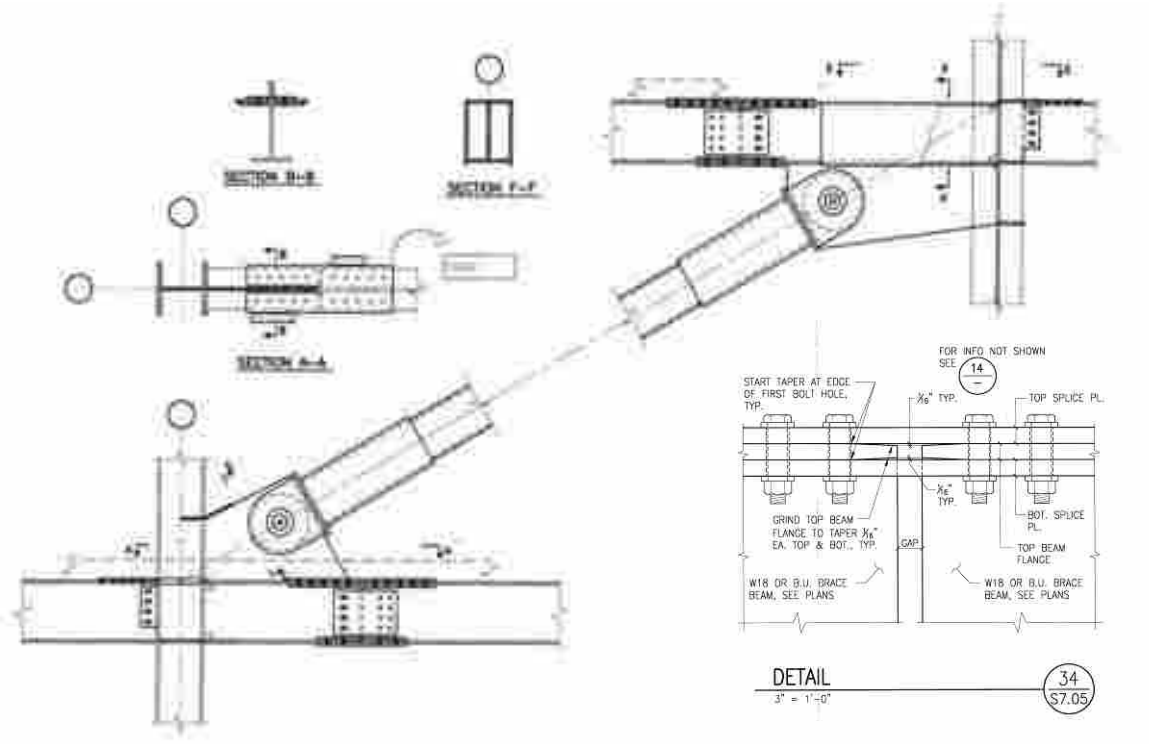

Figure 1-12 Proposed Connection Geometries and Taper Detail (8)

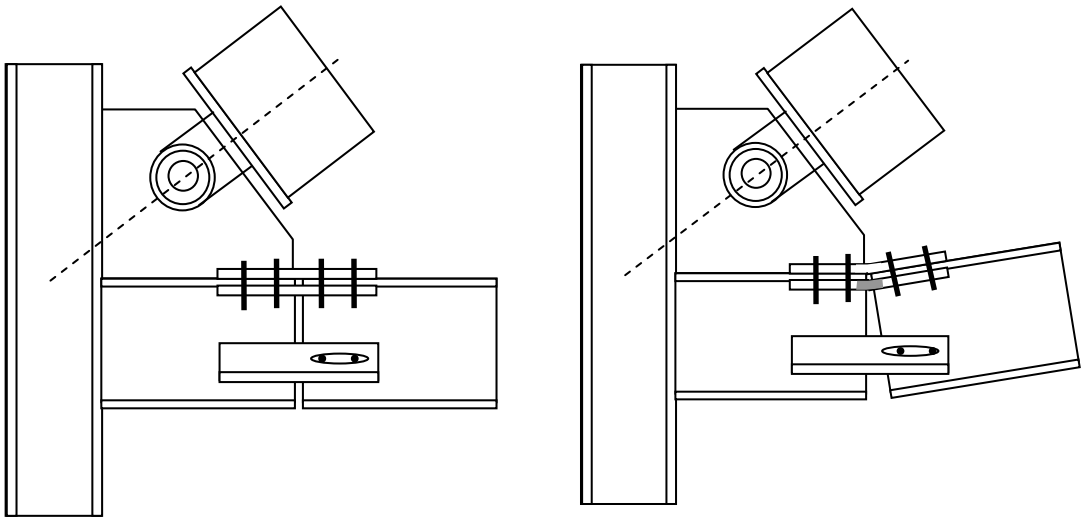

(a) Initial Condition **(b) Deformed Condition**

Figure 1-13 Modified Connection Design Response to Loading

2 Test Setup and Design

To determine the performance of the proposed connection design, specimens were designed and testing was conducted. In general, the procedure was as follows: the prototype bay was determined and designed, the test specimens were designed, the correlation between specimens and the prototype bay was determined, the loading protocols were developed, and the instrumentation plan was established.

2.1 Prototype Bay

A prototype bay with a story height of 13 ft. and bay length of 20 ft. was selected as representative of a typical frame (see Figure 2-1). The dimensions were deemed appropriate for the test setup because connection specimens, which only included the components in the connection vicinity, could be tested at full scale using a self-reacting frame and hydraulic actuators (see Appendix A). The prototype bay was the reference point for the connection design, loading protocols, and data analysis.

2.2 Prototype Bay Design

The beams, columns, and connection components for the prototype bay were designed by performing various steps, including (1) assuming the yield strength and determining the ultimate strength of the prototype brace, (2) designing the beams,

columns, and gusset plates using typical methodology as well as newly developed criteria, and (3) sizing the gap and determining the splice plate configurations using new methodology.

The prototype bay design results encompassed two key areas: the lower beam-column-brace connection (see Figure 2-2) and the upper beam-column-brace connection (see Figure 2-3). A general explanation of the design steps are given next, with calculations provided in Appendix B.

A BRB with a 203 kip yield strength was chosen as the prototype brace due to its common use in industry (16). Using typical factors, the brace ultimate strength was determined to be 402 kips (see Appendix B Section B.1 for calculations). To confine yielding to the brace; the brace ultimate strength was used for the design of the remaining frame components. Using the angle at which the brace connects to the gusset plate, the beam and column axial design forces were determined to be 337 kips and 219 kips, respectively (see Appendix Section B.2 for calculations).

The beams were designed to withstand three failure modes: (1) flexural yielding, (2) tensile yielding of the top flange gross cross-sectional area, and (3) tensile rupture of the top flange net cross-sectional area. Typically, the first failure mode is considered in a beam design and the other two are considered in the design of bolted tension connections. The latter two failure modes are considered in the beam design to ensure the beams are able to pass the entire axial load from the beam top flange to the splice plates. The selected beam was a W16x77 section (see Appendix Section B.3 for calculations).

The column was designed to withstand buckling and have a wider flange than the beam; a wider column flange ensures a simplified beam-column connection. The selected column was a W12x79 section (see Appendix Section B.4 for calculations).

Gusset plates were designed using the Uniform Force Method. The result was two separate geometries: one for the lower connection and one for the upper connection (see Figure 2-1). In both cases, a tapered design was used to accommodate the beam-gusset plate and column-gusset plate connection lengths required by the Uniform Force Method and the bolted brace-gusset plate connection area required by the brace core extension geometry. Both gusset plates were 1.0 in. thick (see Appendix Section B.5 for calculations).

The gap sizing required engineering judgment and geometric calculations. Since the purpose of the hinge is to decrease the moment on the connection, the gap must be placed as close as possible to the column. Nevertheless, the gap still needs to be beyond the edge of the gusset plate to allow for rotation. In addition, there must be enough space to allow for the beam-gusset plate weld. Based on these criteria, gap locations of 1-1/4 in. and 1.0 in. beyond the edge of the gusset plate were chosen for the lower and upper connections, respectively. To allow the gap to fully close under a maximum design drift of 6%, a gap size of 1-1/2 in. was selected (see Appendix Section B.6 for calculations).

The splice plates were designed to withstand four failure modes: (1) shear yielding, (2) global buckling, (3) tensile yielding of the top flange gross cross-sectional area, and (4) tensile rupture of the top flange net cross-sectional area. Because the plates bridge the gap between the beam and beam stub, they must transfer the full shear and

axial loads across the gap without yielding or buckling. As bolted tensile members, the plates must also be designed to withstand tension failure.

Plates were connected to both sides of the top flange (see Figures 2-2 and 2-3) using twelve 7/8 in. A490X bolts in double shear (see Appendix Section B.7 for calculations). Due to the beam web, two plates were used on the inner face of the flange. For the lower connection, two plates were used on the outer face of the flange to accommodate the gusset plate (see Figure 2-2). For the upper connection, only one plate was connected to the outer face of the flange (see Figure 2-3). Though various plate cross sections and configurations were possible for both connections, thinner plates were used to ensure obvious yielding during testing. For the lower connection, all four plates were 4 in. wide and 5/8 in. thick. For the upper connection plates, the two inner plates were 4.0 in. wide and 5/8 in. thick while the outer plate was 9-1/2 in. wide and 5/8 in. thick. To accommodate bolt and edge spacing requirements, the plates were 19-1/2 in. long (see Appendix Section B.8 for calculations).

2.3 Specimen Design and Test Setup

To test the two beam-column-brace connections, two specimens were designed based on the prototype bay. Due to the ability to test full-size connections, the same component design selections were used; no scaling was required. Because the focus of testing was on the connections, the specimens did not consist of the entire bay; instead only the members in the immediate vicinity of the connection were included. In addition, to accommodate the test setup, each specimen incorporated other components, including: a BRB core extension assembly, HSS extension, beam extension, and column pin core

extension assembly (see Appendix C for design calculations). For testing, one specimen at a time was situated on its side and rotated to align the beam and HSS extensions with the corresponding actuators and the column with the self-reacting frame pin connection (see Figures 2-4 and 2-5). Furthermore, lateral bracing and supports were employed above and below the specimen and actuators to limit out-of-plane movement (see Figures 2-6 and 2-7).

2.4 Relationship between Prototype Bay and Test Setup

One difficulty arising from testing an isolated connection, as compared to an entire bay, is the increased complexity of the specimen response. Inter-story drift is a typical variable (given as a percentage) used to measure response, and when testing an entire bay, inter-story drift can be determined directly by calculating the column rotation within the bay. Because the isolated connection does not have a bay to reference, it was determined inaccurate to base the inter-story drift of the specimen on the rotation of the column. Instead, another method was used and is described below.

As the central feature of the proposed connection design and because the specimens utilized the same component design selections as the prototype bay, the gap rotation was deemed the most accurate point of comparison between the test setup and prototype bay. More specifically, the actuator displacement of the test setup and the inter-story drift of the prototype bay are both related to the gap rotation by one-to-one relationships. The result is that every gap rotation value has unique actuator displacement and inter-story drift values to which it corresponds and which thereby correspond uniquely to each other.

The relationships between the gap rotation, actuator displacement, and inter-story drift are helpful in both developing the loading protocols and analyzing test data. For the loading protocols, when given an inter-story drift percentage, the corresponding actuator displacement value can be determined. For the test data, when instruments return actuator displacement values, an estimated inter-story drift can be calculated. Additional explanation and an associated conversion table are given in Appendix D.

2.5 Loading Protocols

Loading protocols were developed for both actuators. The prototype-test conversion table (see Appendix D) was utilized along with the estimated stiffness of the self-reacting frame and the anticipated hysteresis action of the prototype brace. To determine the frame stiffness, small loading cycles were applied to the test specimens. To estimate the brace hysteresis response, a model was developed and validated using results obtained in previous BRB tests; the development and validation are given in Appendix E.

A general explanation of each actuator loading protocol is given below, and detailed calculations are given in Appendix F.

2.5.1 Beam Actuator

The actuator attached to the beam (Actuator 2 in Figures 2-4 and 2-5) was displacement controlled and introduced inter-story drift into the test assembly. The displacement protocol was based on Recommended Provisions (2) and was similar to that used in other test setups (6).

Recommended Provisions (2) suggest a sub-assemblage loading protocol based on BRB deformation in cycles of increasing magnitude. Each cycle consists of two half-cycles: the first is the compressive shortening of the brace to the specified magnitude, and the second is the tensile elongation to the same magnitude. In order to drive the rotational demands of the test specimens to the limit, additional cycles of increasing deformations were added. To more quickly reach the higher-deformation cycles, fewer lower-deformation cycles were applied. The loading protocols for Specimen 1 and 2 are shown in Tables 2-1 and 2-2, respectively.

The variables used in the determination of the protocol are the BRB deformation estimated to occur at the first significant yielding of the prototype BRB (Δ_{by}) and the BRB deformation estimated to occur at the point when the prototype bay is at its design story drift (Δ_{bm}) (2). For the test specimens, the deformation quantities are Δ_{by} = 0.275 in. and Δ_{bm} = 2.590 in.. The initial yielding deformation calculation was based on the yield properties of the brace while the design story drift deformation calculation was based on an inter-story drift of 2%, which is a typical value used in testing (5, 14).

To define the testing protocol, BRB inter-story drift values were translated into corresponding actuator displacement values. To account for movement in the self-reacting frame, the actuator displacement values were adjusted based on the frame stiffness. The resulting protocols are shown in Figures 2-8 and 2-9.

2.5.2 Brace Actuator

The function of the brace actuator (Actuator 1 in Figures 2-4 and 2-5) is to simulate the response of the buckling-restrained brace to the introduced drift. Under cyclic loading, a BRB typically exhibits hysteric behavior, which consists of cyclic

loading displacements and the corresponding forces that result as the brace undergoes strain hardening. Using calculated deformation lengths that relate to the applied displacement of Actuator 2, a force controlled protocol was developed for Actuator 1.

The first step in determining the Actuator 1 protocol was to apply the maximum or minimum inter-story drift for each half-cycle, as specified by the Actuator 2 protocol, to the prototype bay geometry. The deformation value required of the brace to accommodate the shifting bay geometry was then calculated and the brace force expected to oppose the displacement was determined. In performing these calculations, all bay components were assumed to be perfectly rigid, and all hinging was assumed to occur at either the centroid of the splice connection or the idealized hinge point in the BRB transition segment (see Appendix F).

The hystereses for specimens 1 and 2 are shown in Figures 2-10 and 2-11, respectively, and are based on the model described in Appendix E. Due to the multi-linear shapes of the hysteresis half-cycles, intermediate steps were incorporated into each loading protocol half-cycle of Actuator 1.

2.5.3 Actuator Synchronization

A satisfactory performance of the tests necessitated complete correlation between the two actuators. Because intermediate steps for each protocol half-cycle corresponding to the prototype BRB hysteresis discontinuities were required for Actuator 1 to accurately simulate a BRB, corresponding intermediate steps were incorporated into the Actuator 2 protocol. The result was that the displacement values of Actuator 2 and the force values of Actuator 1 corresponding to all points along the BRB hysteresis were included in both protocols.

The two protocols had an equal number of steps and the actuators stepped through the protocols in unison. For each step, the actuators started at a specified displacement or force and moved linearly to the next specified displacement or force; in this way, complete correlation between the actuators was achieved. The complete protocols are included in Appendix G.

2.6 Instrumentation

In order to gather test data for analysis purposes, both test specimens were instrumented. Some modifications were made for the second test and resulted in new instrumentation locations and minor differences in naming conventions; in other words, even though many instruments were placed in similar locations for both tests, they were not necessarily assigned the same name.

Strain gages, rosettes, and string pots were utilized for both tests, and the output was electronically recorded. The splice plates were of particular concern, and were heavily instrumented using post-yield gages.

The instrumentation for Test 1 is shown in Figures 2-12 through 2-15 and consisted of 41 strain gages, 6 rosettes, and 10 string pots. Images of the instrumented specimen are shown in Figures 2-16 and 2-17. The instrumentation for Test 2 is shown in Figures 2-18 through 2-21 and used 30 strain gages, 5 rosettes, and 10 string pots. Images of the instrumented specimen are shown in Figures 2-22 and 2-23.

Table 2-1: BRB Sub-assemblage Loading Protocol (Specimen 1)

Number of Cycles to Perform	BRB Deformation		Corresponding Drift		Actuator 2 Disp. (in.)		Actuator 1 Force (kips)	
	As Specified	*Nominal (in.)*	*Neg.*	*Pos.*	*Neg.*	*Pos.*	*Neg.*	*Pos.*
6	Δ_{by}	0.275	-0.24%	0.24%	-0.33	0.32	200	-200
2	0.5 * Δ_{bm}	1.295	-1.15%	1.14%	-1.54	1.54	233	-251
2	1.0 * Δ_{bm}	2.591	-2.30%	2.28%	-3.06	3.10	275	-271
2	1.5 * Δ_{bm}	3.886	-3.47%	3.43%	-4.57	4.68	305	-284
2	2.0 * Δ_{bm}	5.181	-4.64%	4.57%	-6.06	6.26	325	-297
2	2.5 * Δ_{bm}	6.476	-5.83%	5.71%	-7.54	7.86	345	-304
2 + fatigue*	3.0 * Δ_{bm}	7.772	-7.01%	6.86%	-9.00	9.47	359	-317

*Additional fatigue cycles performed until connection failure.

Table 2-2: BRB Sub-assemblage Loading Protocol (Specimen 2)

Number of Cycles to Perform	BRB Deformation		Corresponding Drift		Actuator 2 Disp. (in.)		Actuator 1 Force (kips)	
	As Specified	*Nominal (in.)*	*Neg.*	*Pos.*	*Neg.*	*Pos.*	*Neg.*	*Pos.*
3	0.3 * Δ_{by}	0.083	-0.07%	0.07%	-0.11	0.10	66	-60
3	0.5 * Δ_{by}	0.138	-0.11%	0.11%	-0.17	0.16	102	-96
6	Δ_{by}	0.275	-0.22%	0.22%	-0.34	0.33	200	-200
2	0.5 * Δ_{bm}	1.295	-1.05%	1.03%	-1.57	1.57	240	-260
2	1.0 * Δ_{bm}	2.591	-2.11%	2.05%	-3.14	3.16	281	-273
2	1.5 * Δ_{bm}	3.886	-3.18%	3.06%	-4.69	4.76	309	-290
2	2.0 * Δ_{bm}	5.181	-4.27%	4.05%	-6.23	6.37	330	-298
2	2.5 * Δ_{bm}	6.476	-5.37%	5.03%	-7.76	7.98	348	-306
2 + fatigue*	3.0 * Δ_{bm}	7.772	-6.49%	6.01%	-9.28	9.60	362	-318

*Additional fatigue cycles performed until connection failure.

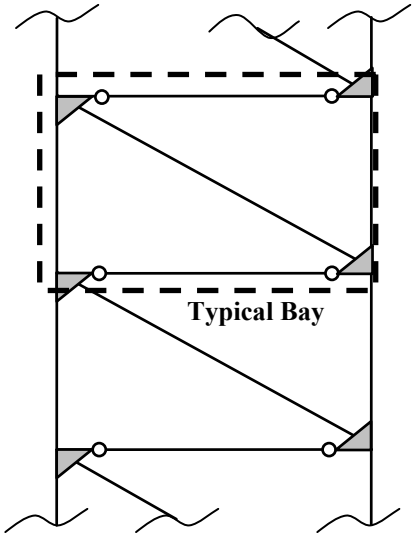

(a) Prototype BRBF with Pinned-Beam Connections

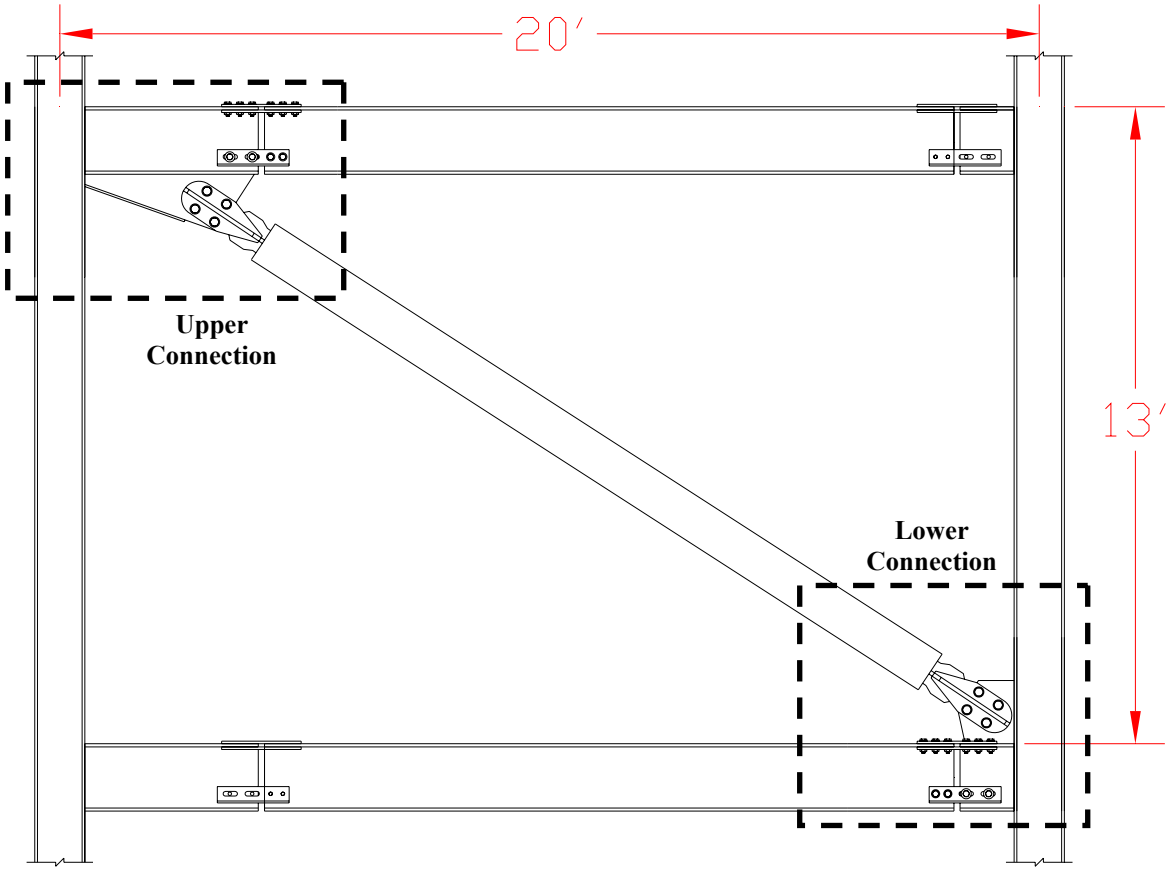

(a) Prototype Bay – Upper and Lower Connections

Figure 2-1 Prototype Bay

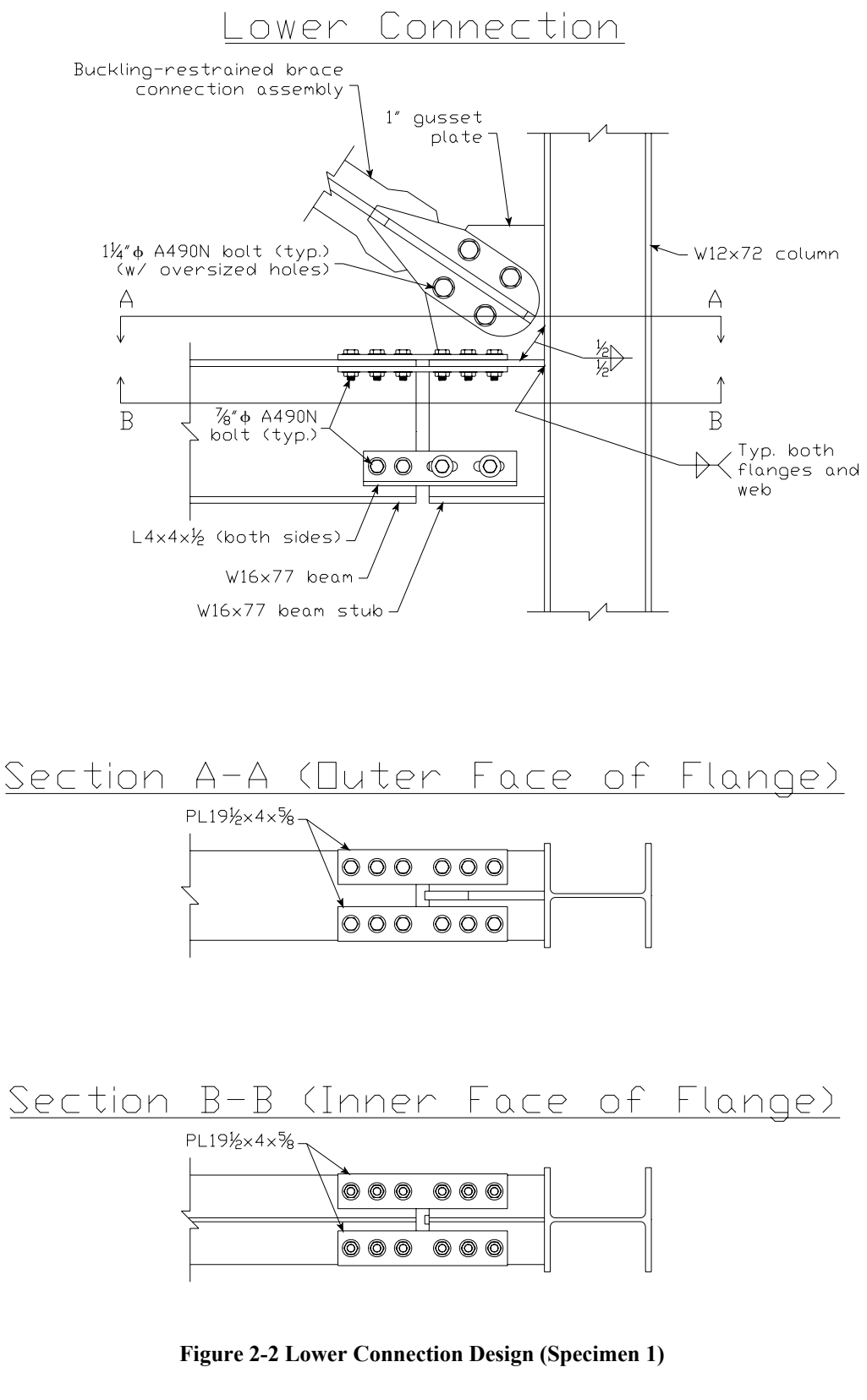

Figure 2-2 Lower Connection Design (Specimen 1)

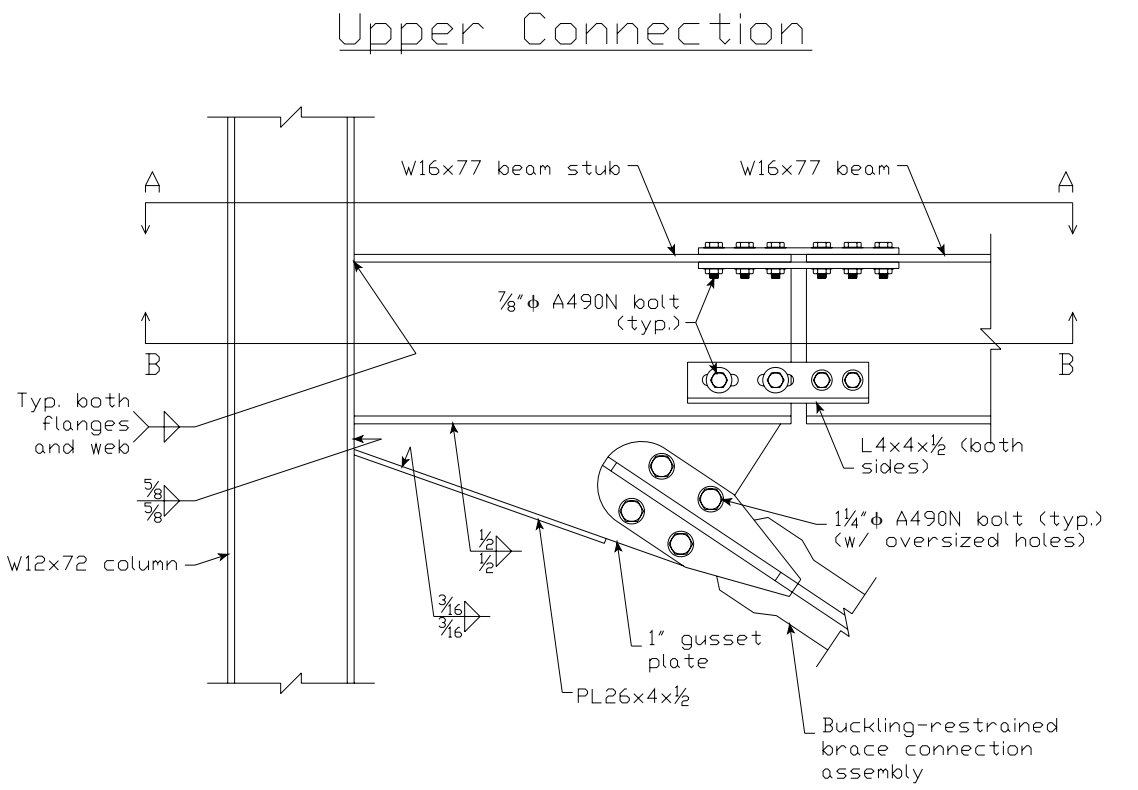

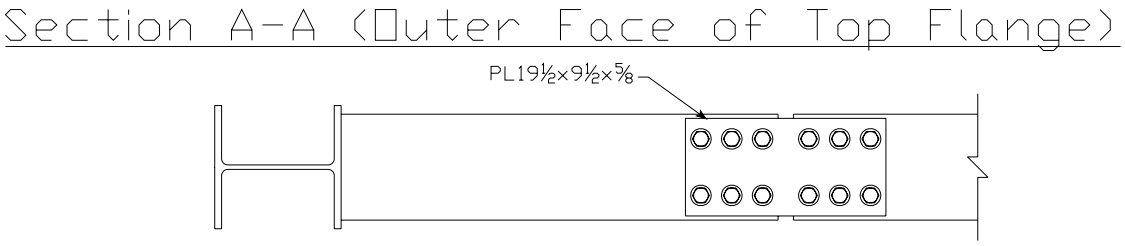

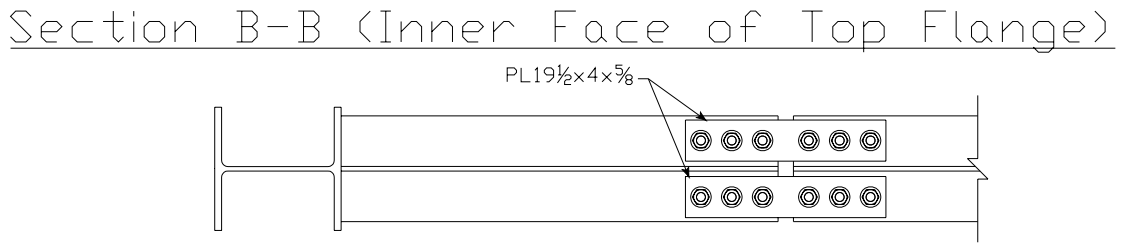

Figure 2-3 Upper Connection Design (Specimen 2)

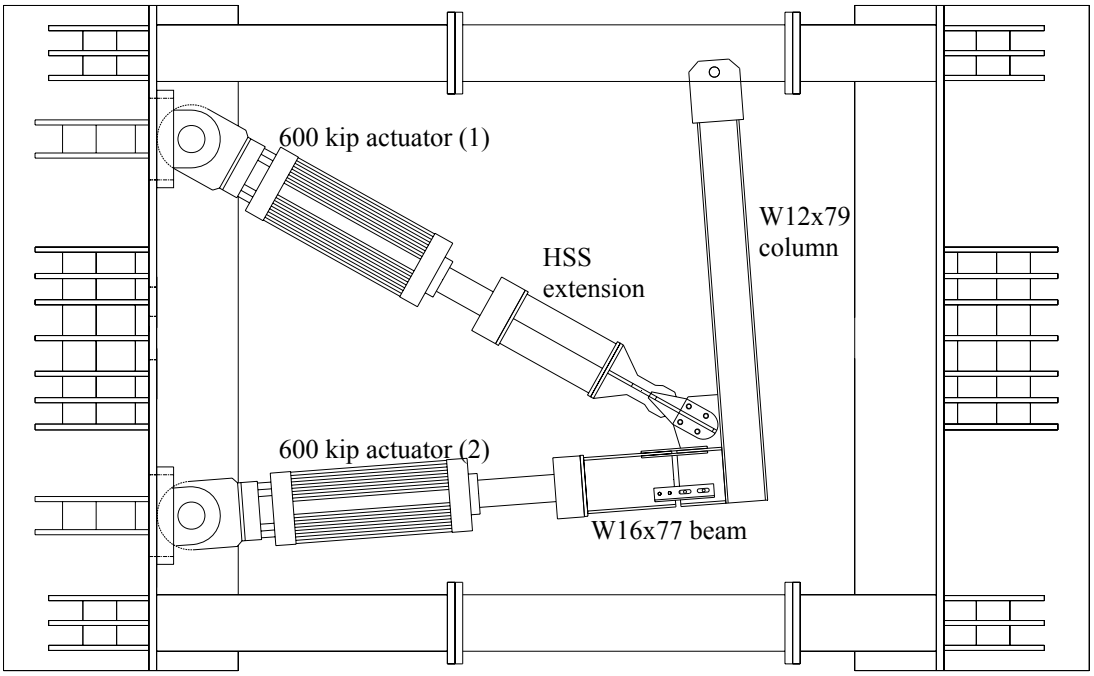

Figure 2-4 Specimen 1 – Configuration in Test Frame

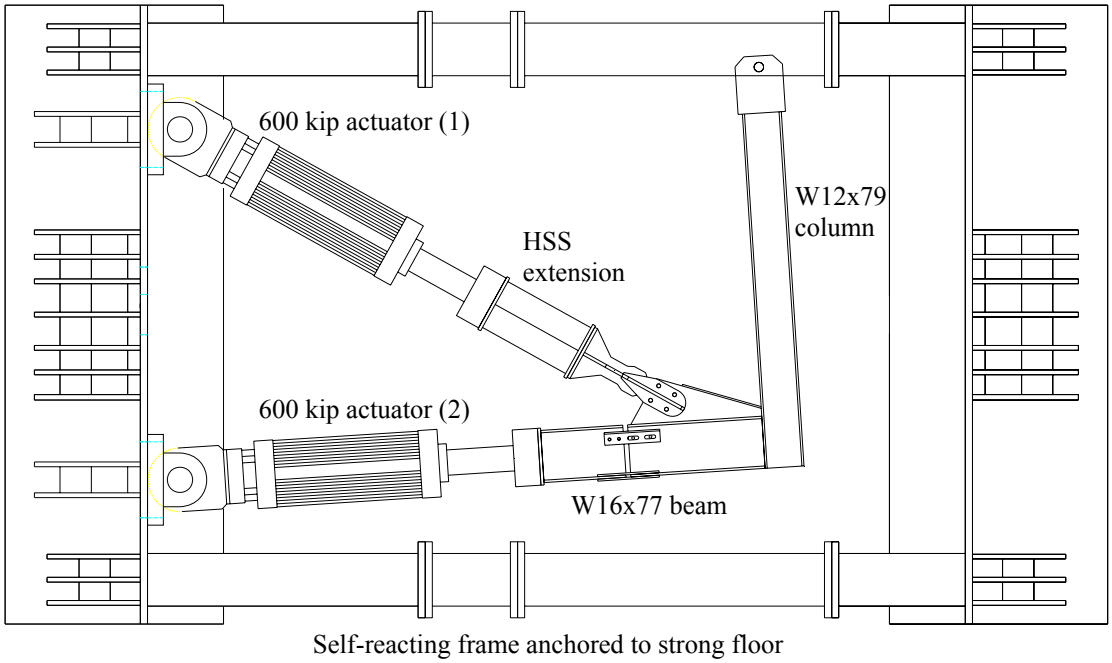

Figure 2-5 Specimen 2 – Configuration in Test Frame

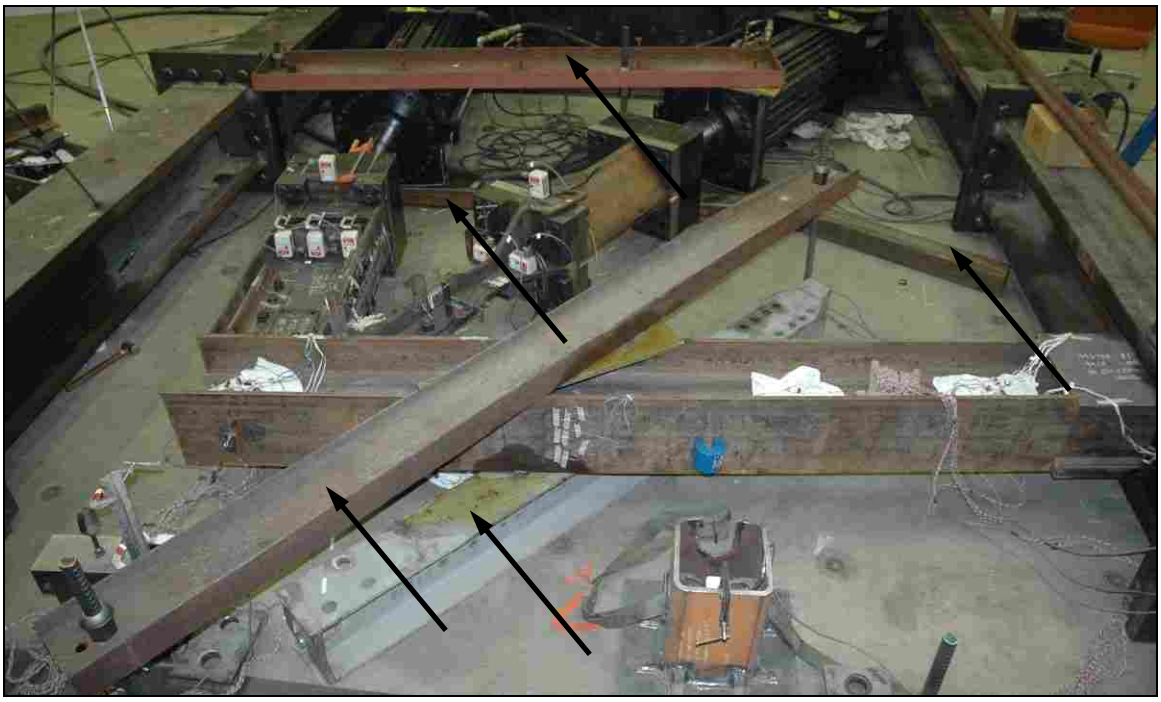

Figure 2-6 Specimen 1 – Out-of-Plane Bracing

Figure 2-7 Specimen 2 – Out-of-Plane Bracing

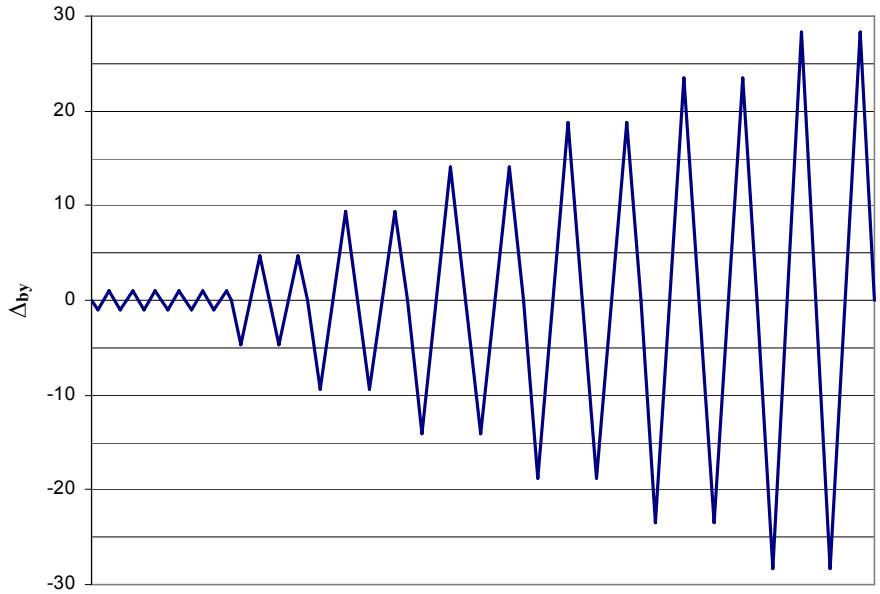

Peak Δ	Cycles
1.0 Δ_{by}	6
4.7 Δ_{by}	2
9.4 Δ_{by}	2
14.1 Δ_{by}	2
18.8 Δ_{by}	2
23.5 Δ_{by}	2
28.2 Δ_{by}	2

Figure 2-8 Specimen 1 – Loading Protocol with Respect to Yield Deformation

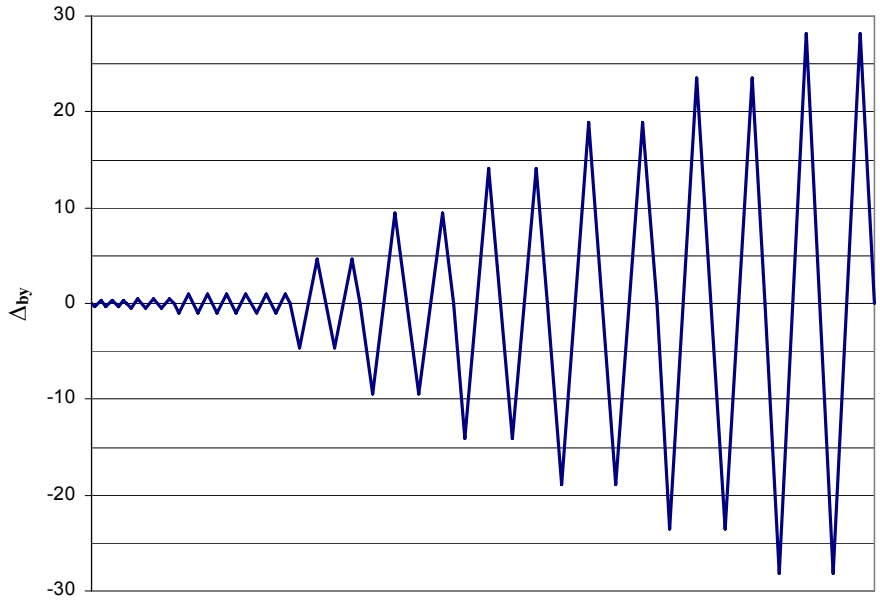

Peak Δ	Cycles
0.3 Δ_{by}	3
0.5 Δ_{by}	3
1.0 Δ_{by}	6
4.7 Δ_{by}	2
9.4 Δ_{by}	2
14.1 Δ_{by}	2
18.8 Δ_{by}	2
23.5 Δ_{by}	2
28.2 Δ_{by}	2

Figure 2-9 Specimen 2 – Loading Protocol with Respect to Yield Deformation

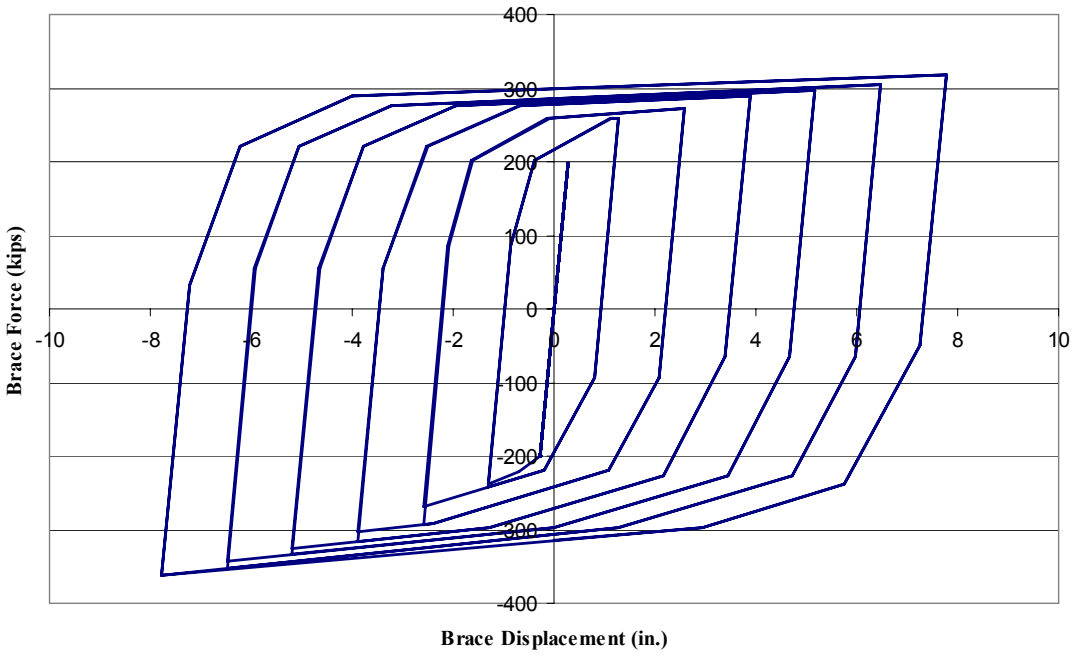

Figure 2-10 Specimen 1 – Estimated Hysteresis of Prototype BRB

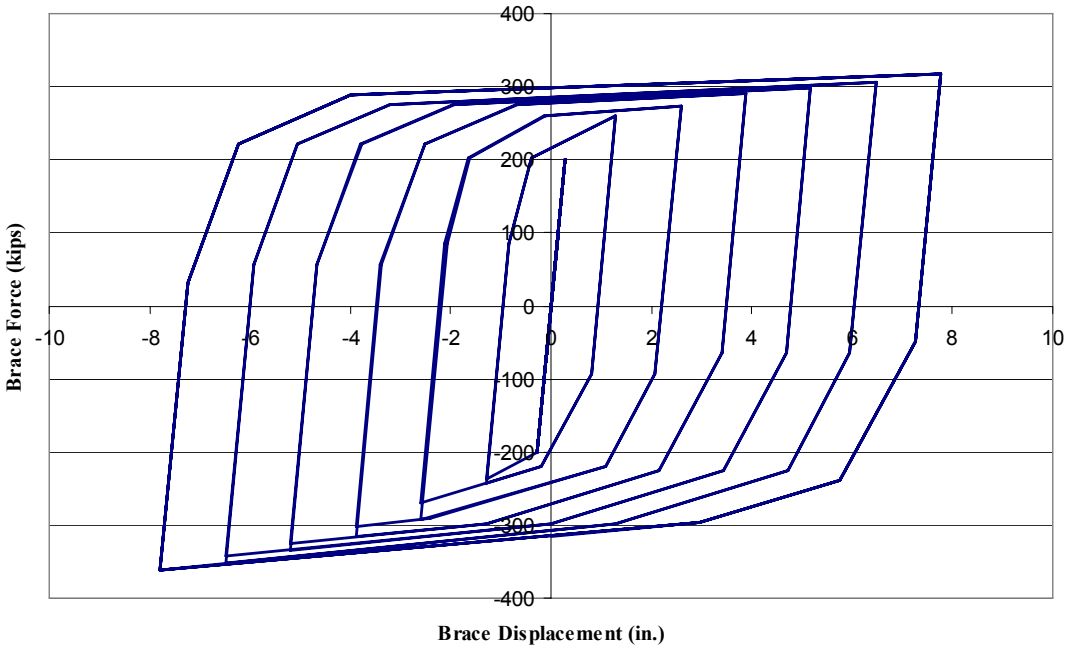

Figure 2-11 Specimen 2 – Estimated Hysteresis of Prototype BRB

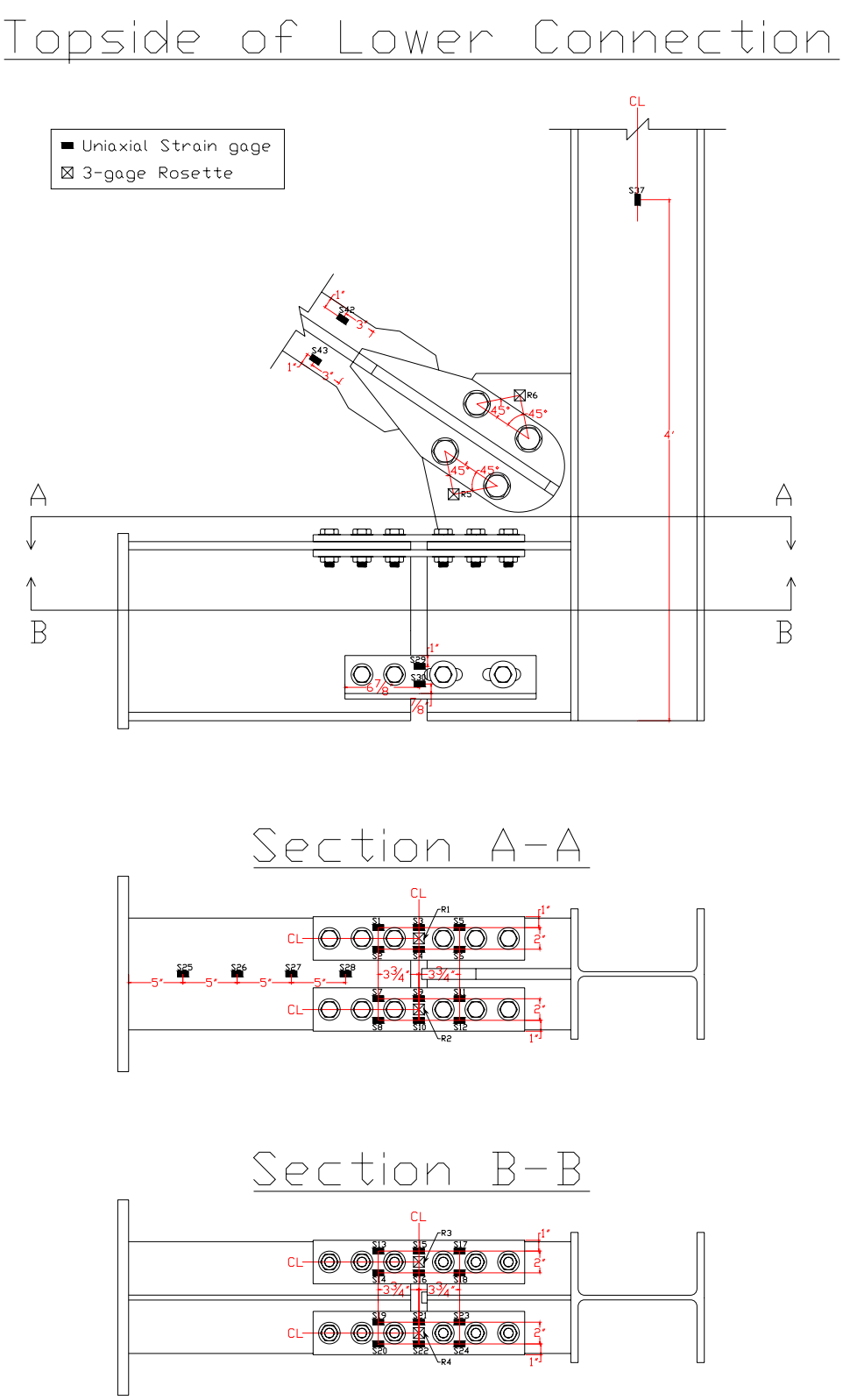

Figure 2-12 Specimen 1 – Instrumentation (Topside)

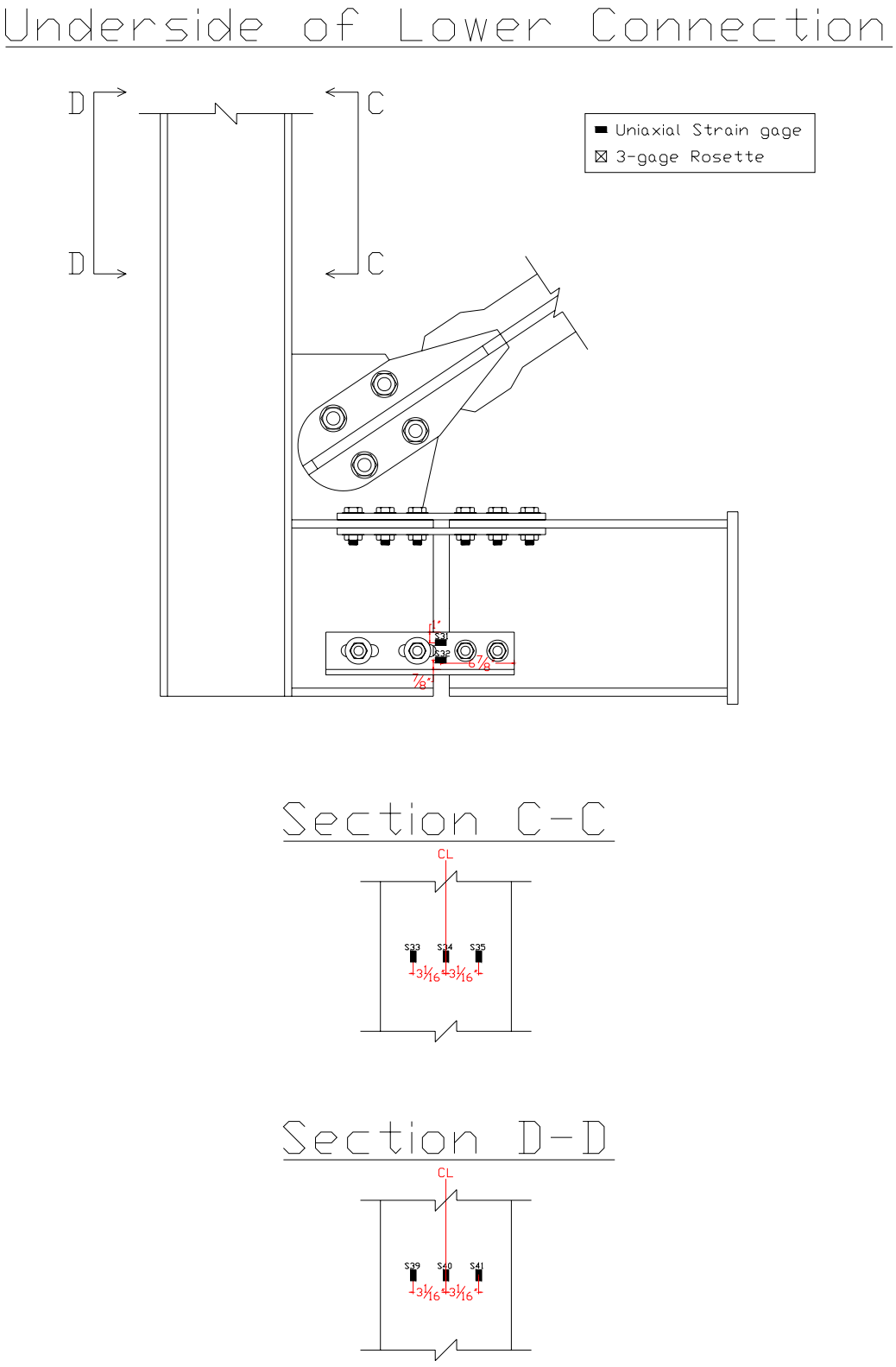

Figure 2-13 Specimen 1 – Instrumentation (Underside)

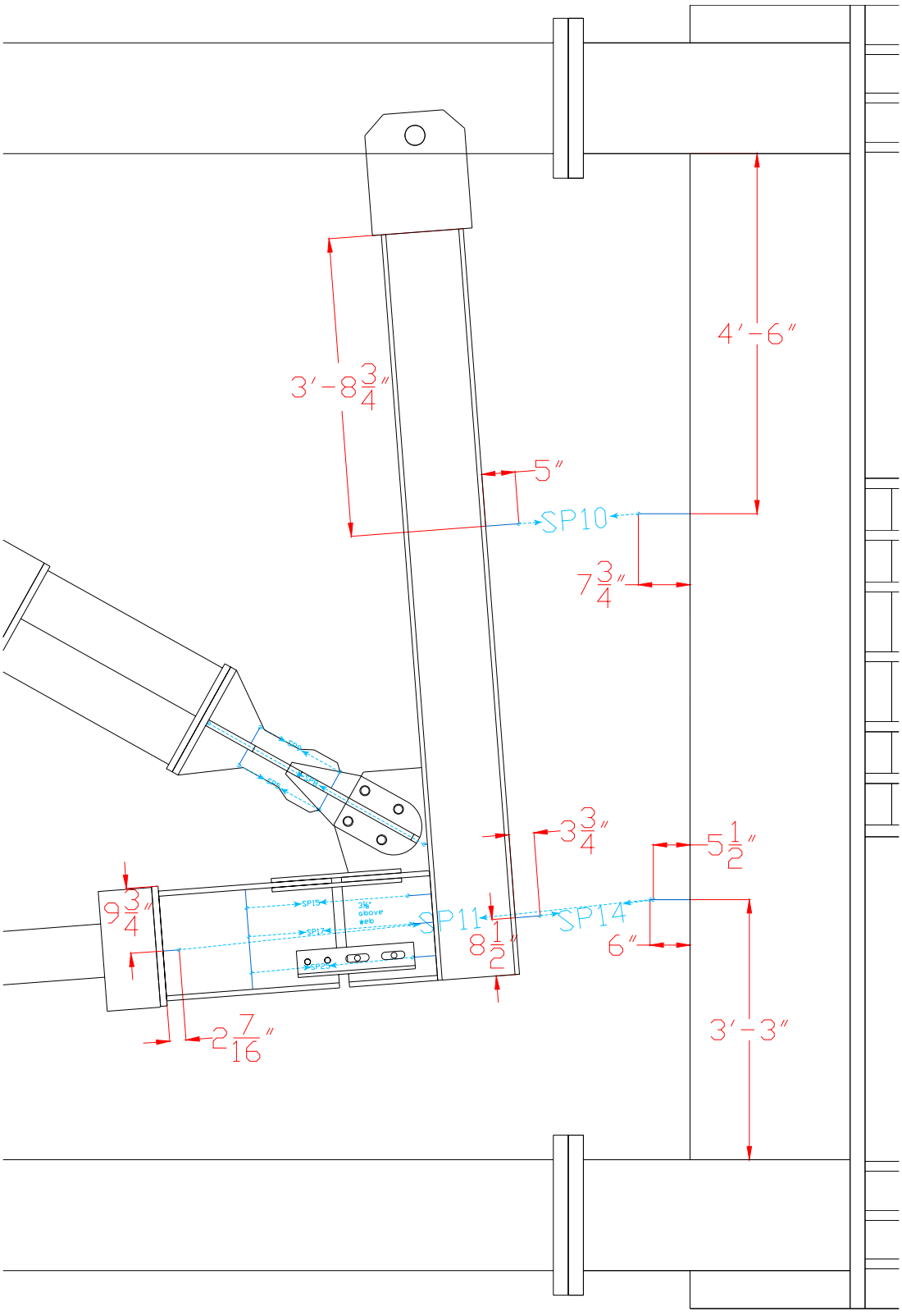

Figure 2-14 Specimen 1 – String Pot Instrumentation

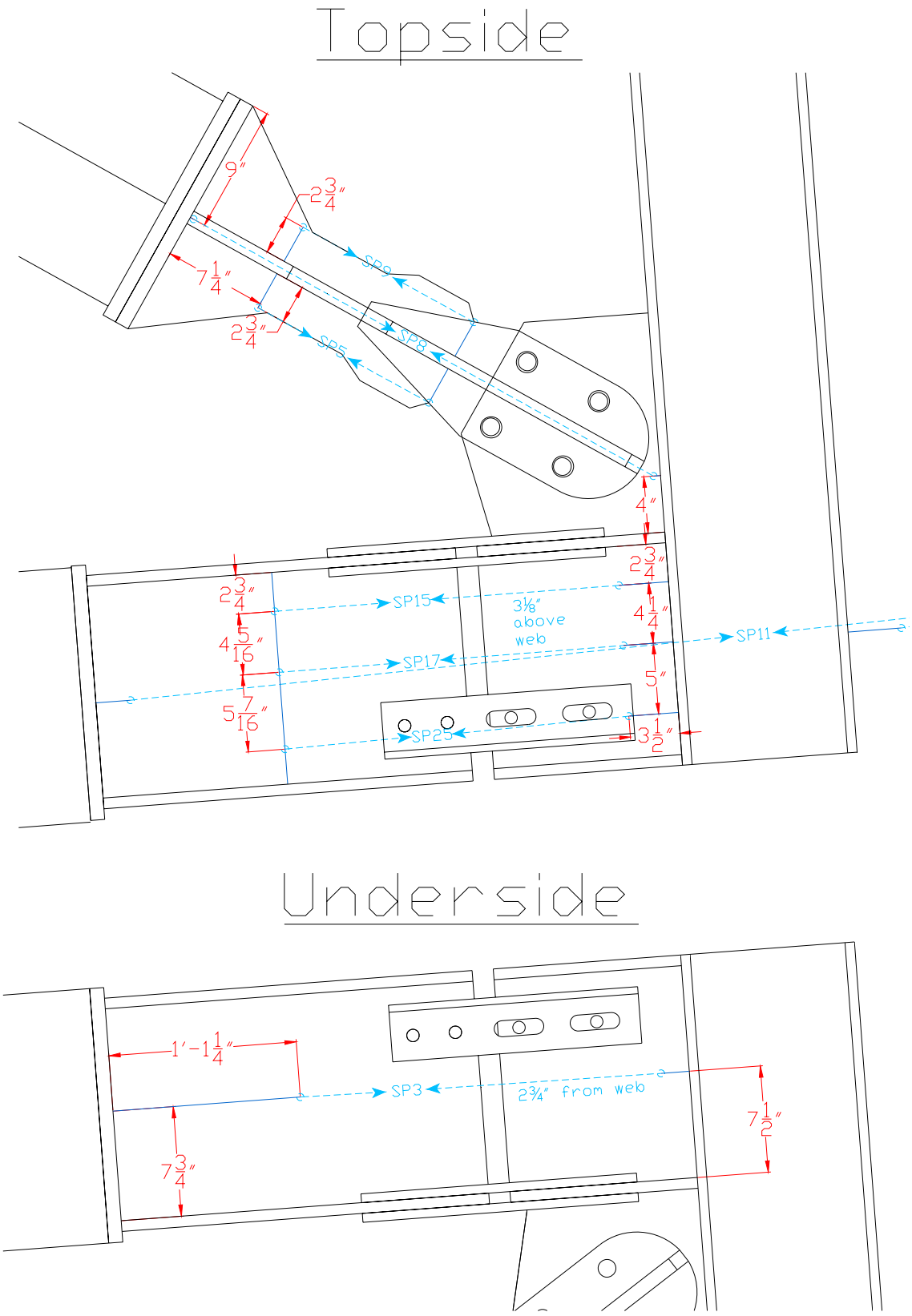

Figure 2-15 Specimen 1 – String Pot Instrumentation (Close-Up)

Figure 2-16 Specimen 1 – Gusset and Splice Plate Instrumentation

Figure 2-17 Specimen 1 – Instrumentation

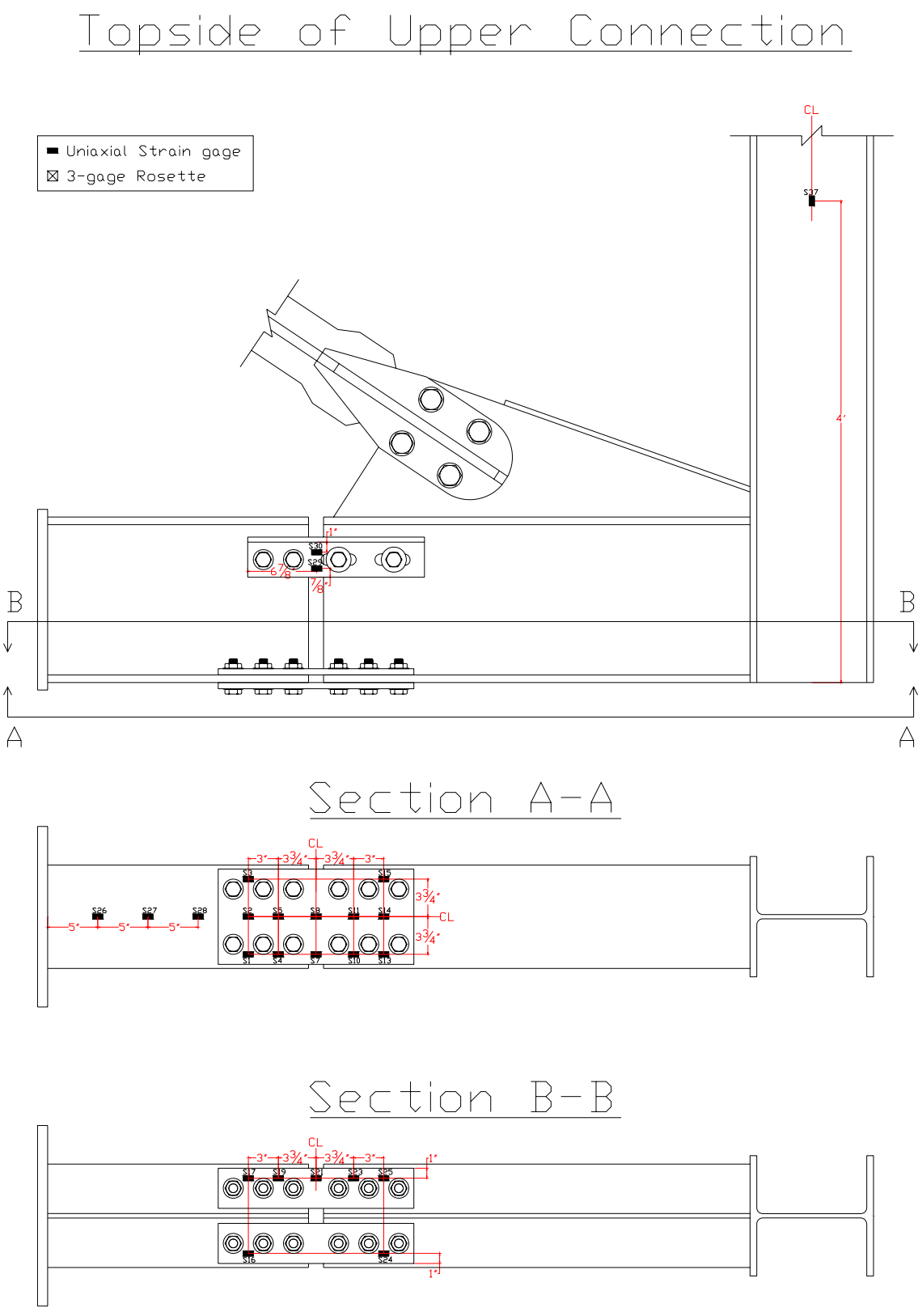

Figure 2-18 Specimen 2 – Instrumentation (Topside)

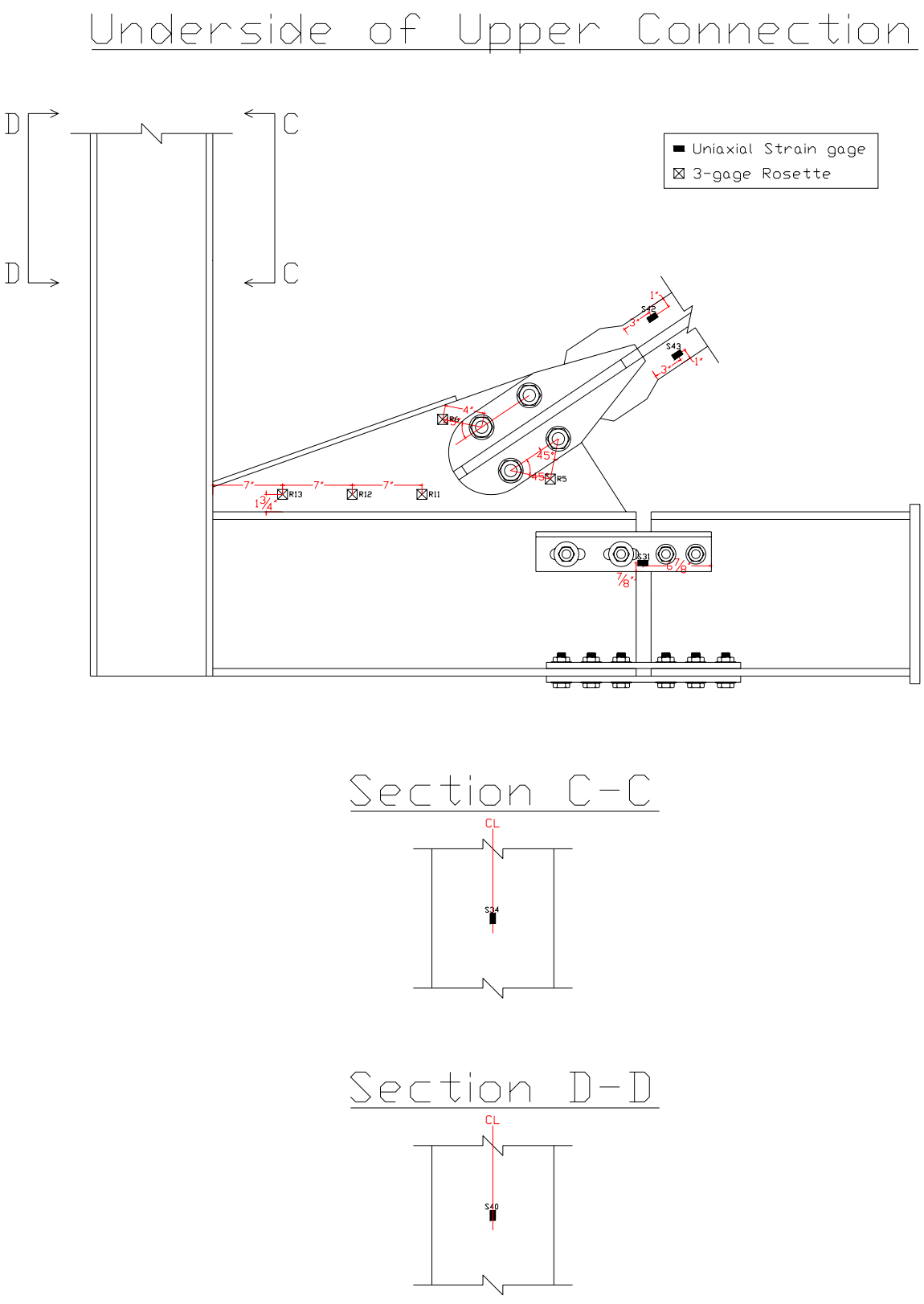

Figure 2-19 Specimen 2 – Instrumentation (Underside)

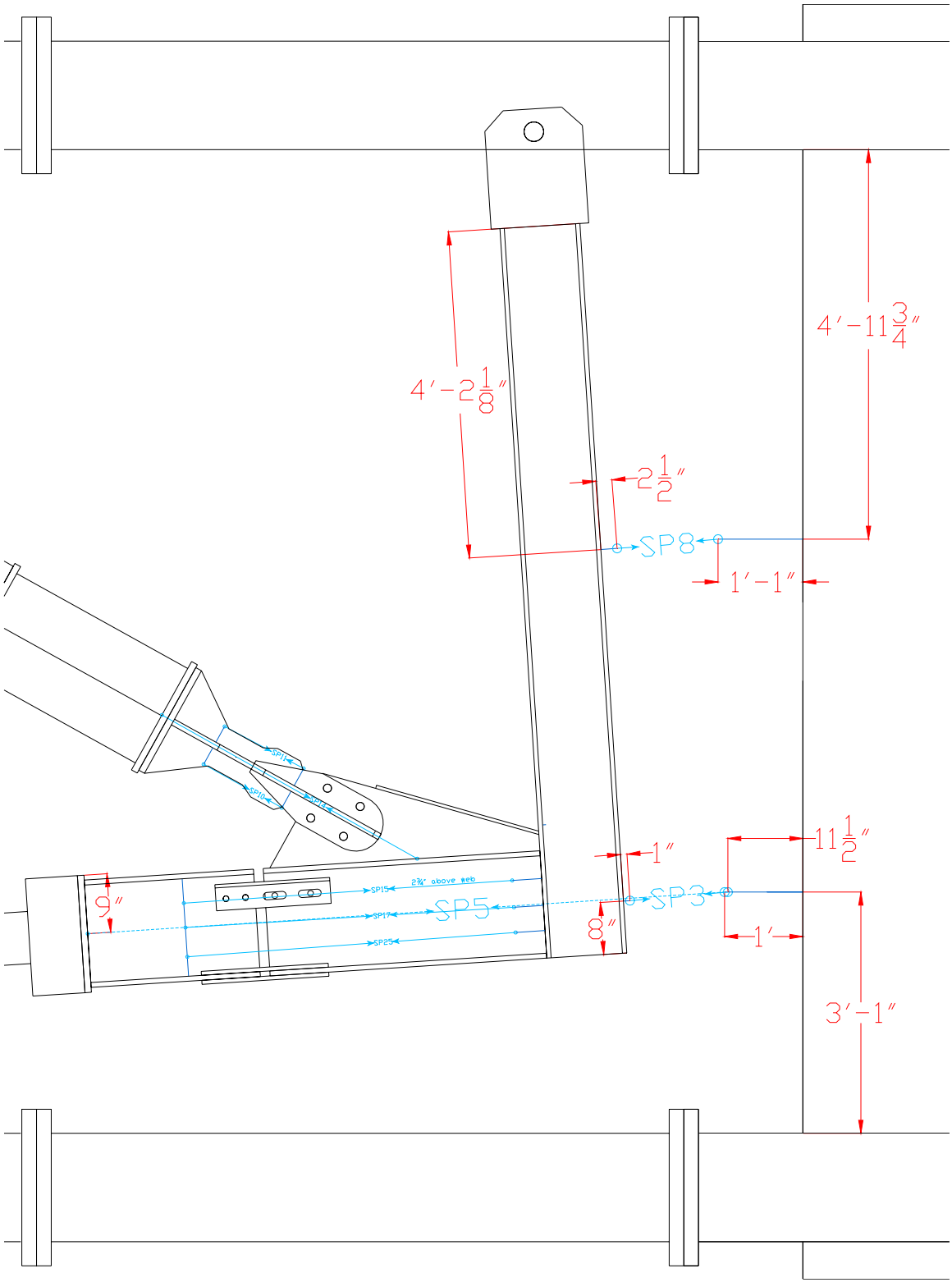

Figure 2-20 Specimen 2 – String Pot Instrumentation

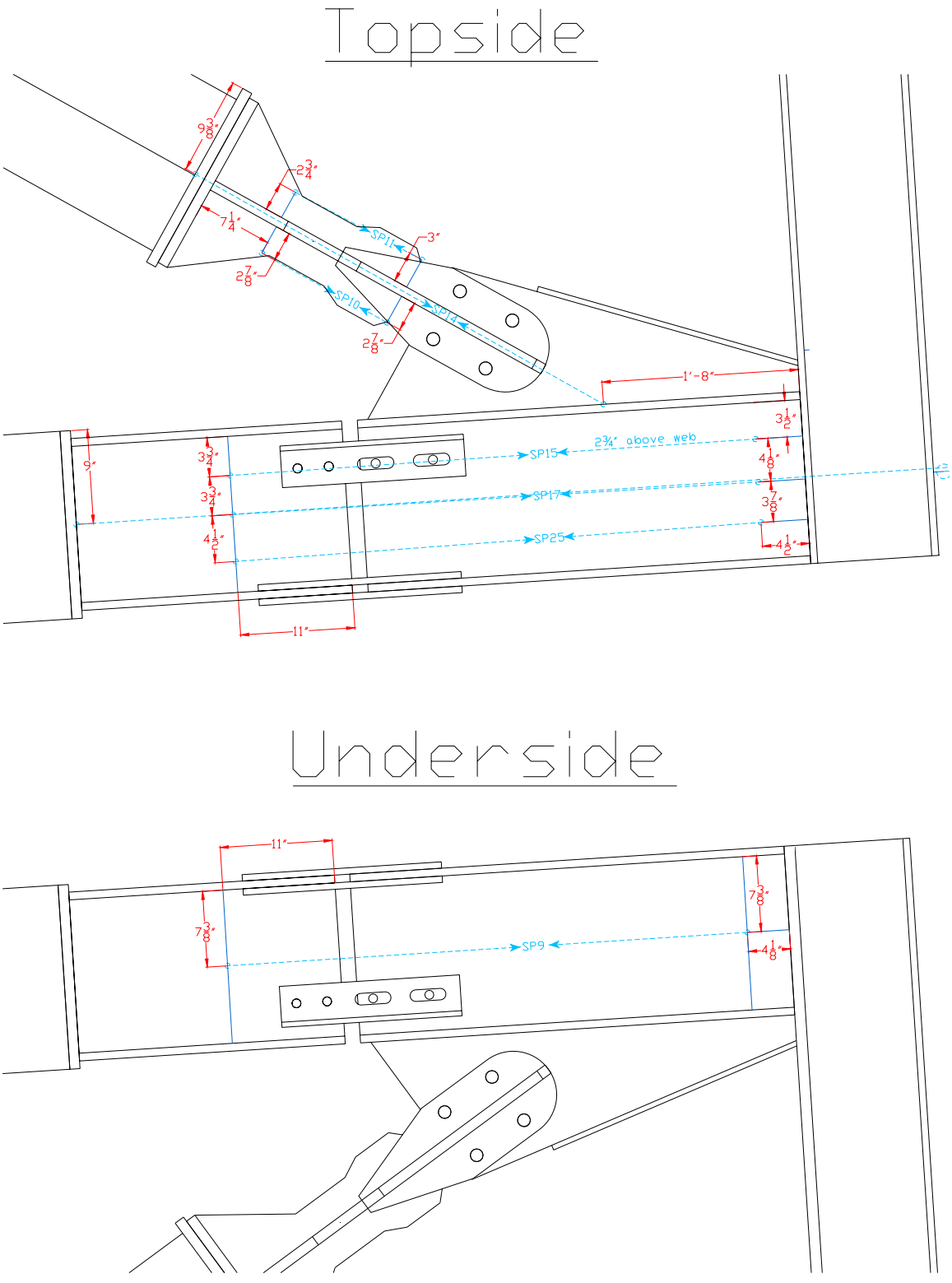

Figure 2-21 Specimen 2 – String Pot Instrumentation (Close-Up)

Figure 2-22 Specimen 2 –Instrumentation (Side View)

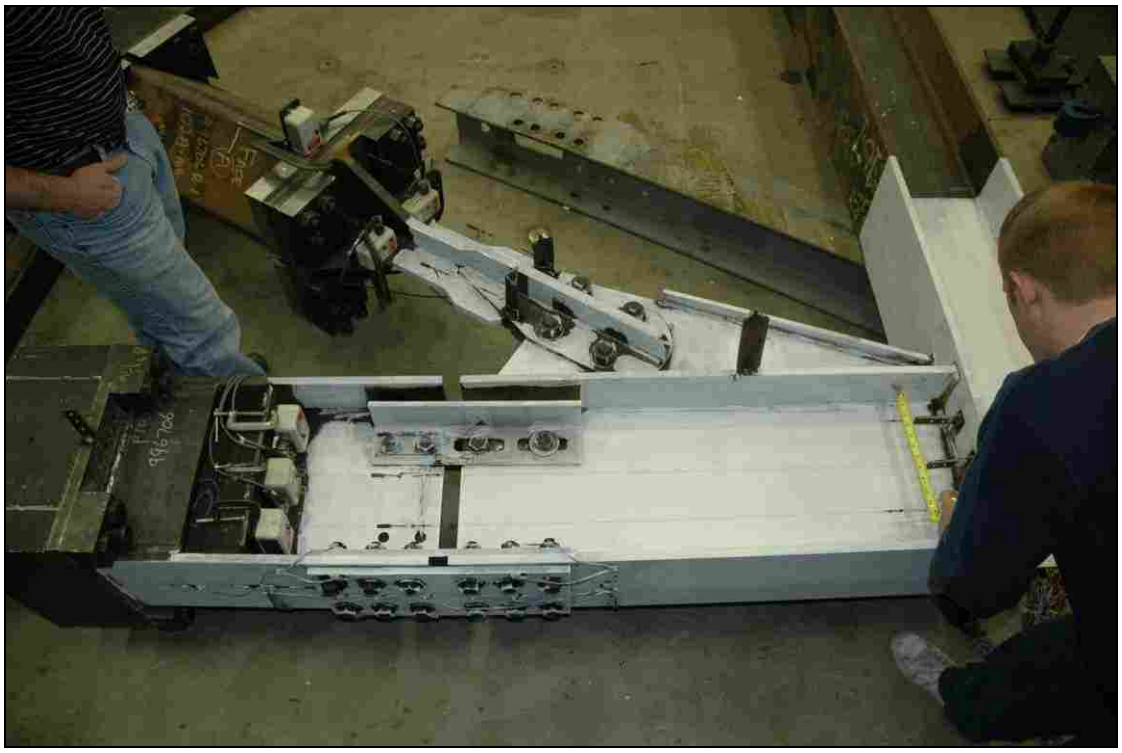

Figure 2-23 Specimen 2 – Instrumentation (Top View)

3 Test Data

The test data consisted of visual observations and recorded data for the two test specimens and are reported in this chapter.

3.1 Test Specimen 1

Testing of the cyclic loading protocol for specimen 1 was performed on December 20, 2006. An additional fatigue test of large displacement cycles was attempted on January 10, 2007.

3.1.1 Observed Performance

The testing began with the test specimen in its non-displaced condition: the gap angle was zero and the gap size was equal to the design width of 1-1/2 in. (see Figure 3-1). The six elastic cycles, which corresponded to the estimated BRB elastic limit, neither noticeably affected the gap size nor appeared to yield the splice plates. The other components of the connection appeared unchanged as well.

Once past the elastic cycles, loud popping sounds were heard consistently throughout the remainder of the testing and were determined to be the result of bolt slippage. Slippage appeared to occur at roughly the same displacement in both half cycles when the opposing actuator force was between 100 and 150 kips. At one point

during the test, the vibrations caused by the slippage were strong enough to knock off the industrial magnets holding sting pot ends. Clamps were used to fasten the magnets more securely.

As testing progressed, the gap opened more on the positive displacements and closed more on the negative displacements. At the target maximum displacement, the gap opening was approximately 3-1/8 in (see Figure 3-2a). At the target minimum displacement, the gap closed completely (see Figure 3-2b). The duration of the gap closure was minimal and did not occur exactly at the point of maximum displacement; instead, it occurred as the displacement began its reversal. One possible reason for such discrepancy was the rapid decrease in the opposing force specified for Actuator 1.

Upon completion of the testing, the specimen components were visually examined. The plates did not experience any significant fatigue, though yielding did appear to have occurred.

In order to test the fatigue limit of the connection, additional loading was applied with the objective to follow the protocol for the maximum displacement cycle. However, before the first fatigue cycle could be completed, a problem in the loading occurred which caused the test to be aborted; due to an equipment command error, the Actuator 1 deviated from the desired force objectives, and forces greater than the test setup could withstand were applied. The results were (1) a tension failure of the bolts connecting the beam stub to Actuator 2 and (2) significant deformation of the splice plates and BRB core extension assembly (see Figures 3-3 through 3-6).

3.1.2 Recorded Response

Actuators

Graphs of the displacement versus force (i.e. the hysteresis action) for Actuators 1 and 2 are shown in Figures 3-7 and 3-8, respectively. Since the pulling force of Actuator 1 was recorded as a negative force even though it corresponds to brace tension, which is usually given as a positive value, the y-axis in Figure 3-7 is reversed to allow for easier comparison with a typical BRB hysteresis.

Strain Gages

Figures 3-9 through 3-13 show the maximum and minimum strains experienced by the strain gages on the plates and BRB core extension assembly at each displacement magnitude. The strains on the outer plates are shown in Figures 3-9 and 3-10. The strains on the inner plates are shown in Figures 3-11 and 3-12. The strains on the BRB core extension assembly are shown in Figure 3-13.

Rosettes

The maximum and minimum shear stresses at each displacement magnitude are shown in Figure 3-14 for the splice plates and in Figure 3-15 for the gusset plate.

String Pots

The string pots on the beam web were used to estimate the gap rotation during testing, and estimation methodology is found in Appendix H. The gap rotation angle is graphed versus Actuator 1 force in Figure 3-16 and Actuator 2 force in Figure 3-17.

3.2 Test Specimen 2

Testing of specimen 2 was conducted on February 2, 2007. Both the cyclic protocol and fatigue protocol were performed in succession.

3.2.1 Observed Performance

Testing began with the test specimen in a non-displaced condition: the gap angle was zero and the gap size was equal to the design width of 1-1/2 in. (see Figure 3-18). The twelve elastic cycles, which corresponded to 30% (3 cycles), 50% (3 cycles), and 100% (6 cycles) of the estimated BRB elastic limit, did not noticeably affect the gap size or splice plates; the other components of the connection appeared unchanged as well.

Starting around 1% drift, bolt slippage was observed and popping sounds were heard consistently. As in Test 1, the sounds occurred during both half-cycles when the opposing actuator force was between 100 and 150 kips.

Starting at 2% drift, flaking of the whitewash in the inner splice plates indicated yielding of the plates (see Figure 3-19). Flaking (and corresponding yielding) continued during the following drift cycles, and by the 4% drift cycle (see Figure 3-20), major flaking was observed. Although yielding was not yet visually observed in the outer plate, considerable deformation of both plates was clearly seen, especially at positive drift extrema (see Figure 3-21).

With each successive cycle, gap opening increased in magnitude during positive displacements and decreased during negative displacements; this is opposite of what occurred in Test 1. At the maximum displacement of the largest cycle, the gap opened to 3-1/2 in (see Figure 3-22a). At the minimum displacement of the largest cycle, the gap

closed completely (see Figure 3-22b). The duration of the gap closure was minimal and did not appear to affect the response of the specimen.

Upon completion of two maximum displacement cycles, the specimen components were visually examined, and no undesirable failure modes were observed (see Figure 3-23). The splice plates did yield considerably but did not appear to experience critical fatigue levels. The outer plate performed well, and on the exposed side only minor yielding was visible (see Figure 3-24). Yielding did appear to have occurred on the underside of some of the plates as evidenced by rust flakes below the specimen, though it was difficult to determine which plate(s) the flakes were associated with. Yielding was also visible on the BRB core extension assembly (see Figure 3-25).

In order to further fatigue the connection, additional maximum displacement cycles were applied; thirteen cycles were performed before a failure occurred in the base plate and bolts attaching the beam stub to Actuator 2 (see Figure 3-26); this was very similar to the test 1 failure, though in the test 2 failure, it was due to cyclic fatigue and was stopped before it caused a significant deformation of the splice plates and BRB core extension assembly.

Following the testing, the specimen components were again visually examined and fracture lines were discovered on the reduced cross-section area of the BRB core extension assembly (see Figure 3-27). Based on the width and propagation length of the facture lines, it appeared that they began during one of the additional maximum displacement cycles and propagated during following cycles until they reached their final condition. Most likely, these fractures were not a result of events associated with the base plate failure.

3.2.2 Recorded Response

Actuators

Graphs of the displacement versus force (i.e. the hysteresis action) for Actuators 1 and 2 are shown in Figures 3-28 and 3-29, respectively. Since the pulling force of Actuator 1 was recorded as a negative force even though it corresponds to brace tension, which is usually given as a positive value, the y-axis in Figure 3-6 is reversed to allow for easier comparison with a typical BRB hysteresis.

Strain Gages

Figures 3-30 through 3-32 show the maximum and minimum strains experienced by the strain gages on the plates and BRB core extension assembly at each displacement extrema. The strains on the outer plate are shown in Figure 3-30. The strains on the inner plates are shown in Figure 3-31. The strains on the BRB core extension assembly are shown in Figure 3-32.

Rosettes

The shear stresses on the gusset plate at each displacement extrema are shown in Figure 3-33.

String Pots

The string pots on the beam web were used to estimate the gap rotation during testing, and estimation methodology is found in Appendix H. The gap rotation angle is graphed versus Actuator 1 force in Figure 3-34 and Actuator 2 force in Figure 3-35.

Figure 3-1 Specimen 1 – Initial Condition

(a) Maximum Negative Drift **(b) Maximum Positive Drift**

Figure 3-2 Specimen 1 – Gap Opening and Closure at Maximum Drifts (6.5% Drift)

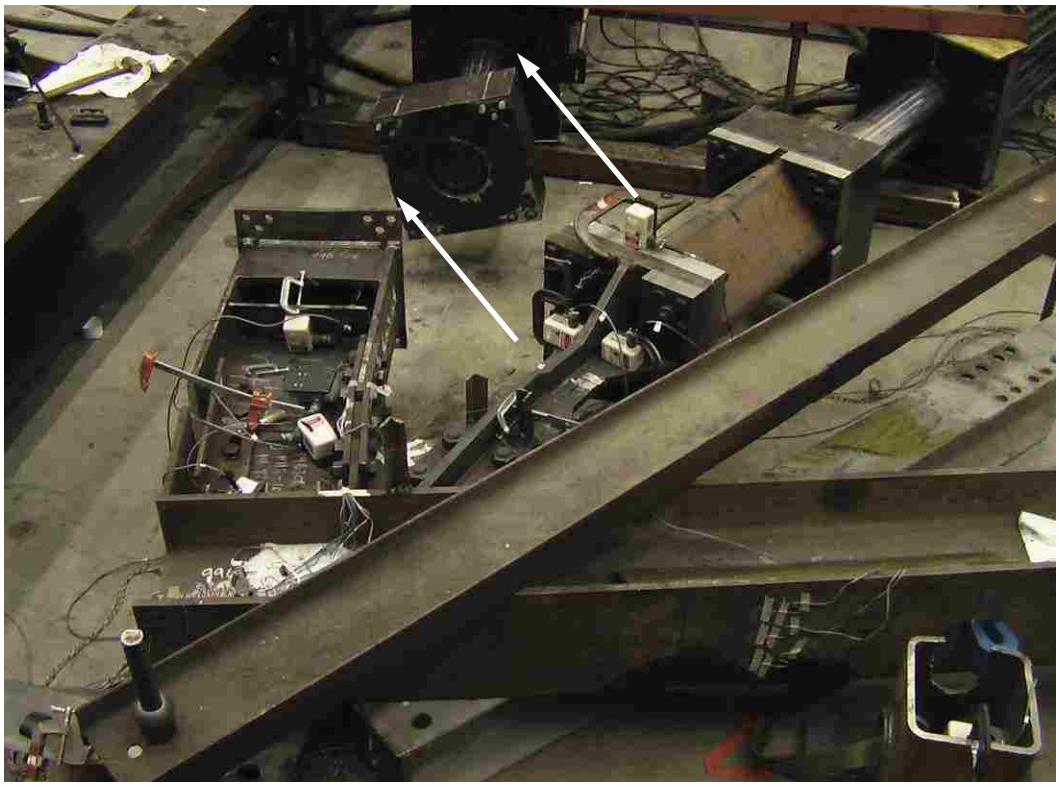

Figure 3-3 Specimen 1 –Bolt Failure at Boundary Plate

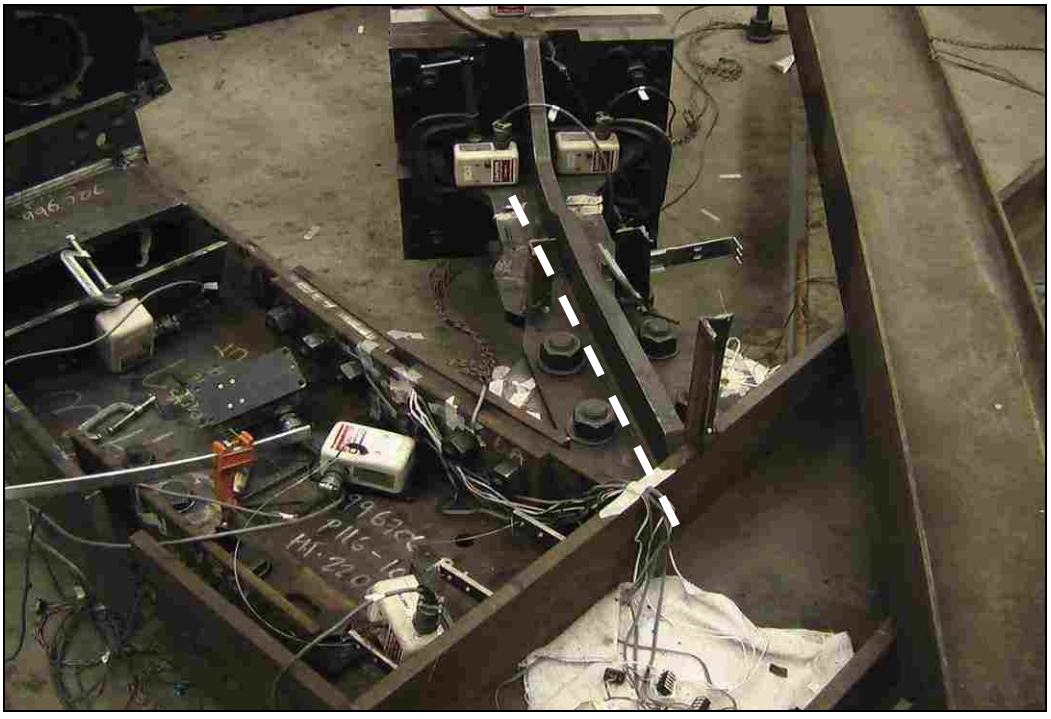

Figure 3-4 Specimen 1 – Connection Deformation Following Boundary Failure

Figure 3-5 Specimen 1 – Core Extension Deformation Following Boundary Failure

Figure 3-6 Specimen 1 – Splice Plate Deformation Following Boundary Failure

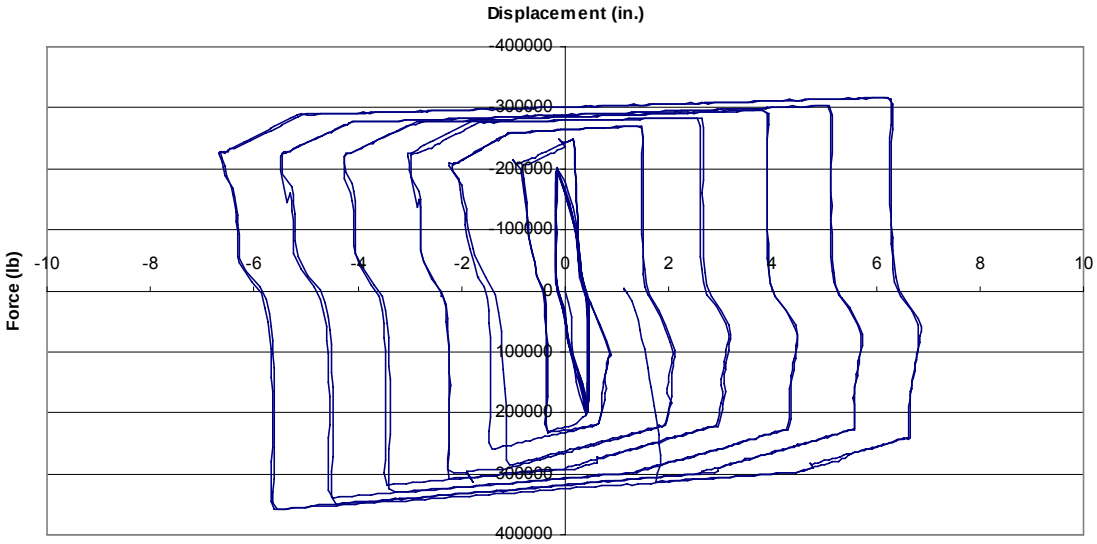

Figure 3-7 Specimen 1 – Actuator 1 Hysteresis Action

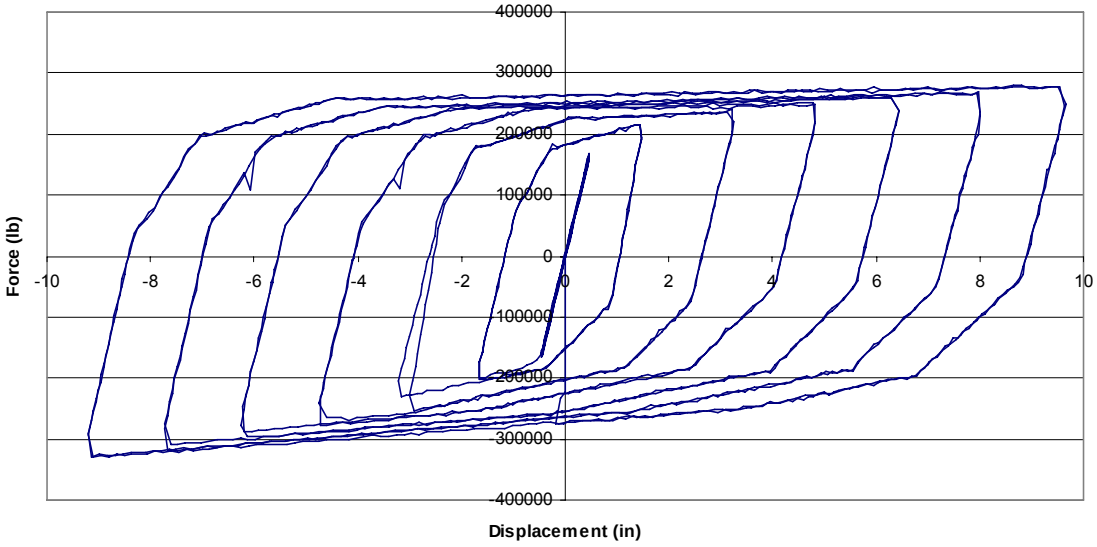

Figure 3-8 Specimen 1 – Actuator 2 Hysteresis Action

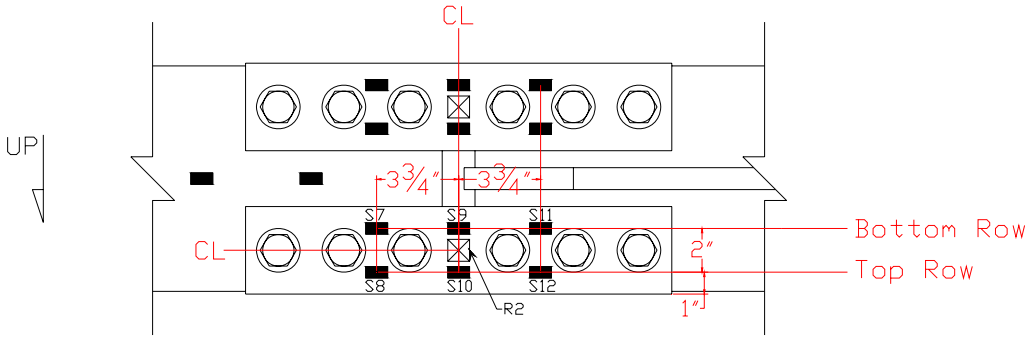

(a) Strain Gage Locations

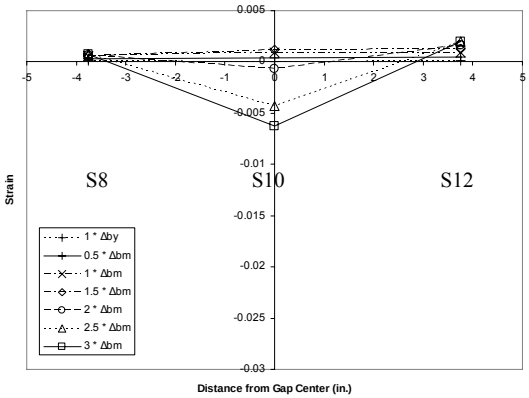

(b) Top Row under Negative Drift

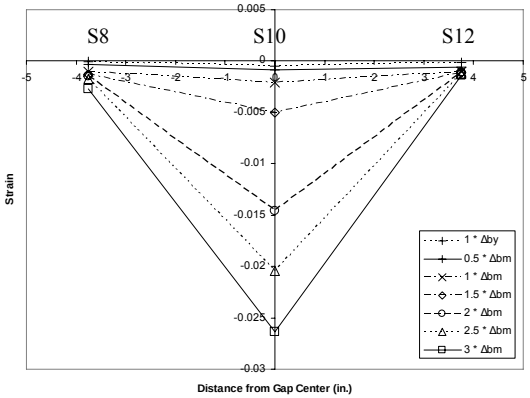

(c) Top Row under Positive Drift

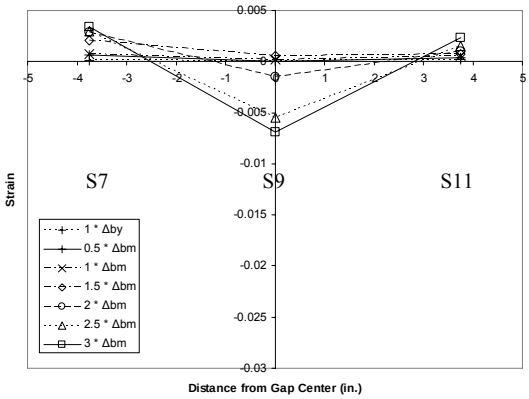

(d) Bottom Row under Negative Drift

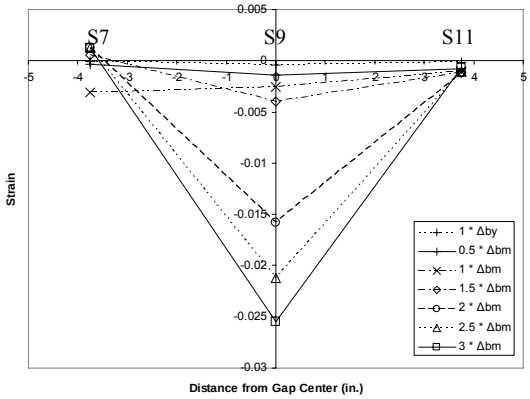

(e) Bottom Row under Positive Drift

Figure 3-9 Specimen 1 – Strain Gage Profiles of Outer Plate 1

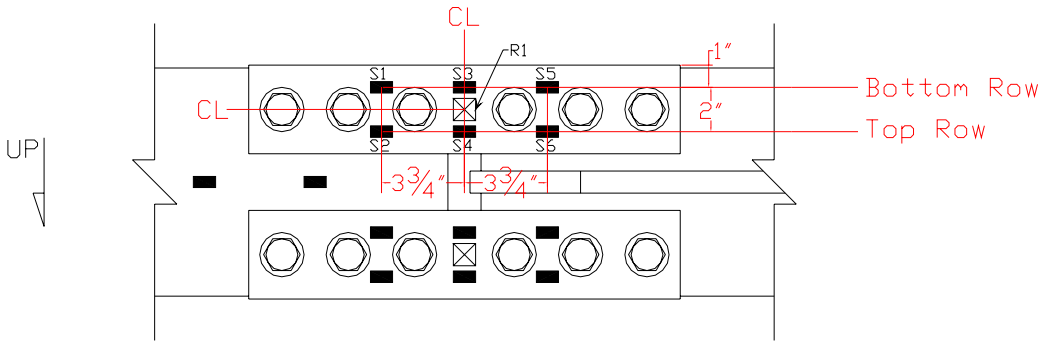

(a) Strain Gage Locations

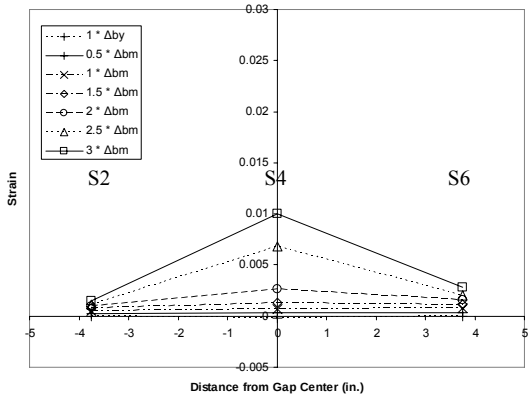

(b) Top Row under Negative Drift

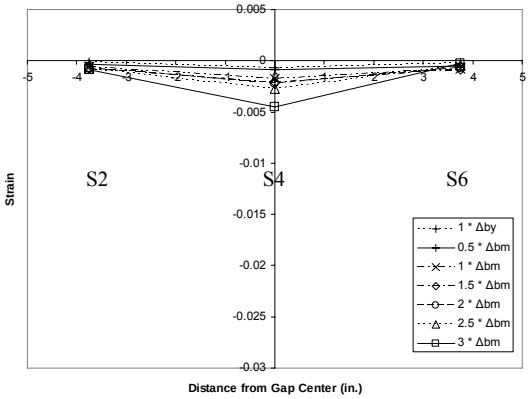

(c) Top Row under Positive Drift

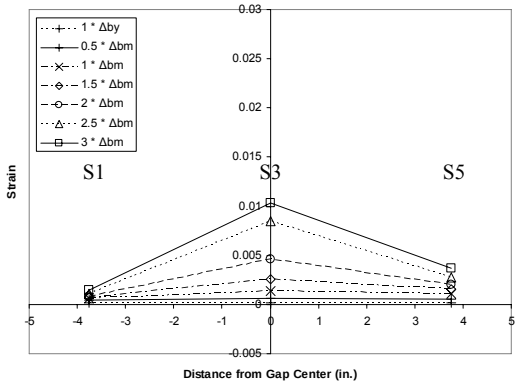

(d) Bottom Row under Negative Drift

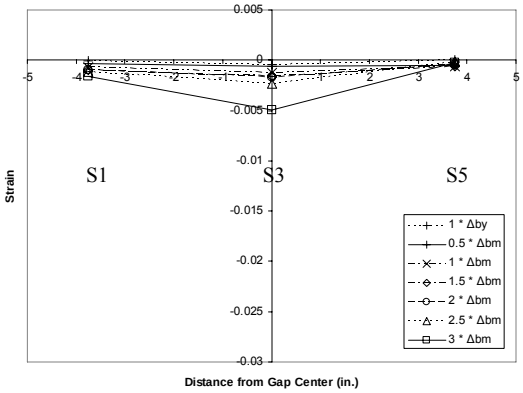

(e) Bottom Row under Positive Drift

Figure 3-10 Specimen 1 – Strain Gage Profiles of Outer Plate 2

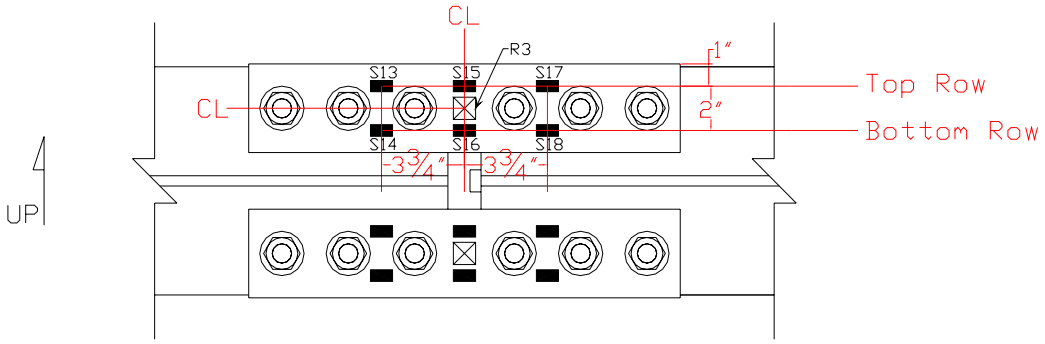

(a) Strain Gage Locations

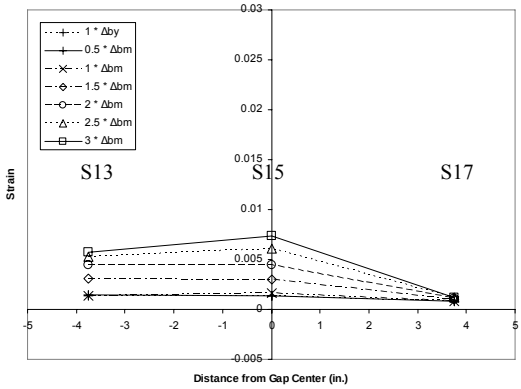

(b) Top Row under Negative Drift

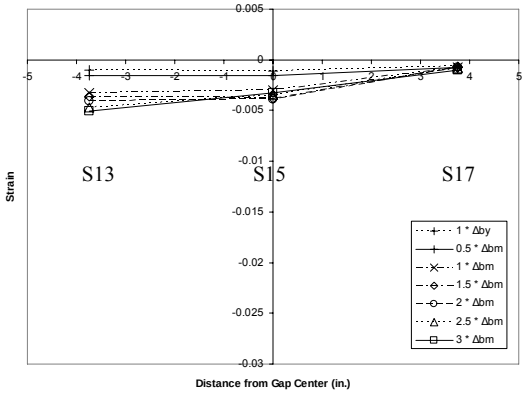

(c) Top Row under Positive Drift

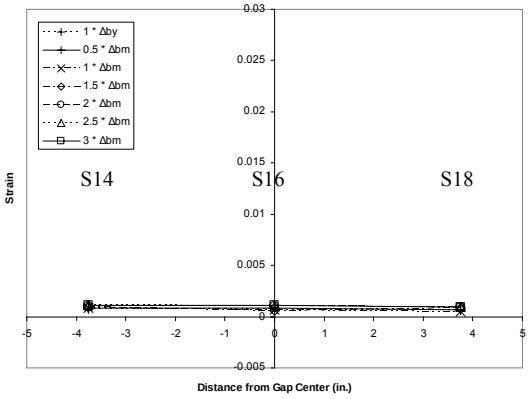

(d) Bottom Row under Negative Drift

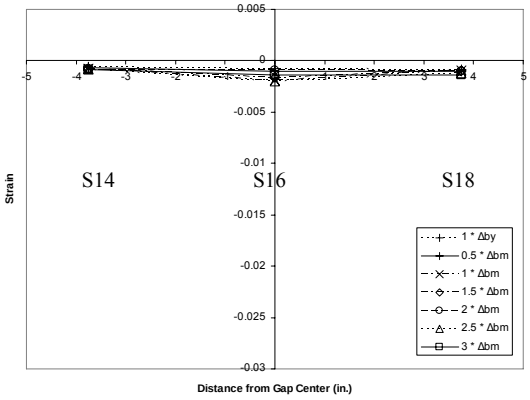

(e) Bottom Row under Positive Drift

Figure 3-11 Specimen 1 – Strain Gage Profiles of Inner Plate 1

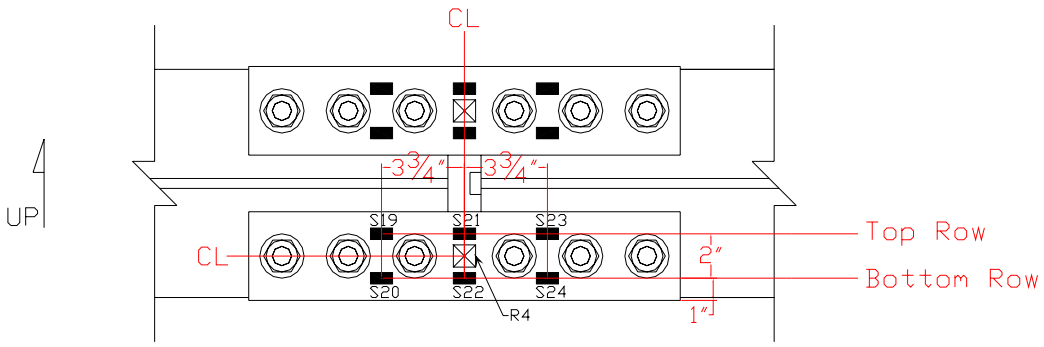

(a) Strain Gage Locations

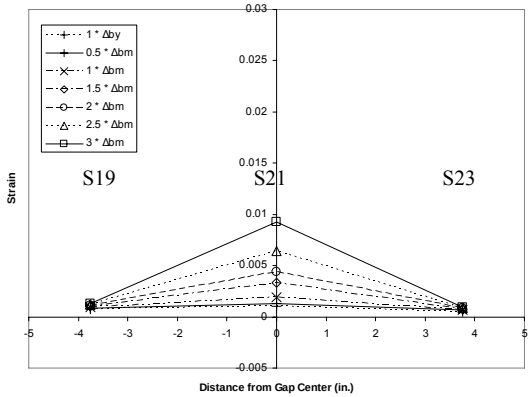

(b) Top Row under Negative Drift

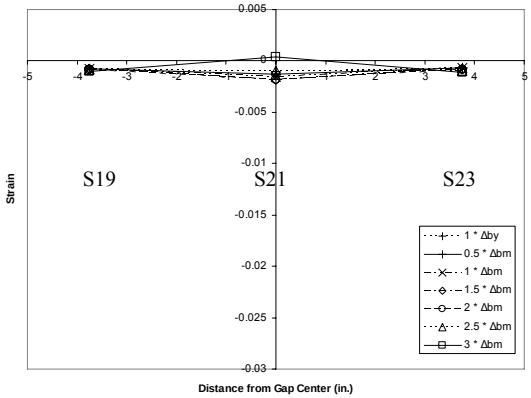

(c) Top Row under Positive Drift

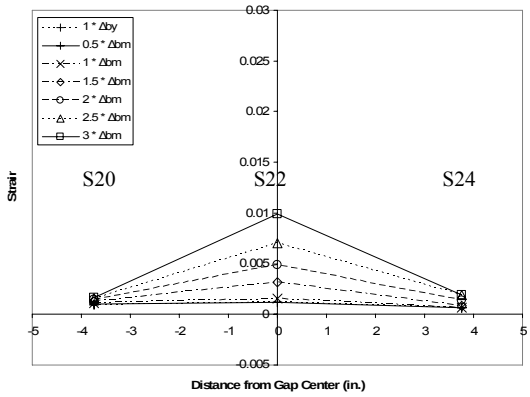

(d) Bottom Row under Negative Drift

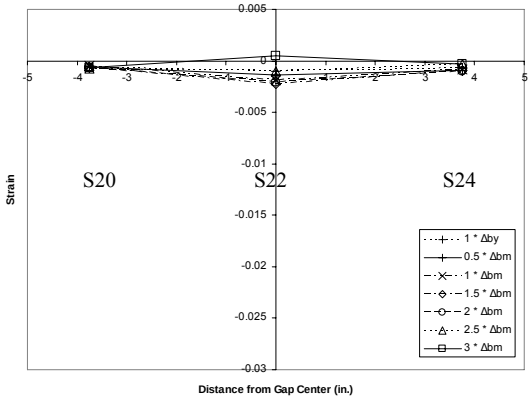

(e) Bottom Row under Positive Drift

Figure 3-12 Specimen 1 – Strain Gage Profiles of Inner Plate 2

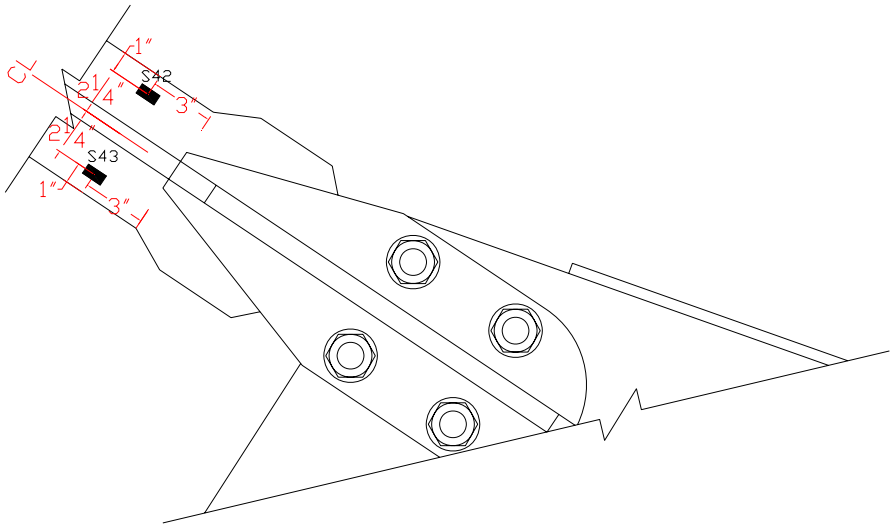

(a) Strain Gage Locations

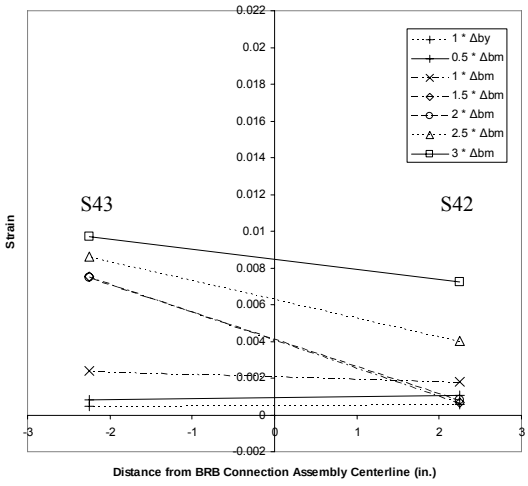

(b) Negative Drift

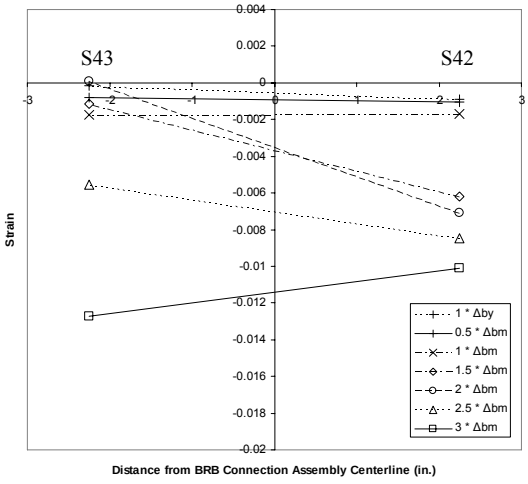

(c) Positive Drift

Figure 3-13 Specimen 1 – Strain Gage Profiles of BRB Core Extension Assembly

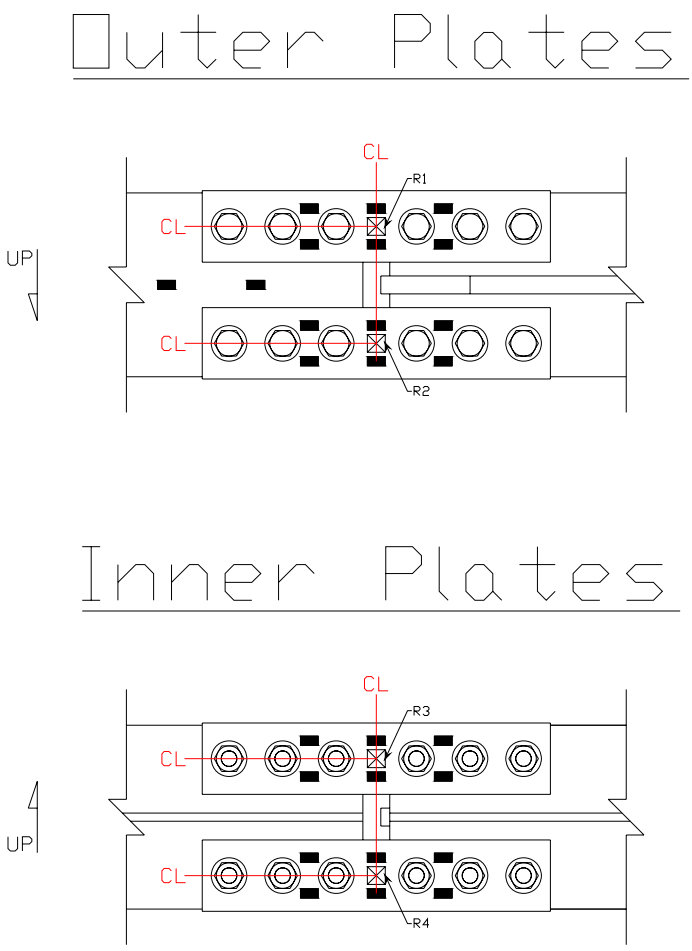

(a) Rosette Locations

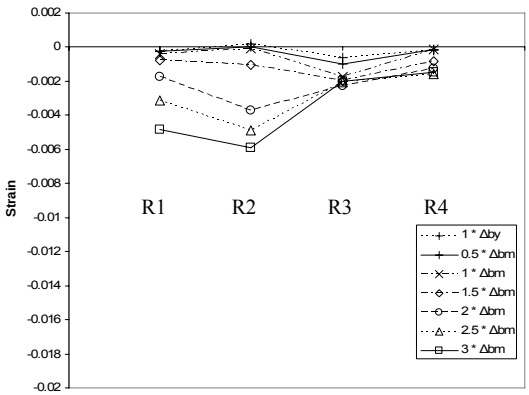

(b) Negative Drift

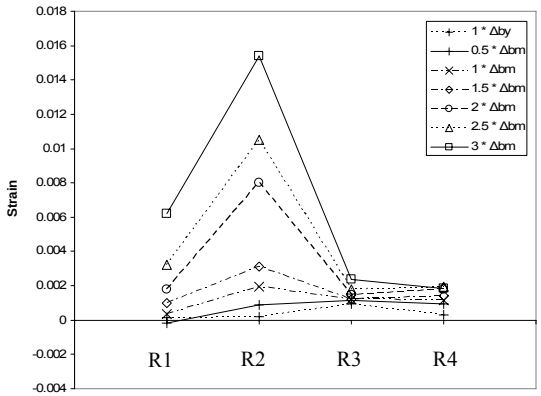

(c) Positive Drift

Figure 3-14 Specimen 1 – Rosette Profiles of Splice Plates

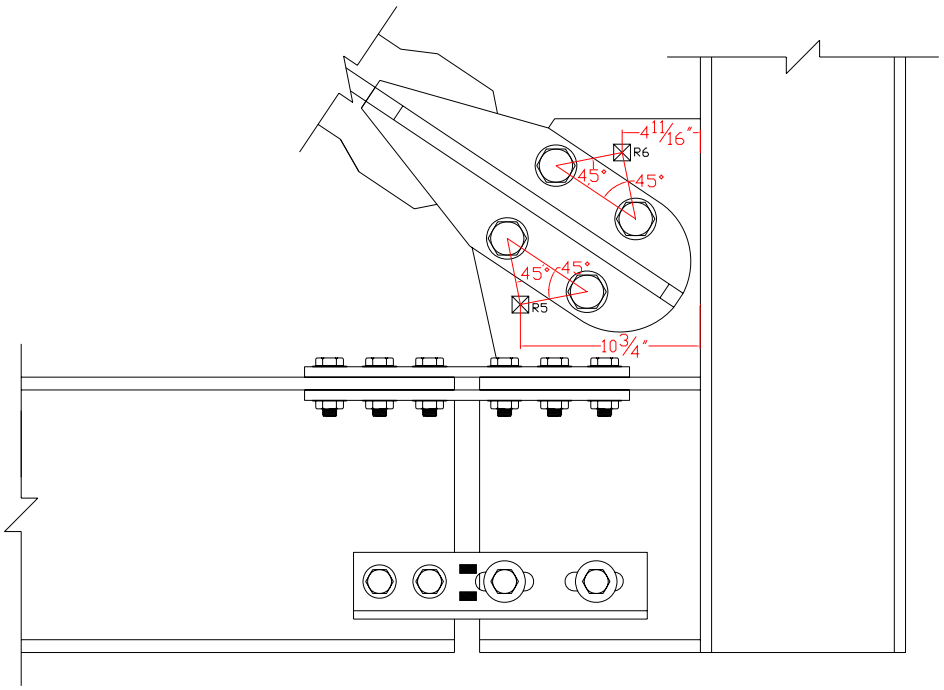

(a) Rosette Locations

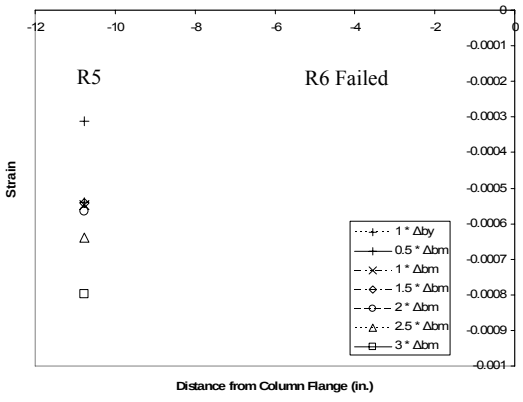

(b) Negative Drift

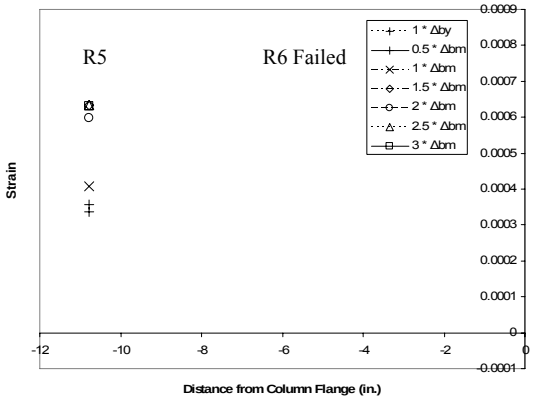

(c) Positive Drift

Figure 3-15 Specimen 1 – Rosette Profiles of Gusset Plate

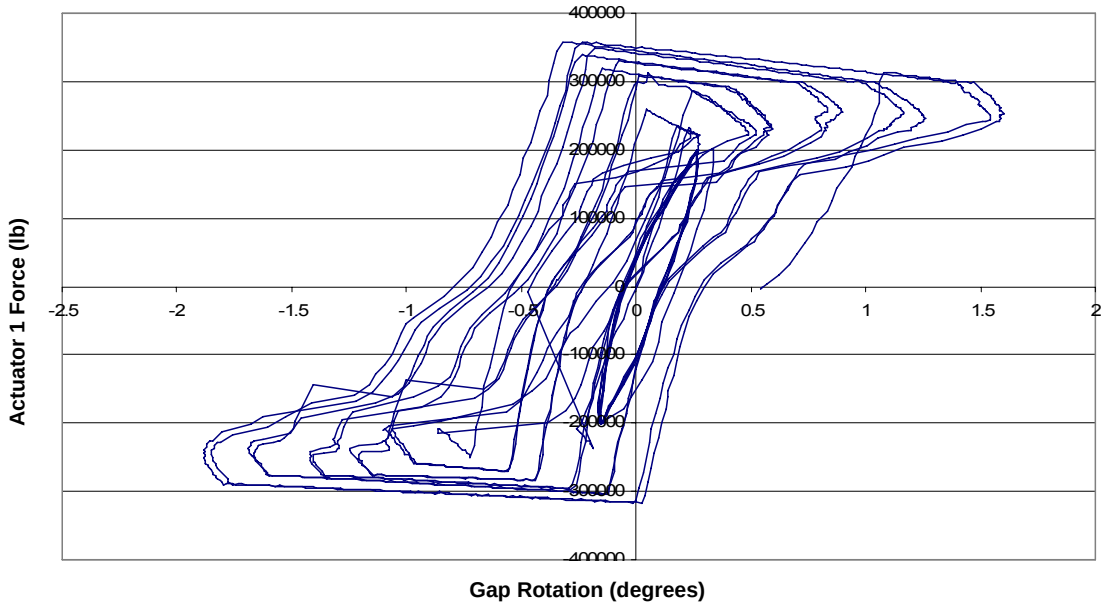

Figure 3-16 Specimen 1 – Estimated Gap Rotation versus Actuator 1 Force

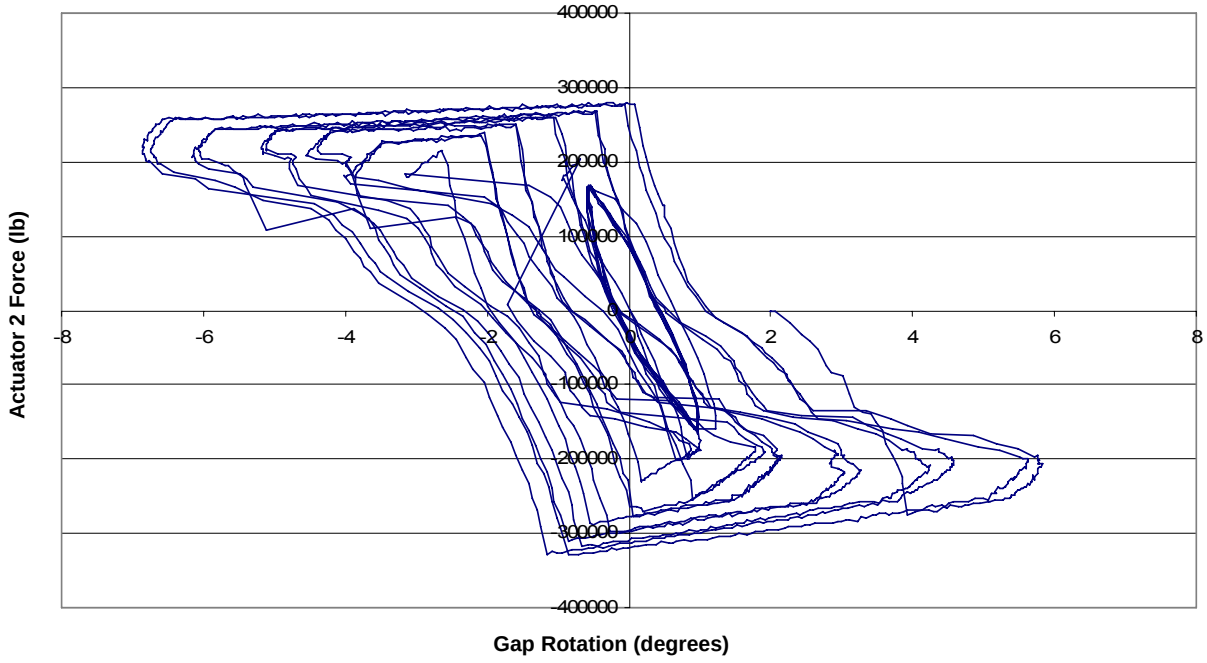

Figure 3-17 Specimen 1 – Estimated Gap Rotation versus Actuator 2 Force

Figure 3-18 Specimen 2 – Initial Condition

Figure 3-19 Specimen 2 – Initial Yielding of Splice Plate (2% Drift)

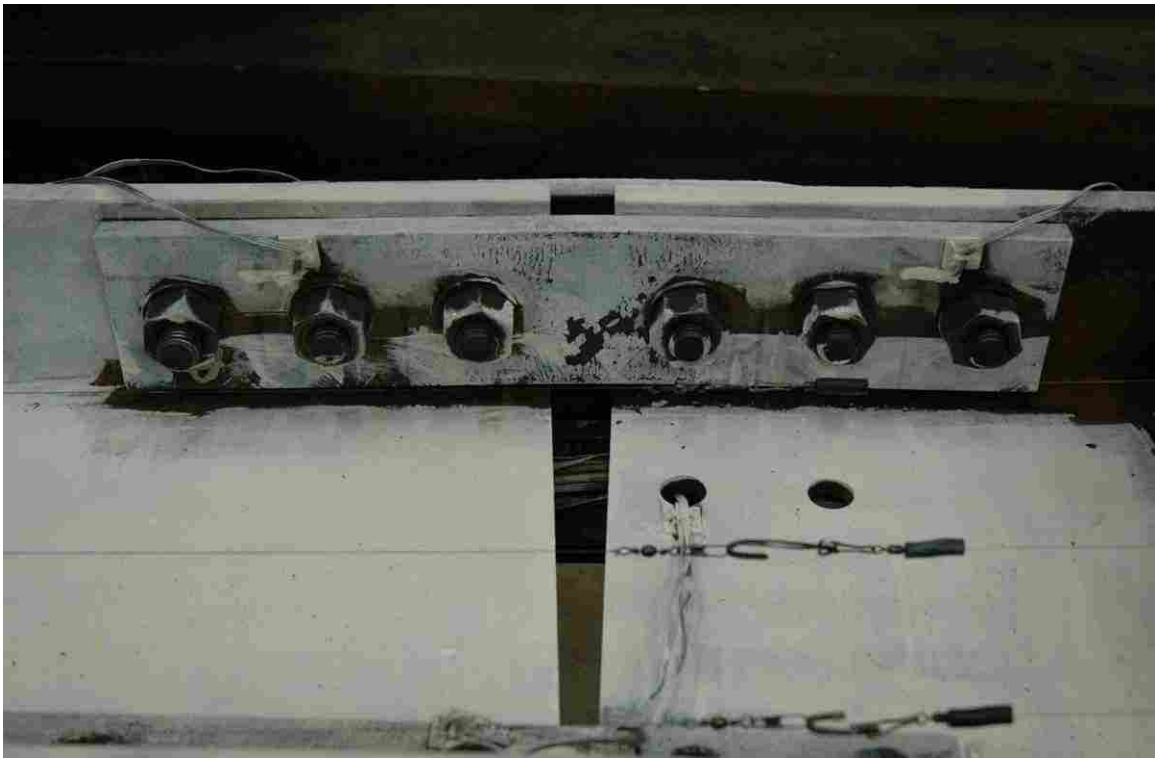

Figure 3-20 Specimen 2 – Significant Yielding of Inner Splice Plate (4% Drift)

Figure 3-21 Specimen 2 – Deformation of Splice Plates (4% Drift)

(a) Maximum Negative Drift

(b) Maximum Positive Drift

Figure 3-22 Specimen 2 – Gap Opening and Closure at Maximum Drifts (6.5% Drift)

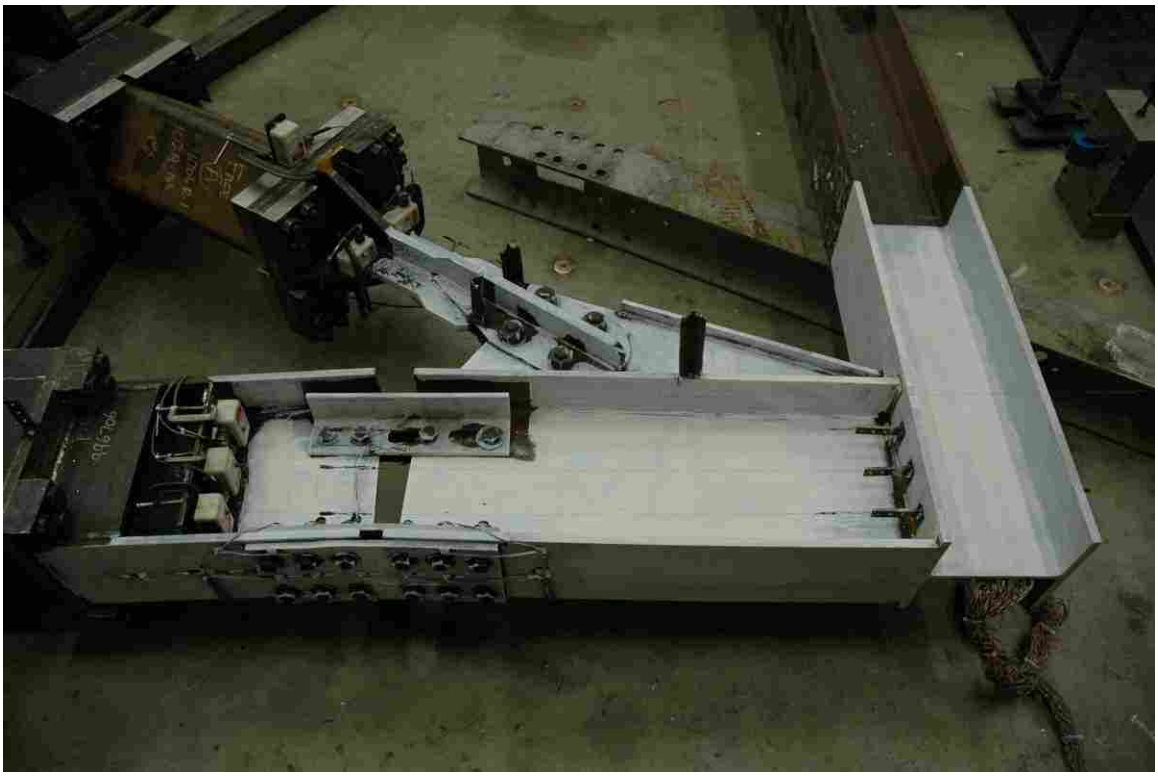

Figure 3-23 Specimen 2 – No Undesirable Failure Modes in Specimen (6.5% Drift)

Figure 3-24 Specimen 2 – Minor Yielding of Outer Splice Plate (6.5% Drift)

Figure 3-25 Specimen 2 –Yielding of BRB Core Extension Assembly (6.5% Drift)

Figure 3-26 Specimen 2 – Boundary Plate Failure

Figure 3-27 Specimen 2 – BRB Core Extension Fracture (6.5% Drift Fatigue Cycles)

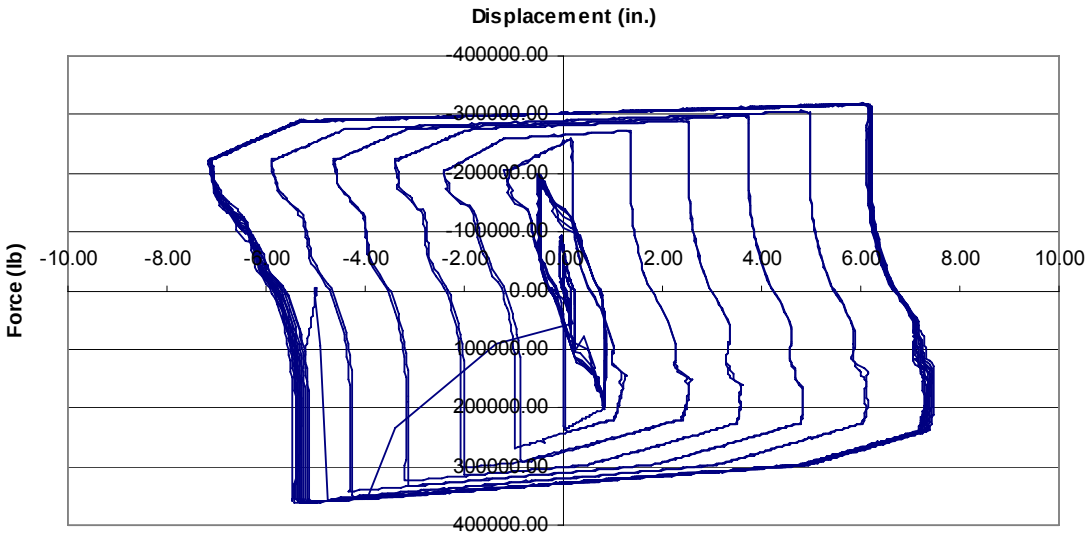

Figure 3-28 Specimen 2 – Actuator 1 Hysteresis Action

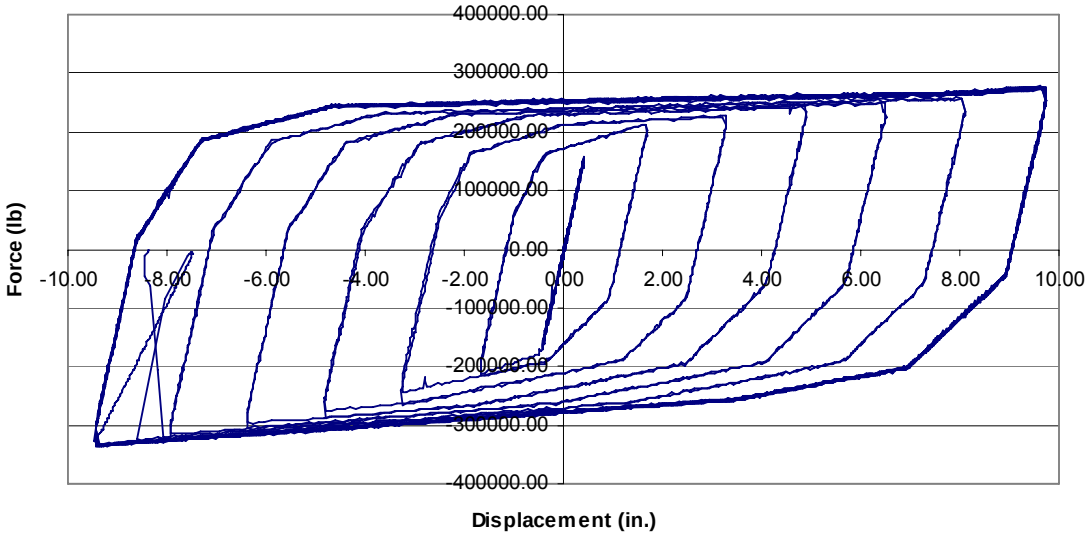

Figure 3-29 Specimen 2 – Actuator 2 Hysteresis Action

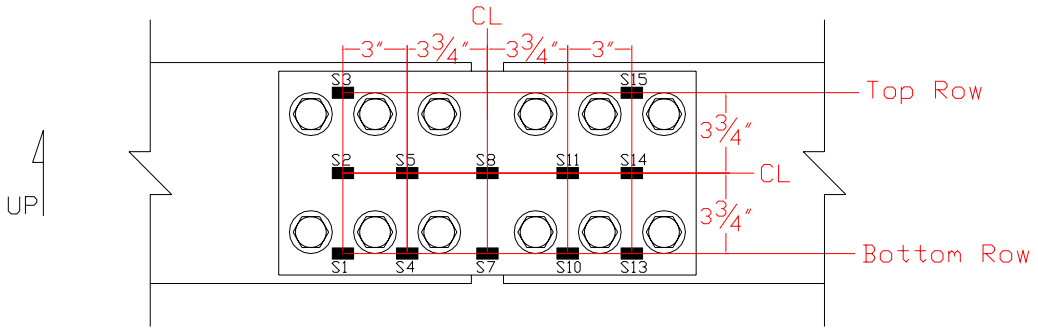

(a) Strain Gage Locations

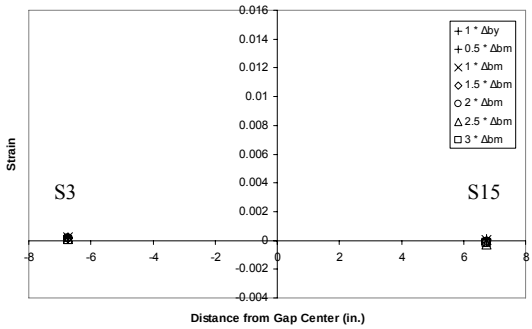

(b) Top Row under Negative Drift

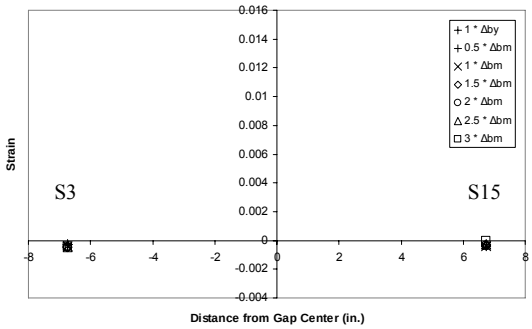

(c) Top Row under Positive Drift

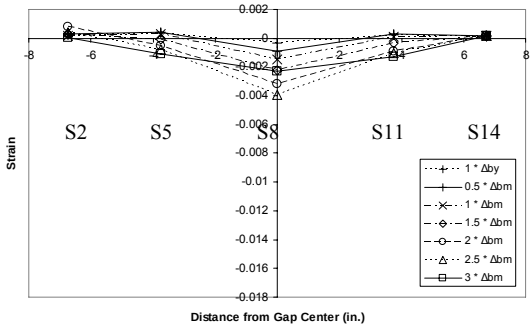

(d) Middle Row under Negative Drift

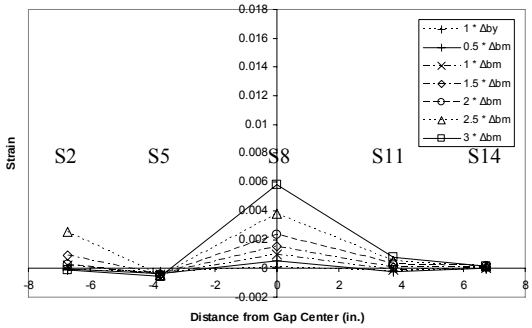

(e) Middle Row under Positive Drift

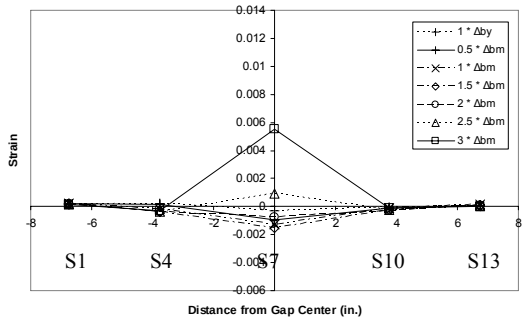

(f) Bottom Row under Negative Drift

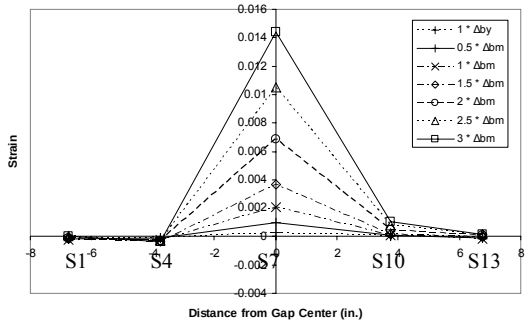

(g) Bottom Row under Positive Drift

Figure 3-30 Specimen 2 – Strain Gage Profiles of Outer Plate

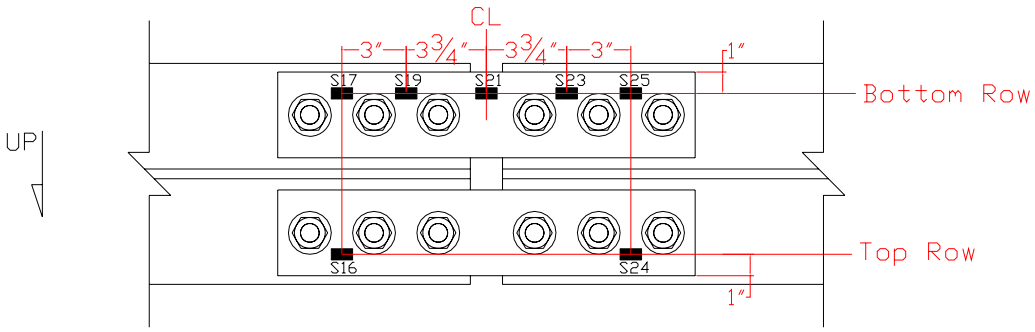

(a) Strain Gage Locations

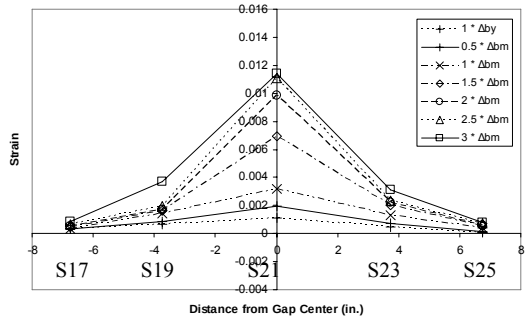

(b) Bottom Row under Negative Drift

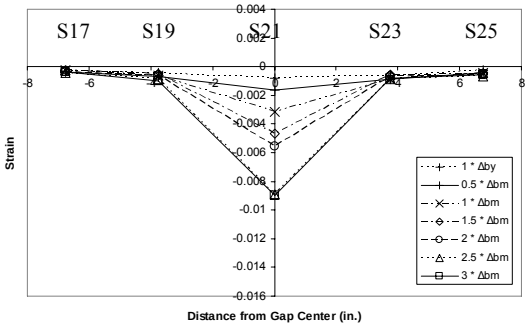

(c) Bottom Row under Positive Drift

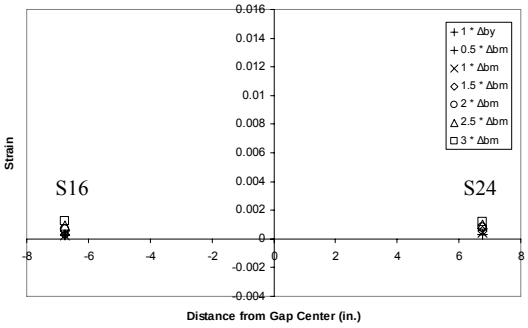

(d) Top Row under Negative Drift

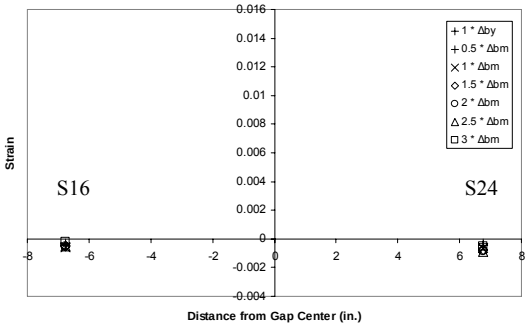

(e) Top Row under Positive Drift

Figure 3-31 Specimen 2 – Strain Gage Profiles of Inner Plates

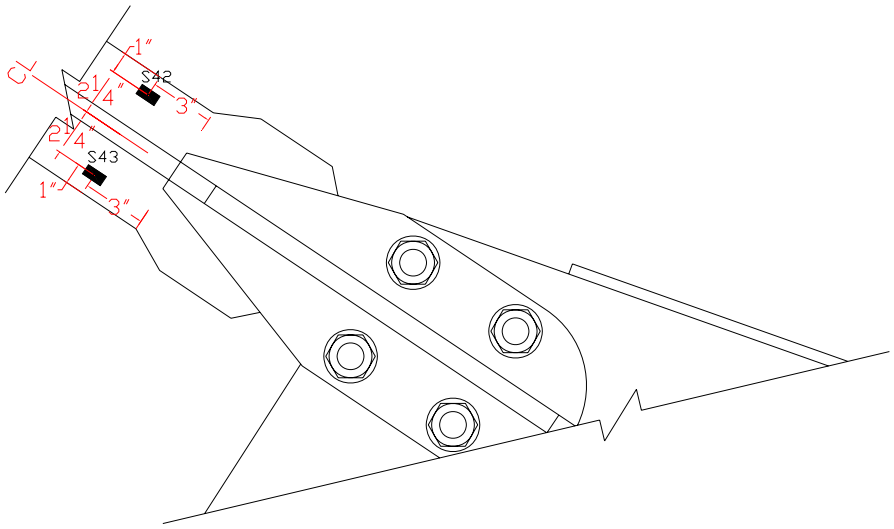

(a) Strain Gage Locations

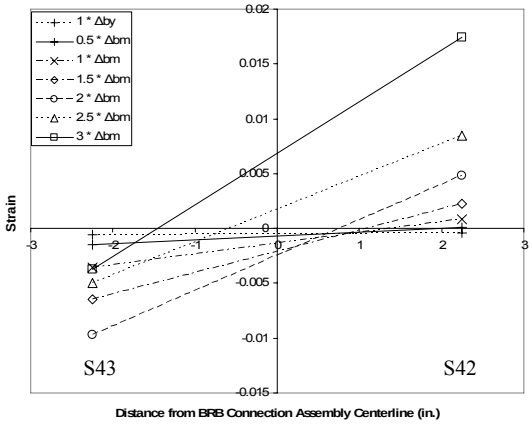

(b) Negative Drift

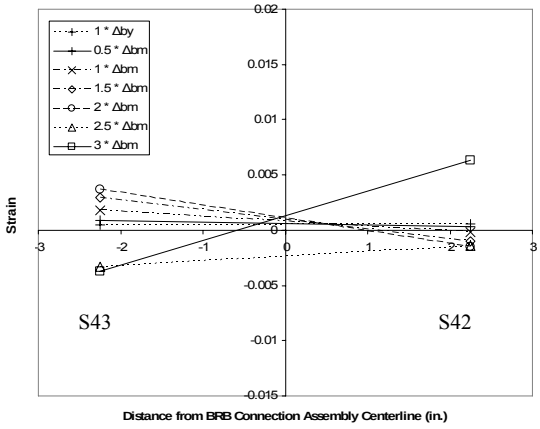

(c) Positive Drift

Figure 3-32 Specimen 2 – Strain Gage Profiles of BRB Core Extension Assembly

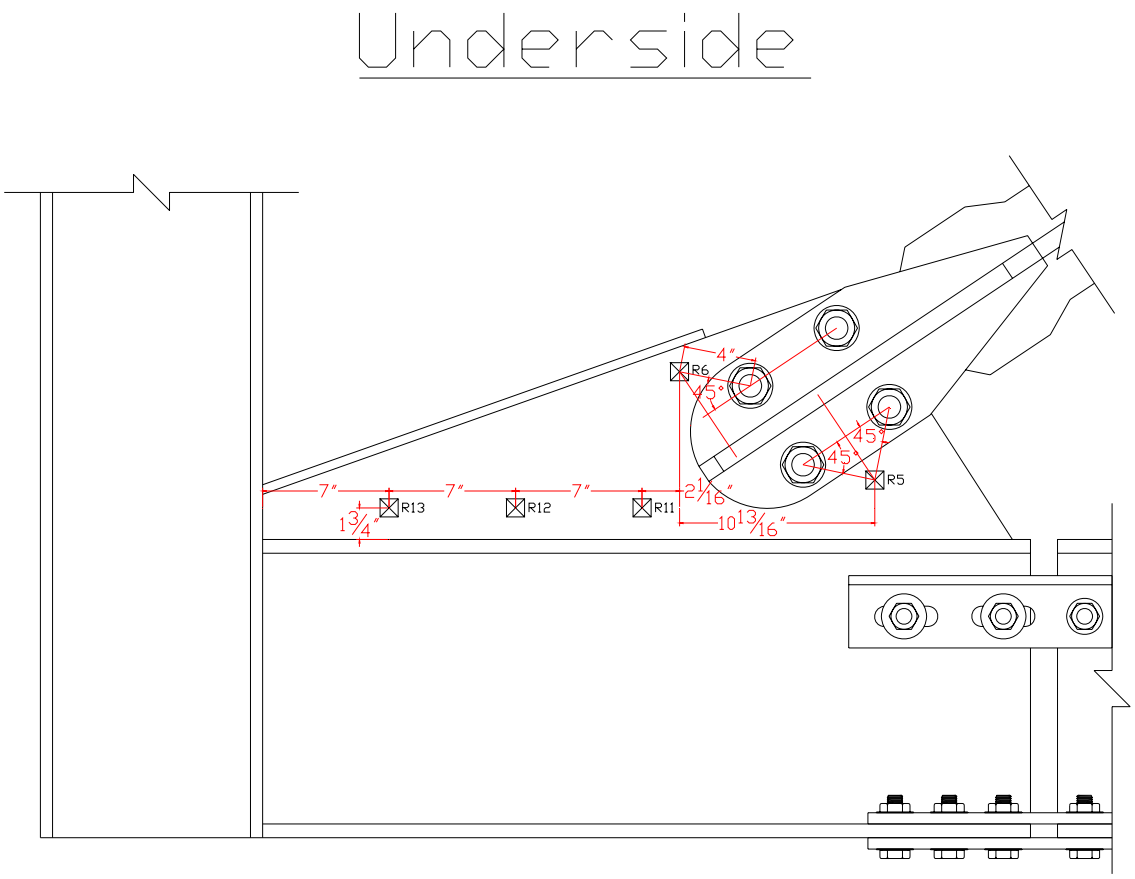

(a) Rosette Locations

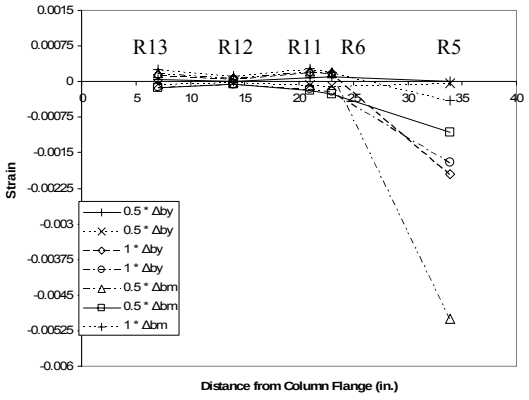

(b) Negative Drift

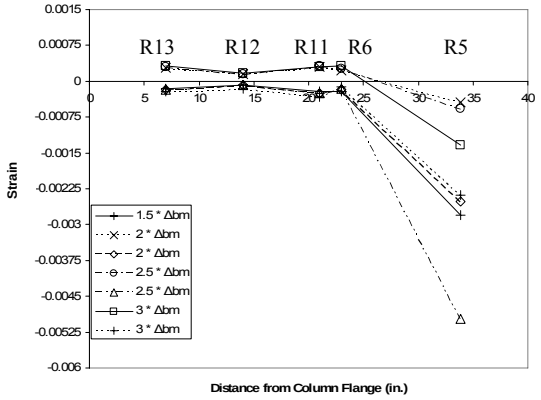

(c) Positive Drift

Figure 3-33 Specimen 2 – Rosette Profiles of Gusset Plate

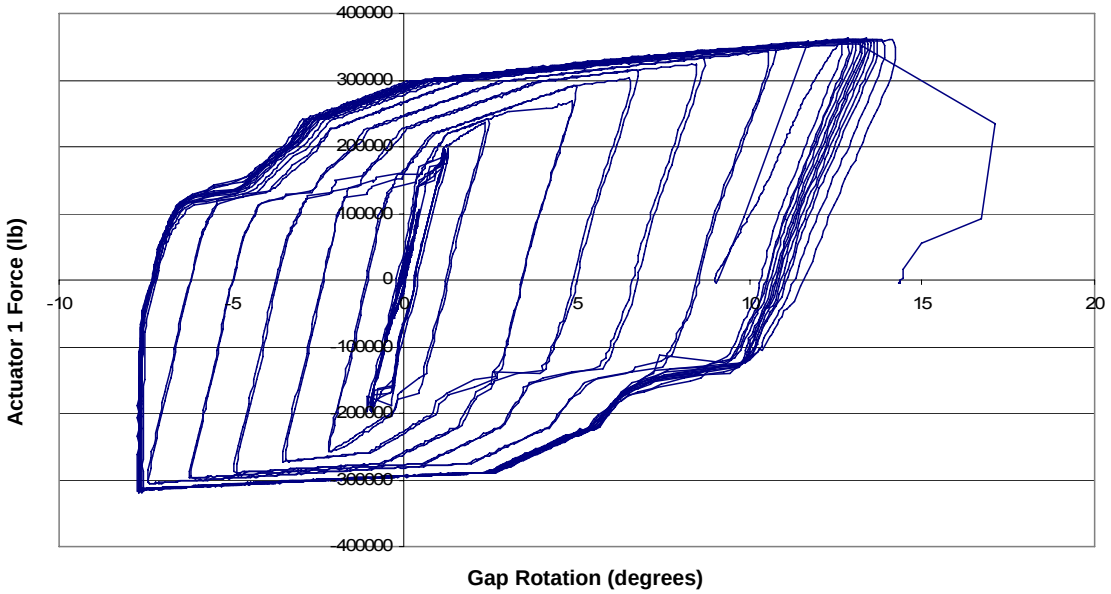

Figure 3-34 Specimen 2 – Estimated Gap Rotation versus Actuator 1 Force

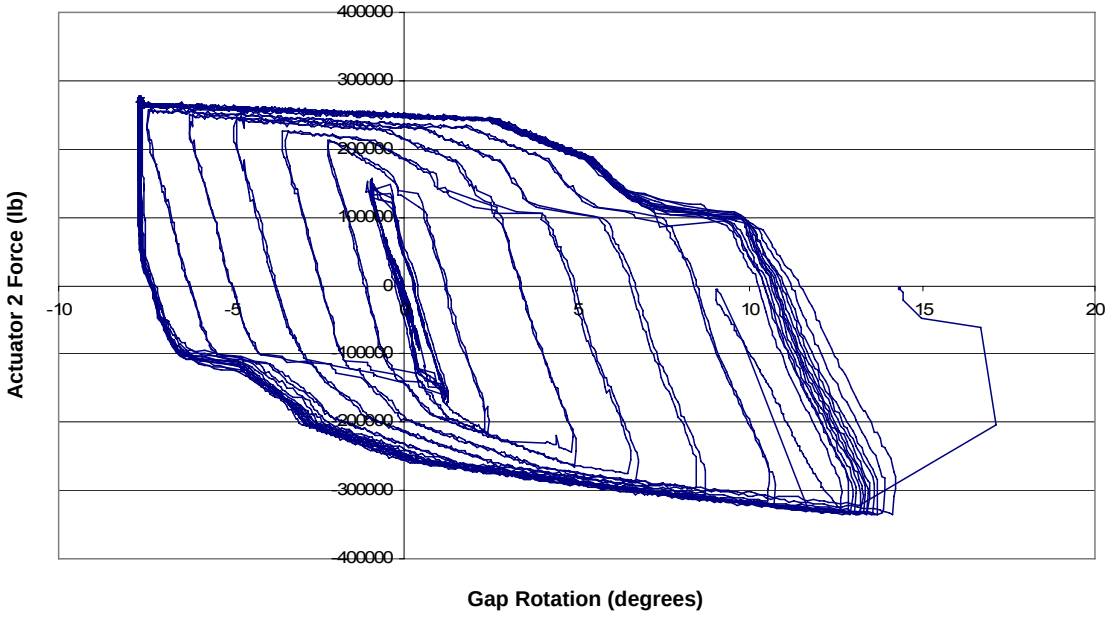

Figure 3-35 Specimen 2 – Estimated Gap Rotation versus Actuator 2 Displacement

4 Discussion of Results

In this chapter, the results reported in Chapter 3 are discussed along with relevant implications. The results of interest are the opening and closing of the connection gap, the magnitudes of the inter-story drifts, the deformation of the splice plates, the shear strain in the gusset plates, the hinging of the BRB core extension assembly, and the avoidance of undesirable failure modes.

4.1 Gap Response

The gaps between beam sections closed completely in both tests but not until the largest applied displacement cycles (see Figures 3-2b and 3-22b). Such a result supports the conclusion that the gap design calculation methodology, which assumes an instantaneous gap closure on the maximum applied displacement, may be accurate. It logically follows that the assumptions of the methodology may be accurate.

One key assumption of the gap design methodology was that all the prototype bay members except the splice plates and brace core extension assembly experience insignificant flexural deformation compared to axial deformation (see Appendix B.6). If this assumption is accurate, then the undesirable buckling failure modes of connection components are unlikely to occur. Observations of the specimens both during and after testing (i.e. minimal flaking of white wash in beams, columns, and gusset plates) support

the assumption that flexural bending was insignificant in all members except the splice plates and brace core extension assembly (see beams, columns, and gusset plates in Figure 3-4 for Specimen 1 and Figure 3-23 for Specimen 2).

4.2 Inter-Story Drift Magnitudes

The maximum opening and closing of the connection gap corresponded to applied inter-story drifts of approximately ±6.5%. At these drift values, minimal damage was observed; the only fracturing occurred at the brace core extension assembly hinge point and the only yielding occurred in the splice plates and the brace core extension assembly (see Figure 3-2 for Specimen 1 and Figures 3-19 through 3-25 for Specimen 2). In other sub-assemblage tests, it was found that a typical buckling-restrained braced frame connection may begin to fail at inter-story drift values of approximately 2.5% (5, 6). Therefore, the proposed connection has a deformation capacity that is more than two and a half times greater than typically experienced by buckling-restrained braced frames. In addition, the drift values were reached without the same significant buckling and yielding failures experienced by the other frames in their beams, columns, and gusset plates (see Figure 3-23).

4.3 Plate Deformation

As expected, deformation was observed to be most pronounced in the portion of the splice plates that was bridging the gap between the beam sections (see Figure 3-6 for Specimen 1 and Figures 3-20 through 3-23 for Specimen 2); it is at this point that the plates must support the entire axial load. The data supported the observations: for nearly

all plates and at almost all drift values, the centermost gages experienced the greatest strains, which were typically two to four times larger than the strains in the other gages (see Figures 3-9 through 3-12 for Specimen 1 and Figures 3-30 through 3-31 for Specimen 2). For example, gage S22 of Specimen 1 experiences strains of approximately ±0.01 in/in under negative drift while the adjacent gages (i.e. S19 and S23) experience strains closer to 0.002 in/in (see Figure 3-12b).

The gage data also supported the observation that significant yielding occurred in the center of the plates. Most of the center gages experienced strains in excess of the typical steel yield strain of 0.002 in/in. In some instances, the strains were ten times larger than the typical steel yield strain; such was the case for the positive drift displacements in the outer plate of Specimen 1 that was closest to the topside of the specimen (see Figure 3-9). Additionally, in most instances yielding was only experienced by the portion of the plates within a few inches of the gap center, as indicated by the lower strains (less than 0.002 in/in) exhibited by the gages near the extremities of the splice plates.

In analyzing the general behavior of the splice plates, data indicates that for Specimen 1, the outer plates experienced as much if not more strain than the inner plates. This is not the preferred result but is considered to have occurred in part because all four plates had the same cross-sectional areas; yielding of the outer plates would be expected to decrease if the outer plates had been designed with a larger total cross-sectional area than the inner plates.

Another possible factor affecting the splice plate yielding was the relative proximity of either the inner plates or the outer plates to the brace actuator (i.e. Actuator

1). In the case of Specimen 1, the outer plates were closer to the brace actuator and experienced more yielding than expected. For Specimen 2, the inner plates were closer and experienced the majority of the yielding. While forces from the brace-gusset plate connection are required to pass through the gusset plate and beam stub and may be distributed in a fairly equal manner between each of the splice plates, it is possible that the forces do not transfer quickly enough and instead forces pass through the closest members.

It is possible that other factors come into play. One result that supports this idea is that there are differences even among plates on the same side of the beam flange. For example, for Specimen 1 the plate that experienced the greatest strain was the outer plate furthest from the floor; the rosette data indicates that shear strains were significantly higher (see Figure 3-14) and the strain gage data indicates that axial strains were large as well, especially under applied positive displacement (see Figure 3.9). One possible cause for the larger strains is greater bolt slippage in the other plates. If the bolts connecting the splice plates to the beam flange had been slightly offset in some holes compared to others or if small differences in bolt hole drilling occurred, then it is possible that this plate was unable to self-adjust as much as the other plates and therefore resisted the majority of the load for the duration of the testing. Another possible explanation is gage malfunction, but it is unlikely due to the high correlation between strain gages S9 and S10 and rosette R2 (see Figure 3.9).

Even though the reasons behind the particular distributions of strains between the splice plates of each specimen are not all clear, the general trends are apparent and do support the finding that yielding occurs in the plates and is greatest across the gap

4.4 Gusset Plate Shear Strain

Shear strains in the gusset plates were measure using rosettes. For Specimen 1, one of the rosettes failed, but the other indicated that shear strains in excess of the typical steel yield strain of 0.002 in/in did occur near the location of the bolted connection (see Figure 3-15). The maximum strain was approximately ±0.008 in/in and corresponded to the maximum drift of the largest applied displacement cycle. It is expected that the forces were dissipated quickly through the gusset plate, and therefore, no obvious yielding or buckling was observed to have occurred.

For Specimen 2, more rosettes were placed on the gusset plate due to the longer beam-gusset plate connection (see Figure 3-33). It was observed that the rosette closest to the brace-gusset plate connection (i.e. farthest from the column) experienced the greatest strains. The strains were roughly ten times greater than at any of location. In looking at the gusset plate geometry, rosette R6 and possibly R11 may be expected to experience a similar axial force as R5. Because they did not, another explanation appears more plausible. When considering the strain gage data on the brace core extension hinge area (see Figure 3-32), the two gages (one on either side of the assembly) experienced asymmetrical strains; therefore, it is probable that the moments occurring in the brace core extension assembly were influencing the forces experienced by the gusset plate. It is expected that, because the gusset plate increases in cross sectional area as it approaches the beam, the gusset plate has sufficient strength to ensure the preclusion of buckling.

4.5 BRB Core Extension Assembly Hinge Point

The BRB hinge point was unable withstand all of the fatigue cycles. Of all the specimen components, it experienced the greatest degree of failure due to its fracturing during the additional fatigue cycles that were applied to Specimen 2. The strain gage data show mild yielding (strains of approximately ±0.01 in/in), but it is anticipated that because the fracture occurred a few inches (approximately 3 in) away from the gages, at some point the gage data becomes unrepresentative of the critical strains experienced by the brace core extension hinge area; had the fracture occurred next to the gage, then it is more likely that the data would give more accurate results. This is true at least up until the point of fracture, after which the strain data nearly becomes obsolete due to the inability of the section to resist forces.

4.6 Avoidance of Undesirable Failure Modes

The overall goal of the proposed connection design was to increase the efficiency of buckling-restrained braced frames by reducing the failures they incur in a major earthquake. The drifts to which the specimens were exposed were considerable and are possibly greater than would be expected to occur in any earthquake. Under these drifts, no yielding, buckling, or fracturing occurred to critical connection components; the beams, columns, and gusset plates of both specimens avoided all undesirable failure modes.

5 Conclusions and Recommendations

Based on the design work and test results of this study, conclusions are made about the connection design methodology, the loading protocol development, and the performance of the test specimens. Recommendations are given regarding implementation of the connection design and follow-up tasks and projects.

5.1 Connection Design Methodology

With a few minor adjustments, the design methodologies utilized for the connection components were deemed reasonable.

The beam flanges were a particular point of concern, and they performed well; they transferred the loads to and from the splice plates without any problems, and in the end showed, no signs of fatigue. Due to potential catastrophic failures, care must always be taken to choose beam sections that have sufficiently large flange cross-sectional areas. It is recommended that flange yielding and fracture checks be performed on the potential beam sections before proceeding further with the design.

For the gusset plate design, the UFM worked well. In addition, tapering did not appear to negatively affect their performance. It is not known if the stiffener on the upper connection was significant.

The splice plate design also was found capable of meeting the connection's rotational and axial demands (the shear demands were not tested), though certain additional criteria are deemed more important than previously considered. The objective to limit yielding in the outer plate(s) while allowing it in the inner plate(s) was not met in the first test but it was in the second test. The difference appears to relate to the comparison of the cross-sectional areas of the inner and outer plates. In Test 1, the inner plates had the same total cross-sectional area as the outer plates and if anything experienced less yielding; in Test 2, the inner plates had only 84% of the area as the outer plate, and it was very obvious that the inner plates yielded significantly while the outer plate did not. As was done in Test 2, it is recommended that the outer plate(s) be designed with a larger total cross-sectional area than the inner plates; though, not enough testing has been performed to specify a certain recommended percentage.

The methodology for choosing the gap size showed itself to be very accurate: in both tests, the gap closed only at the target design drift and with minimal pinching.

5.2 Loading Protocol Development

A great deal of work was involved in developing loading protocols and translating them into specific actuator displacement and force values. The protocols took into account the specimen's deformation response and changing geometry within the test frame, typical BRB hysteresis action, and boundary stiffness, among other things. It was an intense task because the actuators not only had to introduce loads into the test setup, but one had to cause the right amount of drift at the right time and the other had to

simulate a BRB's response to the drift. These needs arose because actual BRBs were not used.

The benefits derived from simulating a BRB had economic and academic significance: the test specimens were more economical and easier to fabricate, testing and design flaws had less significant repercussions, and each connection could be tested and analyzed separately. The main advantage was that the test specimens were more economical. For example, the two main components that are expected to yield in each test are the BRB and the splice plates. If an actual BRB was used in the test specimen, a new one would have to be fabricated for each test. By not using a BRB, only the splice plates and possibly the BRB core extension assembly would have to be changed for each new test, resulting in a significant savings of time and money. Time and money are also saved in the case that an error should occur in the testing; the reasons are that less has been invested in each specimen and the specimens are comprised of more easily transferable components.

5.3 Overall Test Specimen Performance

In both cases, the connections performed very well. They were both able to reach the target drift of ±6.5% with little undesirable duress. For the most part, the yielding of the specimens occurred where desired; the main exception was the near-equal yielding of the inner and outer plates of Specimen 1. The beams, columns, and gusset plates did not show any signs of concentrated moments, and all of the undesirable failure modes were avoided.

5.4 Connection Design Limitations

While the connection design appears to perform in a very satisfactory manner, additional testing is in the planning and intends to address some key issues: the connection's ability to transfer shear loads, how the concrete floor slabs will affect the plates' ability to act as a hinge, and the connection's performance when exposed to out-of-plane loading (e.g. earthquake accelerations hitting a building at an angle). It is recommended that use of the proposed connection design be deferred until further tests are performed.

5.5 Future Testing and Related Efforts at Brigham Young University

Computer modeling of the prototype connection design is already underway by others. The same loading protocol and boundary conditions as used in the lab are being duplicated on the computer in order to compare simulation output with the physical test results. The eventual goal of the analysis is to model how an entire building using the proposed connection design would perform under actual seismic acceleration demands. It is anticipated that future simulation tests can be performed in a similar manner to explore how the connection design performs under slight adjustments: other plate thicknesses, steel decking and concrete slab on top flange, etc.

A new area of interest that has arisen from the testing relates to the BRB core extension assembly hinge. Due to the assembly's fatigue fracturing, more testing and analysis being considered.

References

1. Clark, P., Aiken, I., Kasai, K., Ko, E., and Kimura, I. (1999). "Design Procedures for Buildings Incorporating Hysteretic Damping Devices," Proceedings, 68th Annual Convention, Structural Engineers Association of California, Santa Barbara, California, October 1999.

2. SEAOC-AISC (2001) "Recommended Provisions for Buckling-Restrained Braced Frames", Structural Engineers Association of California and American Institute of Steel Construction.

3. Reaveley, L.D., Okahashi, T., and Farr, C.K. (2004). *CoreBrace Series E Buckling-Restrained Brace Test Results*, University of Utah, Salt Lake City, UT.

4. Ko, E. and Field, C. *The Unbonded Brace: From Research to Californian Practice*.

5. Lopez, W.A., Gwie, D.S., Lauck, T.W., and Saunders, C.M. (2004). *Structural Design and Experimental Verification of a Buckling-Restrained Braced Frame System*, Engineering Journal, 4th Quarter, 2004, 177-186.

6. Christopulos, A. (2006). "Improved Seismic Performance of Buckling Restrained Braced Braces," *Masters Thesis*, University of Washington, Seattle, WA.

7. Fahnestock, L.A., Ricles, J.M, and Sause, R. (2006). "Experimental Study of a Large-Scale Buckling-Restrained Braced Frame Using the Pseudo-Dynamic Testing Method", *Paper No. 1503*, Proceedings, 8th U.S. National Conference on Earthquake Engineering, San Francisco, California, April 2006.

8. Walters, M.T., Maxwell, B.H., Berkowitz, R.A., (2004). *Design for Improved Performance of Buckling-Restrained Braced Frames*, SEAOC 2004 Convention Proceedings, 506-513.

9. Tsai, K.C., Wang, K.J., Chen, C.H., Hsiao, P.C., Lai, W.C., Lai, J.W., Lin, M.L., Weng, Y.T., and Lin, K.C. *Networked Hybrid Tests of Full-Scale Frame Structures in NCREE*.

10. AISC (2005) "Steel Construction Manual," 13th Edition, American Institute of Steel Construction, Chicago, IL.

11. Kaufmann, E.J., Metrovich, B.R., and Pense, A.W. (2001). *Characterization of Cyclic Inelastic Strain Behavior On Properties of A572 Gr. 50 and A913 Gr. 50 Rolled Sections*, Lehigh University, Bethlehem, PA.

12. Sabelli, R., Mahin, S., and Chang, C. (2003). "Seismic Demands on Steel Braced Frame Buildings with Buckling-Restrained Braces", Elsevier Science Ltd., *Engineering Structures*, 25 (2003), 655-666

13. Sabelli, R. and Lopez, W. (2004) "Design of Buckling-Restrained Braced Frames," *Modern Steel Construction*, 44-3 (2004), 67-73

14. Nishimoto, K., Shirai, T., Nakata, Y., Aiken, I., Yamada, S., and Wada, A.. *Sub-Assembly Testing of Large Buckling-Restrained Unbonded Braces*

15. Merritt, S., Uang C.M., and Benzoni, G. (2003). "Subassemblage Testing of CoreBrace Buckling Restrained Braces," *Report No TR-2003/01*, UCSD, La Jolla, CA

16. CoreBrace (2004). *Buckling Restrained Braces*. CoreBrace LLC, West Jordan, UT.

Appendix A. Self-Reacting Frame and Hydraulic Actuators

The self-reacting frame and hydraulic actuators used for testing are described below.

A.1 Self-Reacting Frame

The self-reacting frame (see Figure A-1) has a variable working area roughly 13 ft. wide and between 10 ft. and 30 ft. long, depending on the extensions used. At one end, there are holes available for mounting up to three actuators, and stiffener plates are located directly behind the holes for added strength and support. A 3 in. diameter high-strength pin is also available for use with one of the extension pieces. Holes are located on the floor in a 3 ft. x 3 ft. grid pattern and 1-1/2 in. tension bars are used to hold the frame and equipment in place. The significance of the frame is its total containment of the forces applied within; therefore, strong walls are not needed.

A.2 600-Kip Actuators

Two 600-kip actuators (see Figure A-2) were used for testing. The actuators can be either force or displacement controlled and have a variety of mounting capabilities; their swivel heads on both ends allow free rotation and can be removed to allow for a more rigid connection.

(a) Photograph

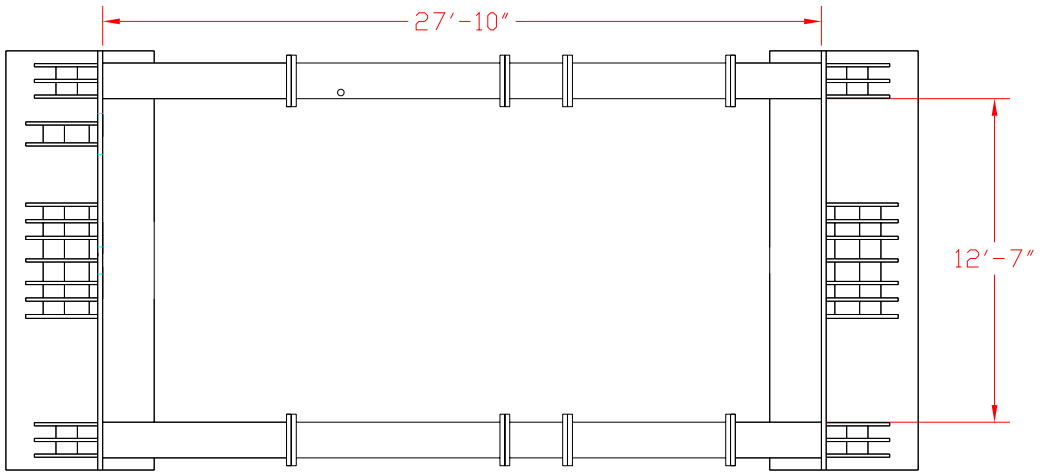

(a) Schematic

Figure A-1 Self-Reacting Frame in Brigham Young University Structures Lab

(a) Photograph

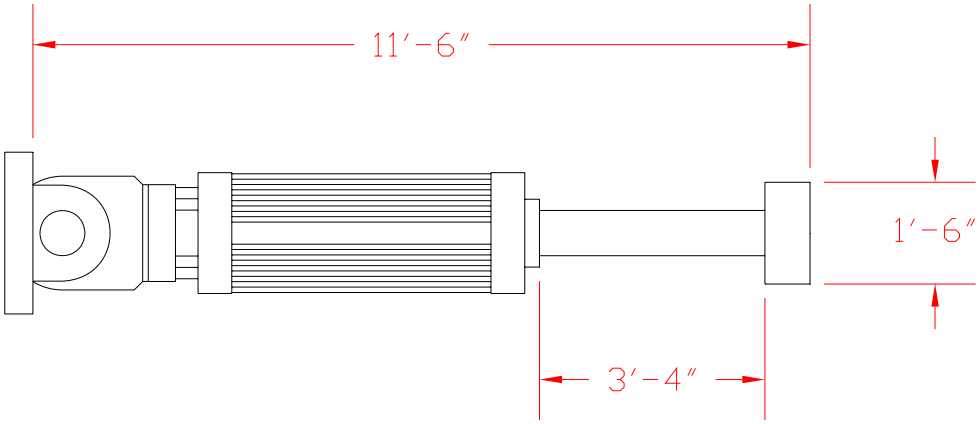

(a) Schematic of Actuator with Head at Maximum Displacement

Figure A-2 600-kip Actuator

Appendix B. Prototype Bay Design Calculations

The calculations used in the prototype bay and test specimen design are explained in the following sections.

B.1 Brace Ultimate Strength Calculations

Three adjustment factors are multiplied to determine the brace ultimate strength (16). They are as follows:

- Strain hardening factor (ω = 1.60); the strain hardening factor takes into account the increasing strength of the steel core as it yields.
- Compression factor (β = 1.06); the compression factor adjusts the yield strength (usually given as a tensile strength) to account for the fact that steel is stronger in compression.
- Real yield stress adjustment factor (R_y = 42 ksi / 36 ksi = 1.167); the real yield stress adjustment factor compensates for how the nominal yield stress is typically lower than the actual yield stress. In most instances, it is conservative to use the nominal value, but in the case of BRBF design, it is conservative to use the real value. The typical steel used in a BRB core has a 36 ksi nominal yield stress and 42 ksi real yield stress.

Multiplying the factors together,

$$B * \omega * R_y = 1.98 \approx 2 \quad \text{(B.1)}$$

This result supports the usual design practice of using a factor of two when exact values of β, ω, and R_y are not available.

A yield strength of P_{ysc} = 203 kip was chosen for the model BRB; this was a value given by CoreBrace as one of their most common brace strengths. Adjusting the brace yield strength to determine its over-strength,

$$F_u = \beta * \omega * R_y * P_{ysc} = 402 \text{ kips} \quad \text{(B.2)}$$

Therefore, the ultimate strength of the brace was determined to be 402 kips. This value was used to determine the beam and column demand forces.

B.2 Beam and Column Design Force Calculations

The beam design force equals the ultimate brace strength multiplied by the cosine of the angle made by the brace and beam (see Figure B-1). The column design force equals the ultimate brace strength multiplied by the sine of the angle. Calculating the initial angle (θ_0) between the beam and BRB,

$$\theta_0 = \tan^{-1}(13 \text{ ft} / 20 \text{ ft}) \approx 33 \text{ degrees} \quad \text{(B.3)}$$

Because rotations are taking place in the BRBF bay, it is better to consider a range of angles and use the most conservative one when determining the beam and column demand forces. Based on the expected rotations, it was determined that the most

appropriate range to consider was 29 to 36 degrees. Recognizing that maximum values will be at the ends of the spectrum and calculating the beam and column demand forces,

$$F_{beam} = F_u * \cos(29°) = 351 \text{ kip} \quad \text{(B.4)}$$

$$F_{column} = F_u * \cos(36°) = 236 \text{ kip} \quad \text{(B.5)}$$

Therefore, the beam will need to be designed to withstand an axial demand force of 351 kips, and the column will need to withstand an axial demand force of 236 kips.

B.3 Beam Design Calculations

Typical beam design focuses on flexural capacity. In seismic design, axial demands must be taken into account due to lateral loads. For the proposed connection design, additional demands are encountered because the beam is required to pass the entire load through splice plates that are attached to the top flange. Taking all the demands into account, there are multiple limit states that must be satisfied in order for a beam to meet design requirements. Many of these states are adaptations from tension member design or connection design.

First, because the top flange of the beam must be designed to withstand the entire beam axial load, tensile yielding of the flange gross cross section ($A_{f,beam}$) must be considered. The required gross section was calculated,

$$A_{f,beam} \geq F_{beam} / \Phi F_y = 351 \text{ kips} / (0.9 * 50 \text{ ksi}) = 7.8 \text{ in}^2 \quad \text{(B.6)}$$

Another important design criterion relates to the flange width. In order for the lower connection to accommodate the gusset plate, associated welds, and splice plates the

flange must be sufficiently wide. Assuming a 1 in. gusset plate, ¾ in. fillet welds on either side, a row of holes on either side, sufficient tightening clearance between holes and gusset plate, and required bolt edge distance, the flange width ($b_{f,beam}$) must equal,

$$b_{f,beam} \geq 1 + 2*(3/4 + 1/2 * 4 + 1.5) = 9.5 \text{ in.} \quad \text{(B.7)}$$

To be consistent with the design used by A. Christopolus (6), W16 shapes were considered for the design. The smallest W16 that met the flange area and width requirement was a W16x77, which has $A_{f,beam} = 7.83$ in^2 and $b_{f,beam} = 10.3$ in.

B.4 Column Design Calculations

The column design of the proposed connection follows typical procedures, which entails finding the design axial load from the different load combinations and then using the "Available Strength in Axial Compression" Table (Table 4-1 in AISC Steel Manual) (10) to size the member based on a given effective length.

For the specimen, the effective length (KL) is the bay height, namely 13 ft. As previously calculated, the column design force equals 236 kips. Based on Table 4-1 (10), most typical column WF shapes (e.g. W8, W10, and W12 shapes) can support the design force; therefore, other criteria were used to select a particular member.

One additional criterion that is suggested for choosing a column is that the flange width of the column should be larger than that of the beam to ensure that the beam-column weld can surround the entire beam cross section. Also, to increase the ease of comparison with the tests performed by A. Christopolus (6), which used a W12x72 column, a similar column shape was used, namely a W12x79. This shape satisfies the flange width criterion with $b_{f,column} = 12.1$ in. > $b_{f,beam}$ 10.3 in.

B.5 Gusset Plate Design Calculations

Due to the unique location of the connection working points, two gusset plate designs were required for the prototype frame: one for the brace connection to the lower beam and the other for the connection to the upper beam (see Figure B-2). In both cases, the working point is inline with the centroid of the beam top flange; the result is that in the lower connection, the working point is almost in line with the gusset-beam weld, while in the upper connection, the working point is nearly a full beam's depth away from the weld. This means that in order for the brace centerline to pass through both working points, the brace must be much closer to the column in the lower connection than in the upper connection.

The initial step in the gusset plate design is to determine the basic geometry of each connection such that the following general requirements are met: sufficient area is provided to bolt the brace core extension to the gusset plate, the brace centerline passes through the connection working point, the gusset plate edge facing the brace core extension assembly is oriented perpendicular to the brace centerline to accommodate the brace-gusset plate connection, the beam-gusset plate weld is short enough to keep the hinge point close to the beam-column-brace connection working point, tapering is such that out-of-plane buckling is precluded, and the gusset plates have discrete dimensions for easy detailing.

The brace-gusset plate bolt connection area was based on the BRB core extension detail (see Figure B-3) supplied by CoreBrace, a brace fabricator involved in the testing. The Uniform Force Method (UFM) was then used to select the connection lengths and to obtain the design forces for the beam-gusset plate and column-gusset plate welds. By

using the UFM, the welds will only be subject to shear and tension forces (10). The principal UFM equation consists of five variables, which are shown in Figure B-4a and defined as follows: θ is the angle of brace with respect to column, e_b is the vertical distance from face of beam to working point, e_c is the horizontal distance from face of column to working point, α is half of the beam-gusset connection length, and β is half of the beam-gusset connection length. The principal UFM equation includes the variables as follows:

$$\alpha - \beta * \tan(\theta) = e_b * \tan(\theta) - e_c \quad \text{(B.8)}$$

Given that the values for variables θ, e_b, and e_c are predetermined by the prototype bay dimensions, design beam properties, and design column properties, respectively, equation (B.13) can be calculated in terms of α and β, which correspond to the beam-gusset plate and column-gusset plate connection lengths (which are assumed to equal the lengths of the corresponding edges of the gusset plates). Because these variables are dependent upon each other, only one connection length can be chosen while the other must be calculated based on the equation, resulting in dependent pairs of connection length values. Multiple options are available and trial and error calculations are helpful in making a decision. It must also be remembered that the connection length values correspond to only two edges of the gusset plate; the other edges should be chosen such that the general requirements previously listed are satisfied.

Based on the selected connection lengths, the vertical and horizontal forces required by the gusset-beam and gusset-column welds (see Figure B-4b) are calculated using UFM equations and used for designing the beam-gusset plate connection and the column-gusset plate connection (10).

The final gusset plate dimension is the thickness, which is based on the distance between the brace core extension bolt plates (see Figure B-3). The fabricator specified a 1.0 in. connection slot, and therefore the gusset plate thickness was 1 in..

B.6 Gap Size Calculations

The gap size was designed to remain open, even if only by a fraction of an inch, at the point when the prototype bay reaches the target inter-story drift (see Figure B-5). One key design step is calculating the maximum gap angle (α_{gap}), which is defined as the angle formed between the beam stub and middle beam member when the bay has reached the desired maximum drift. The following values are included in the calculations and all but the inter-story drift are illustrated in Figure B-6:

δ = 6.0% = inter-story drift design percentage as measured by drift amount divided by story height (B.9)

d = 16-1/2 in = beam depth (B.10)

L = 20 ft = beam length as measured between column midpoints (B.11)

L_{lower} = 20.15 in = lower connection beam-stub length as measured between connection working point and gap centroid (B.12)

L_{upper} = 40.40 in = upper connection beam-stub length as measured between connection working point and gap centroid (B.13)

L_{center} = 170.45 in = beam length as measured between gap centroids (B.14)

The maximum gap angle was determined based on geometric calculations that assume the flexural deformation of prototype bay members is insignificant compared to the axial deformation of those members. In addition, it is assumed that the axial deformation of splice plates is insignificant and that both columns of the prototype bay have the same rotation.

The maximum gap angle can be divided into two components, which include the following: the angle of the beam-stub ($\alpha_{gap,1}$) and the angle of the middle beam ($\alpha_{gap,2}$), which are illustrated in Figure B-7. Assuming no flexural deformation in members, the angle of the beam stub equals the column rotation,

$$\alpha_{gap,1} = \text{column rotation} = \sin^{-1}(\text{drift}) = 3.44° \quad \text{(B.15)}$$

Under the same assumption of no flexural deformation, the angle of the middle beam is based on the lengths of the beam sections as well as the column rotation,

$$\alpha_{gap,2} = \sin^{-1}(\sin(\alpha_{gap,1}) * (L_{lower} + L_{upper}) / L_{center}) = 1.40° \quad \text{(B.16)}$$

The total gap angle is found by summing the two parts,

$$\alpha_{gap} = \alpha_{gap,1} + \alpha_{gap,2} = 4.84° \quad \text{(B.17)}$$

The next step is calculating the required gap size (g_{rec}), which is the smallest gap size that still allows the target inter-story drift to be reached before the gap is completely closed,

$$g_{rec} = 2 * d * \sin(\alpha_{gap} / 2) = 1.39 \text{ in} \quad \text{(B.18)}$$

In order to have clean dimensions for the initial gap size (g_o), the required gap size is rounded up to the nearest eighth inch,

$$g_o = 1.5 \text{ in} \tag{B.19}$$

B.7 Bolt Design Calculations

The entire beam design force (F_{beam} = 351 kip) must pass through the beam flange-splice plate connection. The AISC Steel Design Manual (10) gives the design strength ($\Phi_v r_n$) of A490X bolts in double shear,

$$\Phi_v r_n = 67.6 \text{ kip/bolt} \tag{B.20}$$

Based on the bolt strength and design force, the required number of bolts (n_{bolts}) is calculated and rounded up to ensure symmetry in the connection,

$$n_{bolts} = F_{beam} / \Phi_v r_n = (351 \text{ kip}) / (67.6 \text{ kip/bolt}) = 4.98 \text{ bolts} \approx 6 \text{ bolts} \tag{B.21}$$

B.8 Splice Plate Configuration Design Calculations

The entire beam design force (F_{beam} = 351 kip) must pass through the splice plates, which are connected to both the sides of the beam top flange. The lower connection splice plate configuration includes four splice plates, each with a 4 in x 5/8 in cross section. The upper connection splice plate configuration includes three plates, including: two with a 4 in x 5/8 in cross section and one with a 9-1/2 in x 5/8 in cross section. All plates were 19-1/2 in long.

The plates were required to satisfy various tension and compression member limit states, including: shear yielding, global buckling, tensile yielding of gross section, and tensile rupture in net section.

The following design parameters will be assumed:

$$\Phi_y = 0.9 \tag{B.22}$$

$$\Phi_u = 0.75 \tag{B.23}$$

$$U = 1.0 \tag{B.24}$$

All splice plates have the following properties:

$$F_y = 36 \text{ kip} \tag{B.25}$$

$$F_u = 58 \text{ kip} \tag{B.26}$$

The bolt calculations are as follows,

$$d_{bolt} = 7/8 \text{ in} \tag{B.27}$$

$$d_{effective} = 7/8 + 1/16 = 0.9375 \text{ in} \tag{B.28}$$

B.8.1 Lower Connection Splice Plate Configuration

The lower connection plates have the following properties:

$$w_{plate} = 4 \text{ in} \tag{B.29}$$

$$t_{plate} = 5/8 \text{ in} \tag{B.30}$$

$$A_{f,plate} = w_{plate} * t_{plate} = 4 * 5/8 = 2.5 \text{ in}^2 \quad \text{(B.31)}$$

$$A_f = 4 * A_{f,plate} = 4 * 2.5 = 10.0 \text{ in}^2 \quad \text{(B.32)}$$

$$A_n = A_f - (\pi * (d_{effective} / 2)^2) * 4 * t_{plate} = 10.0 - (3.14 * (0.9375 / 2)^2) * 4 * 5/8$$
$$= 8.275 \text{ in}^2 \quad \text{(B.33)}$$

$$A_e = A_n * U = 8.275 * 1.0 = 8.275 \text{ in}^2 \quad \text{(B.34)}$$

The limit state calculation for shear rupture of gross section is greater than the demand from gravity floor loads,

$$\Phi_u V_n = 194 \text{ kip} \geq 44 \text{ kip} \quad \text{(B.35)}$$

Though the limit state calculation for global buckling is less than the design force, it was deemed sufficiently close,

$$\Phi_y P_n = 320 \text{ kip} < 351 \text{ kip} \quad \text{(B.36)}$$

Though the limit state calculation for tensile yielding of gross section is less than the design force, it was deemed sufficiently close,

$$\Phi_y P_n = \Phi F_y * A_f = 0.9 * 36 * 10.0 = 324 \text{ kip} < 351 \text{ kip} \quad \text{(B.37)}$$

The limit state calculation for tensile rupture of net section is greater than the design force,

$$\Phi_u P_n = \Phi_u F_u * A_e = 0.75 * 58 * 8.275 = 360 \text{ kip} \geq 351 \text{ kip} \quad \text{(B.38)}$$

B.8.2 Upper Connection Splice Plate Configuration

The upper connection plates have the following properties:

$$w_{plate,inner} = 4 \text{ in} \tag{B.39}$$

$$w_{plate,outer} = 9\text{-}1/2 \text{ in} \tag{B.40}$$

$$t_{plate} = 5/8 \text{ in} \tag{B.41}$$

$$A_f = (2 * w_{plate,inner} + w_{plate,outer}) * t_{plate} = (2 * 4 + 9\text{-}1/2) * 5/8 = 10.94 \text{ in}^2 \tag{B.42}$$

$$A_n = A_f - (\pi * (d_{effective} / 2)^2) * 4 * t_{plate} = 10.94 - (3.14 * (0.9375 / 2)^2) * 4 * 5/8$$
$$= 9.21 \text{ in}^2 \tag{B.43}$$

$$A_e = A_n * U = 9.21 * 1.0 = 9.21 \text{ in}^2 \tag{B.44}$$

The limit state calculation for shear rupture of gross section is greater than the demand from gravity floor loads,

$$\Phi_u V_n = 213 \text{ kip} \geq 44 \text{ kip} \tag{B.45}$$

Though the limit state calculation for global buckling is less than the design force, it was deemed sufficiently close,

$$\Phi_y P_n = 350 \text{ kip} < 351 \text{ kip} \tag{B.46}$$

The limit state calculation for tensile yielding of gross section is greater than the design force,

$$\Phi_y P_n = \Phi F_y * A_f = 0.9 * 36 * 10.94 = 354 \text{ kip} \geq 351 \text{ kip} \tag{B.47}$$

The limit state calculation for tensile rupture of net section is greater than the design force,

$$\Phi_u P_n = \Phi_u F_u * A_e = 0.75 * 58 * 9.21 = 400 \text{ kip} \geq 351 \text{ kip} \quad \text{(B.48)}$$

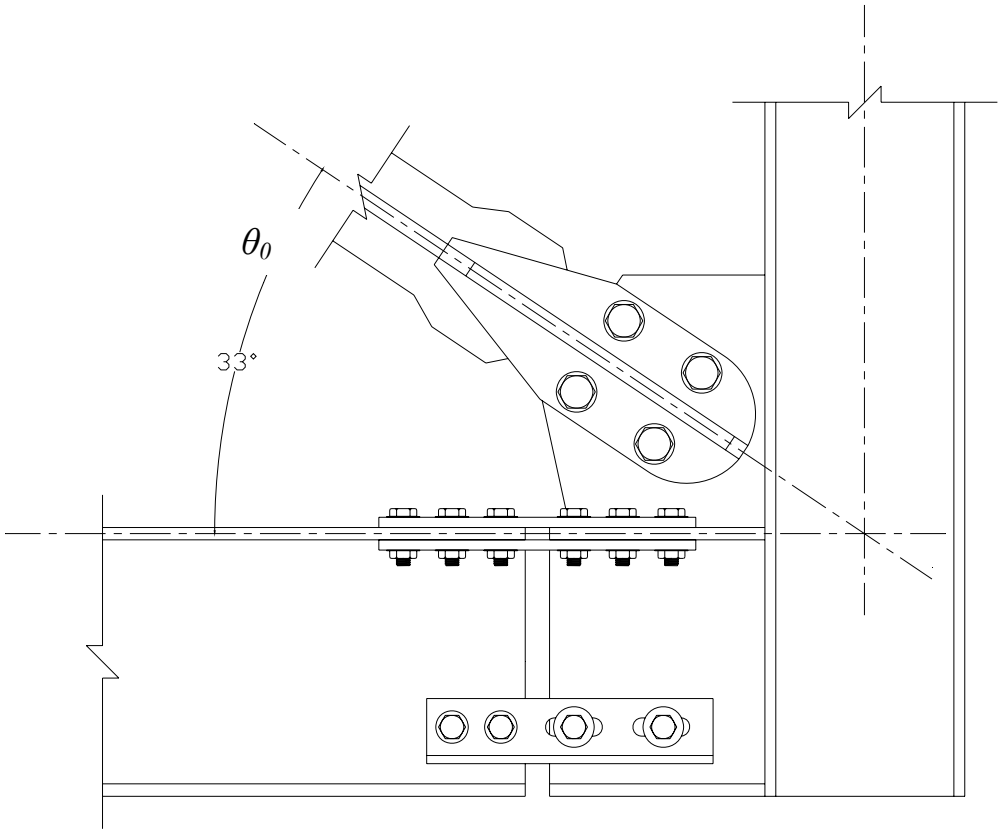

Figure B-1 Brace Angle in Relation to Beam

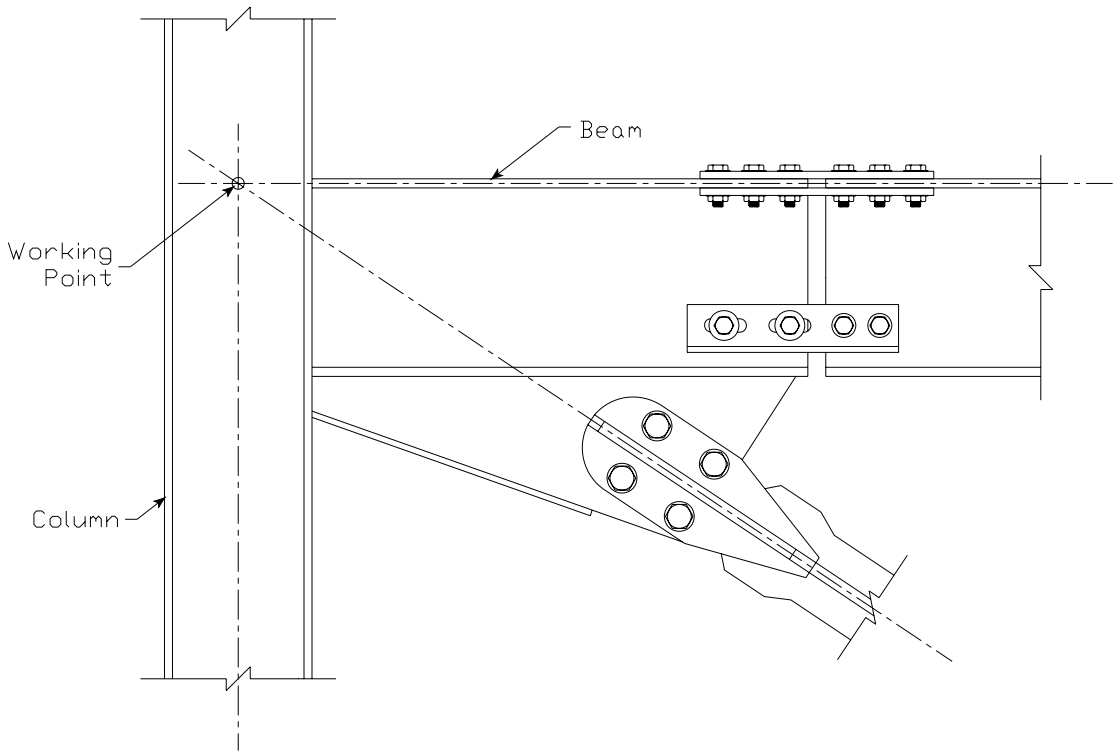

(a) Upper Connection

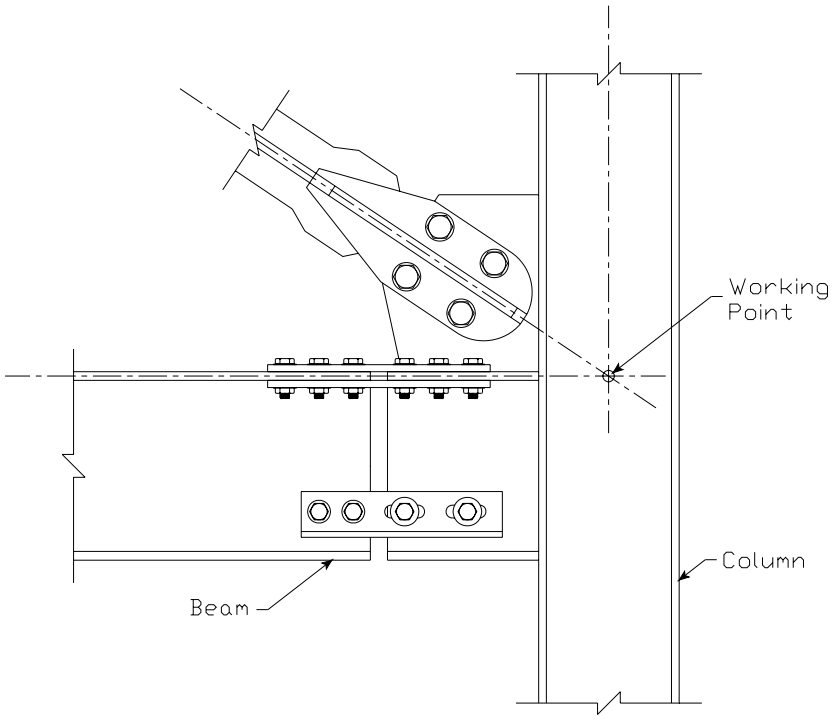

(b) Lower Connection

Figure B-2 Connection Working Point Locations

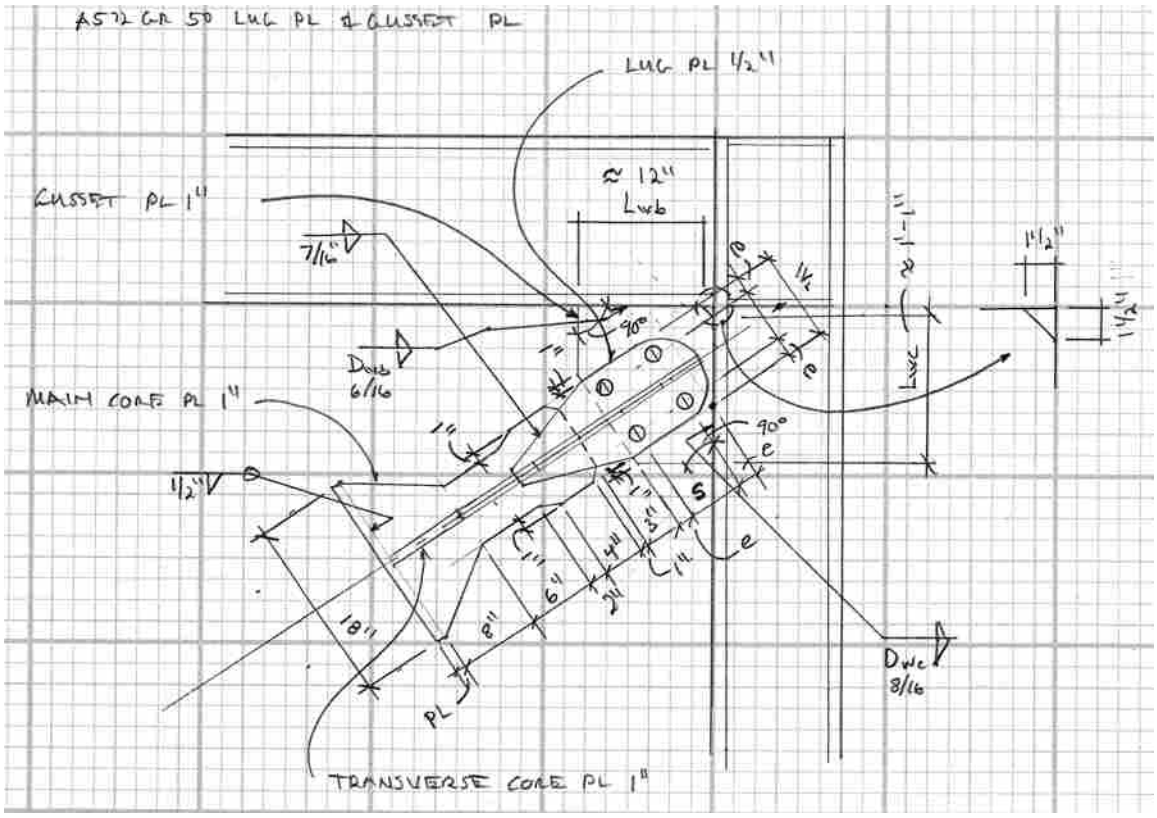

Figure B-3 CoreBrace Core Extension Detail

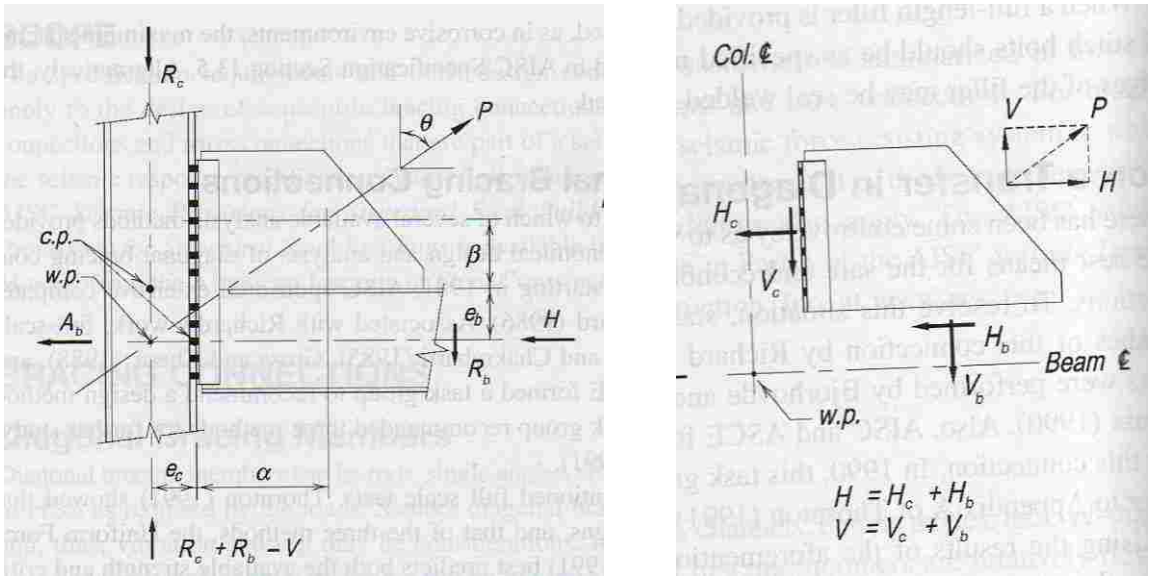

(a) Diagonal Bracing Connection and External Forces **(b) Gusset Free-Body Diagram**

Figure B-4 Uniform Force Method (10)

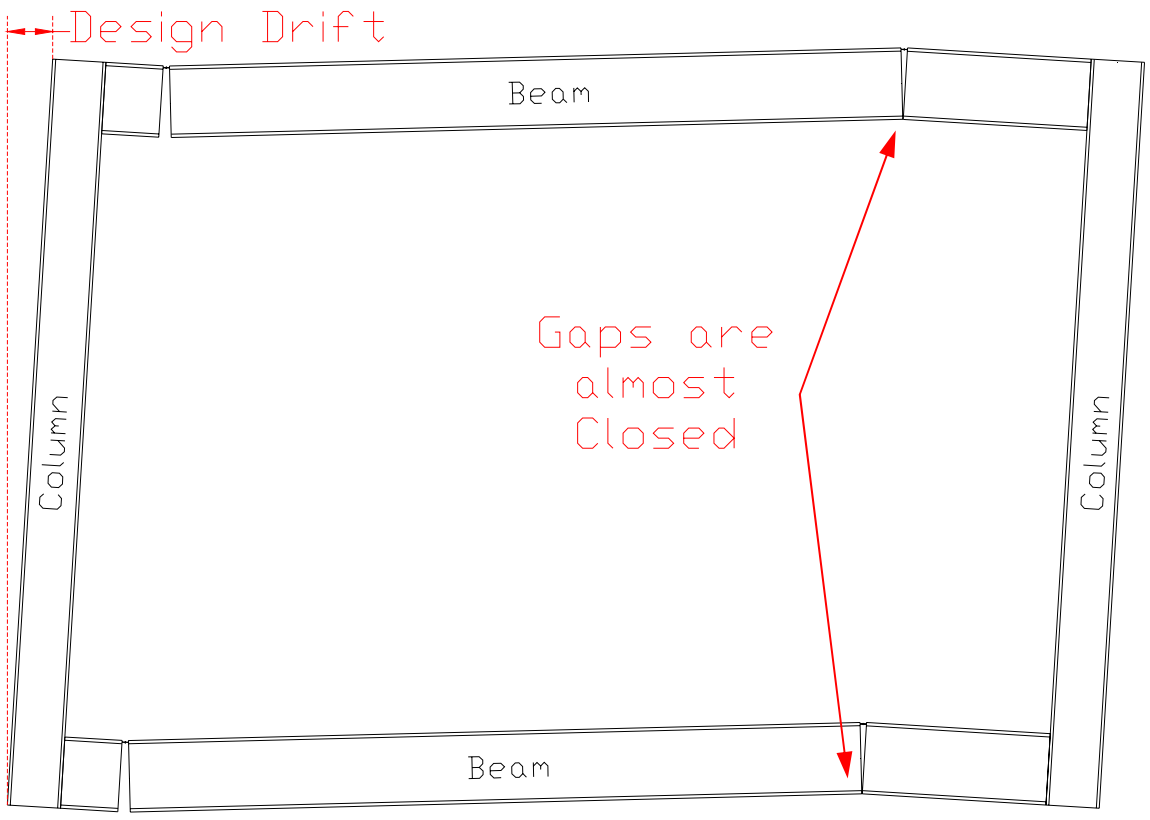

Figure B-5 Gap Calculation Width

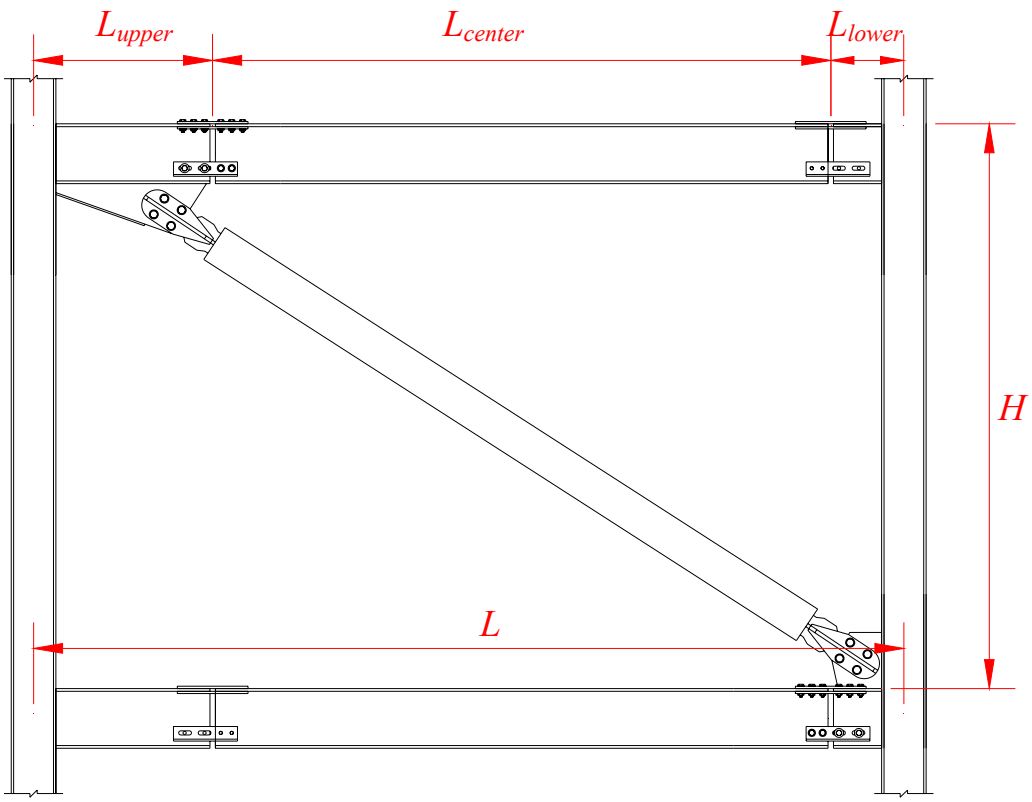

Figure B-6 BRBF Bay Variables

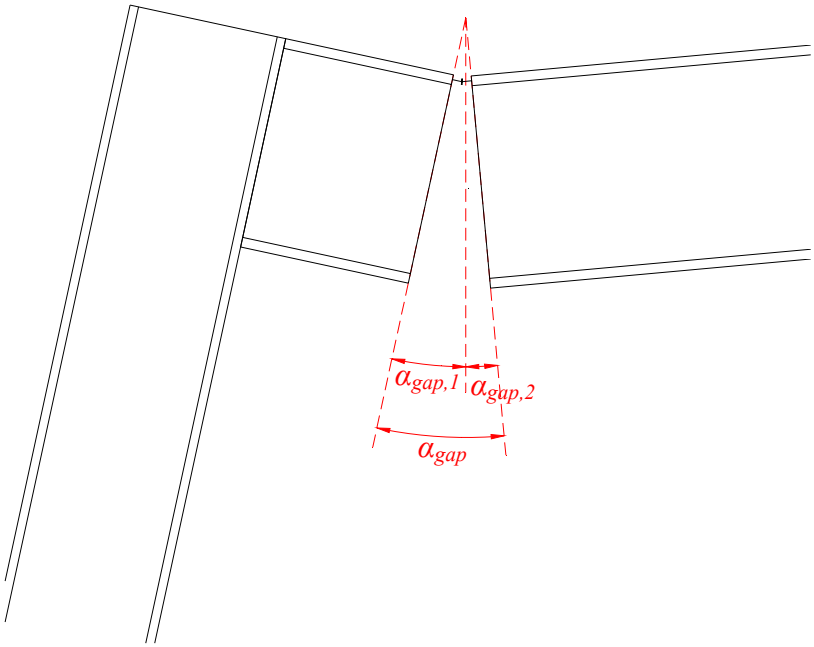

Figure B-7 Gap Angle Calculation

Appendix C. Additional Component Design Calculations

To accommodate the test setup, additional components were designed.

C.1 BRB Proxy

The fabricators designed the brace core extension assembly (see Figure C-1) based on (1) the typical BRB core extension design utilized by CoreBrace and (2) the bolt-hole configuration required for the connection to the HSS extension. A section of the core extension transition area was included in the design with the purpose of acting as a hinge point. A core extension assembly was supplied for each specimen.

C.2 HSS Extension for Brace Replicating Actuator

The brace replicating actuator was not sufficiently long to connect directly to the BRB core extension assembly and still maintain an adequate available stroke length. The optimum extension length was chosen to be 30 inches so that the BRB actuator could start at mid-stroke. An economical piece was needed that could easily support 400 kips (the strain-hardened design force of the brace) while avoiding local and global buckling.

A square HSS 12 x 12 x 1/2 with an 18 x 18 x 1 plate welded at either end was selected (see Figure C-2). The HSS extension's bolt-hole configuration was designed to be the same for both end plates and was based on the actuator's bolt configuration. The

HSS was rotated 45 degrees to allow the HSS to fit within the required bolt configuration. Based on Table 4-4 in the AISC Manual (10), 3/8 in. was the minimum thickness to avoid being slender for compression. Based on the fabricator's availability, the thickness was increased to 1/2 in. The component was sufficiently strong to be used in multiple tests.

C.3 Beam Section Attached to Actuator 2

A beam extension was designed to transfer forces from Actuator 2 into the connection specimen in the same manner as a typical beam. As such, the beam extension was the same design shape (W16x77) as the prototype beam and was long enough (i.e. greater than the beam depth) to allow the transfer of forces from the actuator into the beam, up to the beam top flange, into the splice plates, and across the gap into the connection. In addition, the beam extension was designed to allow a sufficient stroke length for Actuator 2, to line up splice plate bolt holes, and to accommodate specimen placement with the self-reacting frame. The only difference between the beam extension designs for the upper and lower connections were the bolt hole placements.

The beam extension design (see Figure C-3) was a W16x77 with a length of 25-15/16 in. and welded onto a 1 in. plate at one end in order to allow attachment to the actuator. Based on the design, the actuator stroke range was roughly –12-1/2 in. to +27-1/2 in., which allows the necessary ±10 in..

C.4 Column Pin Connection to Self-Reacting Frame

The column was connected to the self-reacting frame using a pin connection (3 in. pin with corresponding holes drilled in self-reacting frame) that allowed the transfer of

forces while the column rotated. To withstand the maximum design force, a section of each of the four flange edges of the column was notched and plates were welded on either side of the column at the notches (see Figure C-4). The plates were extended past the end of the column to ensure the pin passed through the two plates but not the column web.

With the column on its side, the plate width was designed to extend between the flanges and to be welded onto the outer edges of the flanges. The depth of the design column is 12 in. and assuming 1-1/2 in. of clear space on either side (for the weld, etc.), the required plate width was calculated to equal 15 in.

The plates were also designed to support the entire column load. Given the plate width of 15 in., various limit states were checked, and it was determined that a plate thickness of 1-1/2 in. was adequate. The limit state calculations are summarized below.

The pin bearing on the plate was checked to ensure preclusion of plate fracture,

$$\Phi_u R_n = 2 * \Phi_u * (1.2 * L_c * t * F_u) = 2 * 0.75 * (1.2 * 2 * 1.5 * 58) = 314 \text{ kip}$$
$$\geq 220 \text{ kip} \qquad \text{(C.1)}$$

The bearing of the pin on the plate was checked to ensure the preclusion of hole elongation in the plate,

$$\Phi_u R_n = 2 * \Phi_u * (2.4 * d_{pin} * t * F_u) = 2 * 0.75 * (2.4 * 3 * 1.5 * 58) = 940 \text{ kip}$$
$$\geq 220 \text{ kip} \qquad \text{(C.2)}$$

The tensile yielding of the plate gross cross section was checked to ensure the preclusion of plate yielding,

$$\Phi_y P_n = \Phi F_y * A_f = 0.9 * 36 * 45 = 1458 \text{ kip} \geq 220 \text{ kip} \qquad \text{(C.3)}$$

The tensile yielding of the plate net cross section was checked to ensure the preclusion of plate fracture,

$$\Phi_u P_n = \Phi_u F_u * A_e = 0.75 * 58 * 35.625 = 1550 \text{ kip} \geq 220 \text{ kip} \quad \text{(C.4)}$$

A 3 in. chamfer of the unwelded plate corners was designated to allow the column to rotate while still maintaining sufficient clearance with the self-reacting frame web. A clear distance of at least 1/2 in. from the edge of the web fillet was found and determined sufficient.

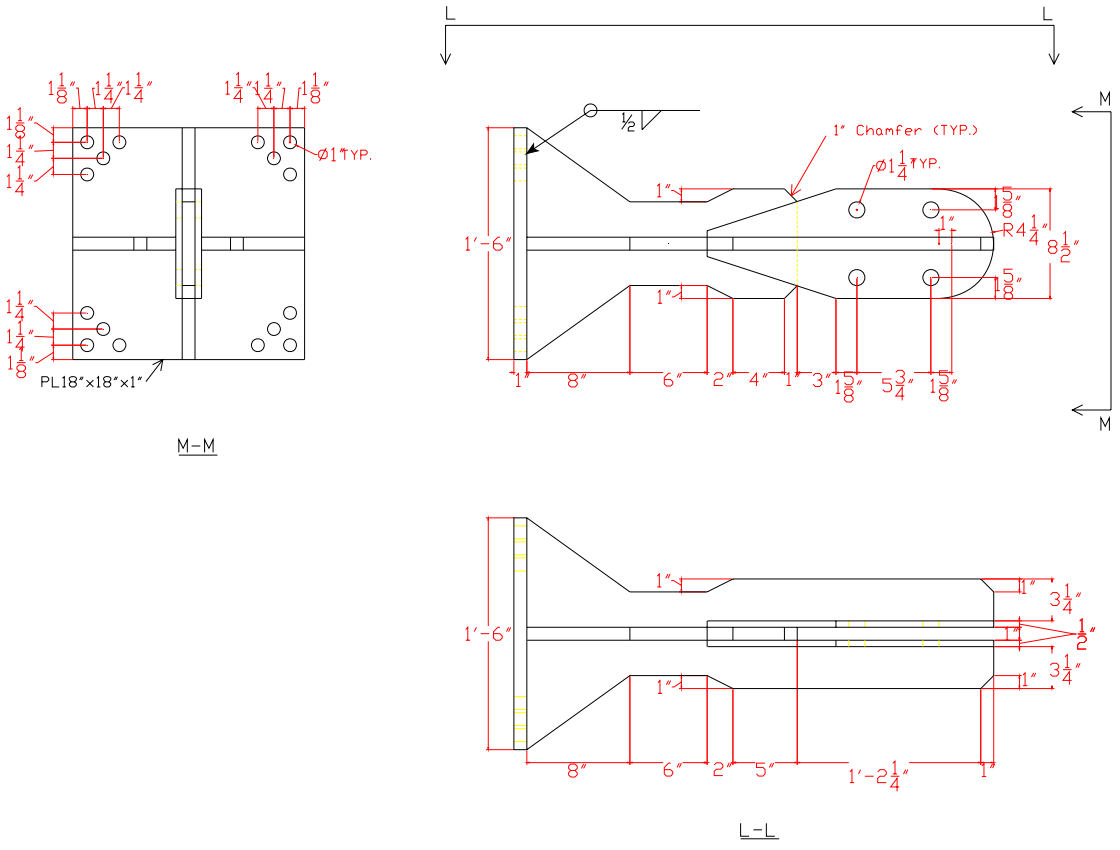

Figure C-1 BRB Core Extension Assembly Detail

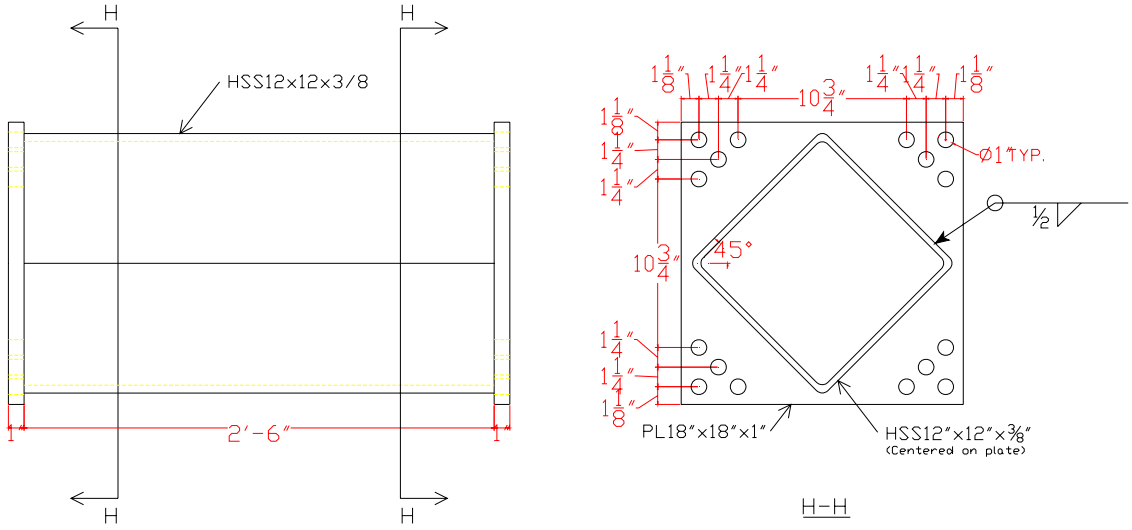

Figure C-2 HSS Detail

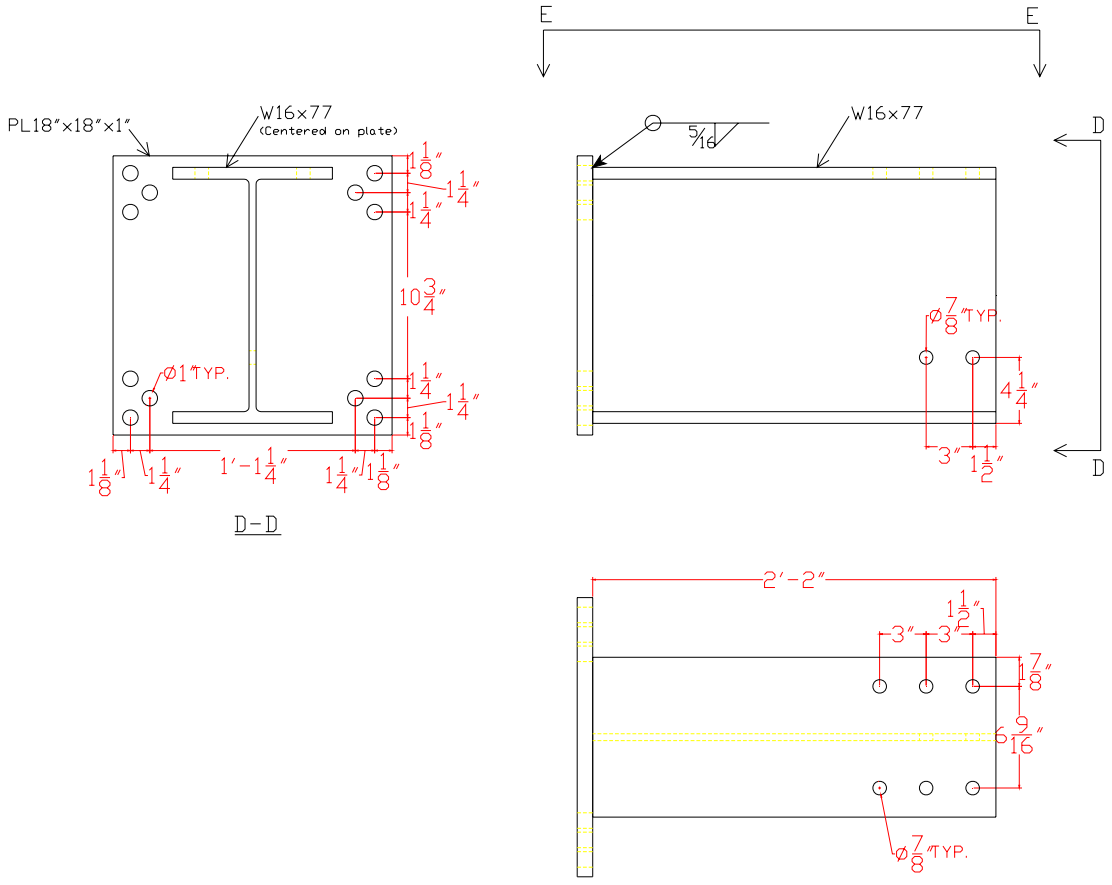

Figure C-3 Beam Extension Detail

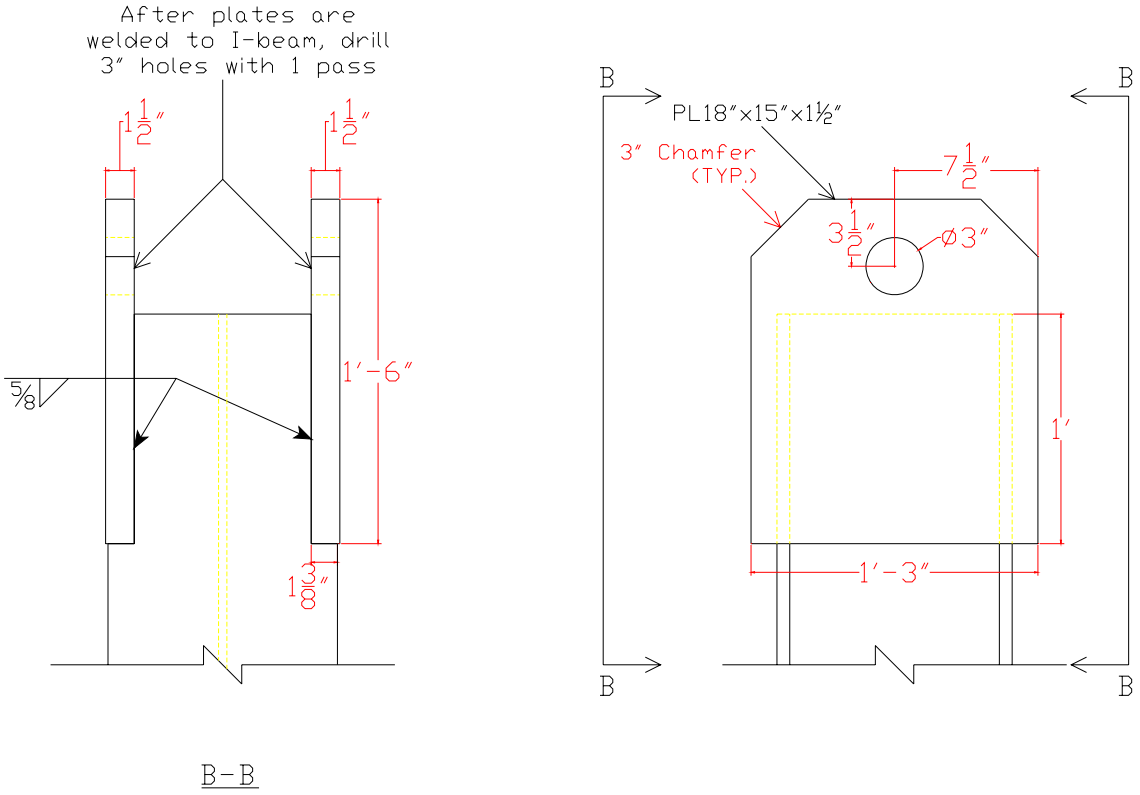

Figure C-4 Column Pin Connection Detail

Appendix D. Prototype-Test Relationship and Conversion

An important tool used for both the loading protocol preparation and data reduction efforts is the relationship between the prototype bay and the test setup. The chosen method for relating the test setup to the prototype bay was to compare the gap angles formed in each. For the prototype, the gap angle is measured between the beam-stub and middle beam and has been discussed previously. For the test setup, the gap angle is measured between the beam-stub and beam extension in a similar manner. The two main advantages of this method are that (1) the gap design is the exact same in both instances and (2) the gap is receiving the most attention, which is ideal because it is the most critical point of the design.

The most important variable for the test setup was the main actuator displacement; for the prototype frame, it was the interstory drift. In order to use the gap angle to make translations from the test setup's actuator displacement to the prototype bay's interstory drift and vice-versa, the behavior of each in relation to the angle was determined. Using the determined relationships, the displacement in the test setup or drift in the prototype bay could be used to find the gap angle, and using that angle, the corresponding drift or displacement of the other could be calculated. The calculations were based on geometry and the results are given in Tables D-1 and D-2. The tables give

the actuator displacement values in 1/4 in. increments between -9-3/4 in. and 10 in. along with the corresponding drift values for both test specimens.

In addition to calculating the corresponding drift values, the associated brace angles for both the test setup and prototype frame were calculated. The error was computed in order to check the accuracy of the conversion. The error range was between ± 2.2%, which is very small, and therefore the conversion was considered sufficiently accurate.

Table D-1: Prototype-Test Conversion Table for Specimen 1

Actuator Displacement	Inter-Story Drift	Brace Angle		
		Test	Real	% Difference
-9.75	-7.63%	28.80	29.44	-2.17%
-9.50	-7.43%	28.91	29.54	-2.14%
-9.25	-7.22%	29.02	29.65	-2.11%
-9.00	-7.01%	29.14	29.75	-2.08%
-8.75	-6.81%	29.25	29.86	-2.04%
-8.50	-6.60%	29.36	29.97	-2.01%
-8.25	-6.40%	29.47	30.07	-1.99%
-8.00	-6.20%	29.58	30.18	-1.96%
-7.75	-6.00%	29.70	30.28	-1.93%
-7.50	-5.79%	29.81	30.38	-1.91%
-7.25	-5.59%	29.92	30.49	-1.88%
-7.00	-5.39%	30.02	30.59	-1.86%
-6.75	-5.19%	30.13	30.70	-1.83%
-6.50	-4.99%	30.24	30.80	-1.81%
-6.25	-4.79%	30.35	30.90	-1.79%
-6.00	-4.59%	30.46	31.01	-1.77%
-5.75	-4.40%	30.57	31.11	-1.75%
-5.50	-4.20%	30.67	31.21	-1.73%
-5.25	-4.00%	30.78	31.31	-1.71%
-5.00	-3.81%	30.88	31.42	-1.69%
-4.75	-3.61%	30.99	31.52	-1.68%
-4.50	-3.42%	31.10	31.62	-1.66%
-4.25	-3.22%	31.20	31.72	-1.65%
-4.00	-3.03%	31.31	31.83	-1.63%
-3.75	-2.83%	31.41	31.93	-1.62%
-3.50	-2.64%	31.51	32.03	-1.61%
-3.25	-2.45%	31.62	32.13	-1.59%
-3.00	-2.26%	31.72	32.23	-1.58%
-2.75	-2.07%	31.82	32.33	-1.57%

Table D-1 – *Continued*

Actuator Displacement	Inter-Story Drift	Brace Angle		
		Test	Real	% Difference
-2.50	-1.88%	31.93	32.43	-1.56%
-2.25	-1.69%	32.03	32.53	-1.55%
-2.00	-1.50%	32.13	32.63	-1.54%
-1.75	-1.31%	32.23	32.73	-1.53%
-1.50	-1.12%	32.33	32.83	-1.52%
-1.25	-0.93%	32.43	32.93	-1.52%
-1.00	-0.74%	32.53	33.03	-1.51%
-0.75	-0.56%	32.63	33.13	-1.50%
-0.50	-0.37%	32.73	33.23	-1.50%
-0.25	-0.19%	32.83	33.33	-1.49%
0.00	0.00%	32.93	33.43	-1.49%
0.25	0.18%	33.03	33.53	-1.48%
0.50	0.37%	33.13	33.63	-1.48%
0.75	0.55%	33.23	33.73	-1.48%
1.00	0.74%	33.33	33.82	-1.47%
1.25	0.92%	33.42	33.92	-1.47%
1.50	1.10%	33.52	34.02	-1.47%
1.75	1.28%	33.62	34.12	-1.47%
2.00	1.47%	33.72	34.22	-1.47%
2.25	1.65%	33.81	34.32	-1.47%
2.50	1.83%	33.91	34.41	-1.47%
2.75	2.01%	34.00	34.51	-1.47%
3.00	2.19%	34.10	34.61	-1.47%
3.25	2.37%	34.19	34.71	-1.47%
3.50	2.55%	34.29	34.80	-1.47%
3.75	2.73%	34.38	34.90	-1.47%
4.00	2.90%	34.48	35.00	-1.48%
4.25	3.08%	34.57	35.09	-1.48%
4.50	3.26%	34.67	35.19	-1.48%
4.75	3.43%	34.76	35.29	-1.49%
5.00	3.61%	34.85	35.38	-1.49%
5.25	3.79%	34.95	35.48	-1.50%
5.50	3.96%	35.04	35.58	-1.50%
5.75	4.14%	35.13	35.67	-1.51%
6.00	4.31%	35.23	35.77	-1.51%
6.25	4.49%	35.32	35.86	-1.52%
6.50	4.66%	35.41	35.96	-1.53%
6.75	4.83%	35.50	36.05	-1.53%
7.00	5.01%	35.59	36.15	-1.54%
7.25	5.18%	35.68	36.24	-1.55%
7.50	5.35%	35.77	36.34	-1.56%
7.75	5.52%	35.87	36.44	-1.56%
8.00	5.70%	35.96	36.53	-1.57%
8.25	5.87%	36.05	36.63	-1.58%
8.50	6.04%	36.14	36.72	-1.59%
8.75	6.21%	36.23	36.81	-1.60%

Table D-1 – *Continued*

Actuator Displacement	Inter-Story Drift	Brace Angle		
		Test	Real	% Difference
9.00	6.38%	36.32	36.91	-1.61%
9.25	6.55%	36.40	37.00	-1.62%
9.50	6.72%	36.49	37.10	-1.63%
9.75	6.89%	36.58	37.19	-1.64%
10.00	7.06%	36.67	37.29	-1.65%

Table D-2: Prototype-Test Conversion Table for Specimen 2

Actuator Displacement	Inter-Story Drift	Brace Angle		
		Test	Real	% Difference
-9.75	-6.84%	29.23	29.70	-1.58%
-9.50	-6.65%	29.34	29.79	-1.52%
-9.25	-6.47%	29.44	29.88	-1.46%
-9.00	-6.28%	29.54	29.96	-1.41%
-8.75	-6.10%	29.64	30.05	-1.35%
-8.50	-5.91%	29.74	30.13	-1.30%
-8.25	-5.73%	29.84	30.22	-1.25%
-8.00	-5.55%	29.94	30.30	-1.20%
-7.75	-5.37%	30.04	30.39	-1.15%
-7.50	-5.18%	30.14	30.47	-1.10%
-7.25	-5.00%	30.24	30.56	-1.05%
-7.00	-4.82%	30.33	30.64	-1.00%
-6.75	-4.64%	30.43	30.73	-0.96%
-6.50	-4.46%	30.53	30.81	-0.91%
-6.25	-4.29%	30.63	30.90	-0.87%
-6.00	-4.11%	30.72	30.98	-0.83%
-5.75	-3.93%	30.82	31.06	-0.78%
-5.50	-3.75%	30.92	31.15	-0.74%
-5.25	-3.58%	31.01	31.23	-0.70%
-5.00	-3.40%	31.11	31.31	-0.66%
-4.75	-3.23%	31.20	31.40	-0.63%
-4.50	-3.05%	31.29	31.48	-0.59%
-4.25	-2.88%	31.39	31.56	-0.55%
-4.00	-2.70%	31.48	31.65	-0.52%
-3.75	-2.53%	31.58	31.73	-0.48%
-3.50	-2.36%	31.67	31.81	-0.45%
-3.25	-2.19%	31.76	31.89	-0.41%
-3.00	-2.02%	31.85	31.97	-0.38%
-2.75	-1.84%	31.94	32.06	-0.35%
-2.50	-1.67%	32.04	32.14	-0.32%
-2.25	-1.50%	32.13	32.22	-0.29%
-2.00	-1.34%	32.22	32.30	-0.26%
-1.75	-1.17%	32.31	32.38	-0.23%
-1.50	-1.00%	32.40	32.46	-0.20%

Table D-2 – *Continued*

Actuator Displacement	Inter-Story Drift	Brace Angle		
		Test	Real	% Difference
-1.25	-0.83%	32.49	32.55	-0.17%
-1.00	-0.66%	32.58	32.63	-0.15%
-0.75	-0.50%	32.67	32.71	-0.12%
-0.50	-0.33%	32.76	32.79	-0.10%
-0.25	-0.17%	32.85	32.87	-0.07%
0.00	0.00%	32.93	32.95	-0.05%
0.25	0.16%	33.02	33.03	-0.02%
0.50	0.33%	33.11	33.11	0.00%
0.75	0.49%	33.20	33.19	0.02%
1.00	0.65%	33.28	33.27	0.04%
1.25	0.82%	33.37	33.35	0.06%
1.50	0.98%	33.46	33.43	0.08%
1.75	1.14%	33.54	33.51	0.10%
2.00	1.30%	33.63	33.59	0.12%
2.25	1.47%	33.72	33.67	0.14%
2.50	1.63%	33.80	33.75	0.16%
2.75	1.79%	33.89	33.83	0.17%
3.00	1.95%	33.97	33.91	0.19%
3.25	2.10%	34.06	33.99	0.21%
3.50	2.26%	34.14	34.06	0.22%
3.75	2.42%	34.22	34.14	0.24%
4.00	2.58%	34.31	34.22	0.25%
4.25	2.74%	34.39	34.30	0.27%
4.50	2.89%	34.48	34.38	0.28%
4.75	3.05%	34.56	34.46	0.29%
5.00	3.21%	34.64	34.54	0.31%
5.25	3.36%	34.72	34.61	0.32%
5.50	3.52%	34.81	34.69	0.33%
5.75	3.67%	34.89	34.77	0.34%
6.00	3.83%	34.97	34.85	0.35%
6.25	3.98%	35.05	34.92	0.36%
6.50	4.13%	35.13	35.00	0.37%
6.75	4.29%	35.21	35.08	0.38%
7.00	4.44%	35.29	35.16	0.39%
7.25	4.59%	35.37	35.23	0.40%
7.50	4.74%	35.45	35.31	0.41%
7.75	4.90%	35.53	35.39	0.41%
8.00	5.05%	35.61	35.47	0.42%
8.25	5.20%	35.69	35.54	0.43%
8.50	5.35%	35.77	35.62	0.43%
8.75	5.50%	35.85	35.70	0.44%
9.00	5.65%	35.93	35.77	0.44%
9.25	5.80%	36.01	35.85	0.45%
9.50	5.95%	36.09	35.93	0.45%
9.75	6.09%	36.17	36.00	0.46%
10.00	6.24%	36.24	36.08	0.46%

Appendix E. Prototype Brace Hysteresis Development

The relationship between deformation and brace force is dependent upon the brace properties. In previous tests, buckling-restrained braces (BRBs) have shown hysteretic behavior (as described in Chapter 1); in other words, as displacements have been applied in a cyclic fashion, the brace forces change due to the strain hardening that occurred in previous cycles. The hysteretic behavior needs to be predicted in order to estimate the displacement-force relationship.

The main difficultly that lies in predicting hysteretic behavior is that every BRB has different properties, including the yield length, core cross-section area, and yield stress. The combination of these properties affects the relationship between displacements and forces in the brace; therefore, unless a brace of almost exactly the same properties has been tested, it is difficult to know how the BRB will behavior unless an accurate method for predicting it can be developed. The basic shape is straightforward, and the displacements are given, but the forces are not as easy to determine due to strain hardening and residual strain.

E.1 Hysteretic Behavior Estimation Using Multiple Stress-Strain Relationships

To account for strain hardening effects, a hysteretic behavior estimation method was developed wherein the cyclic frame displacement protocol is used to predict the

cyclic stress-strain behavior of the prototype brace. The method was applied to the test specimens and is described in the following paragraphs.

First, the frame displacements were translated into brace displacements by using the brace yield stress, brace yield length, and frame dimensions (this process is explained in Appendix F and the results for the two specimens are given in Appendix G).

Then, the stress-strain relationship of the prototype brace was estimated using stress-strain data from cyclic coupon testing (11). In order to account for strain hardening, the stress-strain relationships at four different levels (i.e. initial, low, medium, and high) of strain were obtained (see Figures E-1). Each relationship consisted of a positive half-cycle and a negative half-cycle, and each level was assigned a particular strain threshold (see Table E-1).

At the start of the protocol, the brace was assigned the *initial* strain relationship. Stresses were determined by following this relationship through the protocol cycles (i.e. up to the maximum strain of the cycle and then down to the minimum strain) until the initial strain threshold was exceeded, at which point the brace began to follow the *low* strain relationship in a similar manner. As each successive threshold was exceeded, the next strain relationship level was applied to the brace. The brace followed the appropriate relationships until the end of the protocol, and in this way, a stress-strain relationship was developed that incorporated strain hardening.

The brace core area was then used to translate the strains into corresponding brace forces. To check the results, the hysteretic behavior estimation method was followed using properties of previously tested buckling-restrained braces (3). In comparing the estimation results with the actual test data, it was determined that the estimation gave

satisfactory results, as shown in Figures E-2 through E-7; in these figures, the actual hysteretic behaviors are shown in green and the estimated behaviors are in blue.

E.2 Equivalent Spring Properties for Hysteretic Brace Behavior Modeling

In addition to the estimation method performed using multiple stress-strain relationships, equivalent spring properties were developed to provide a simpler modeling method. The tradeoff is a lower level of accuracy, and for particular situations, the increased simplicity is worth it. The manner by which the method can be implemented is explained below.

First of all, the yield force ($P_{y,brace}$) is calculated using the brace area (A_{brace}) and brace yield stress ($F_{y,brace}$), and the brace yield length ($L_{BRB,yield}$) is estimated using bay dimensions, including the bay length (L_{bay}), bay height (H_{bay}), beam depth (d_{beam}), and an estimated brace core extension length ($L_{BRB,core}$). The calculations are as follows:

$$P_{y,brace} = A_{brace} * F_{y,brace} \tag{E.1}$$

$$L_{BRB,yield} = ((L_{bay}^2 + (H_{bay} - d_{beam})^2)^{½} - 2* L_{BRB,core}) * 0.85 \tag{E.2}$$

The brace yield length ($L_{BRB,yield}$) equation includes two portions: the estimated buckling-restrained brace sleeve length and a factor to account for the transition segment within the sleeve length. Furthermore, the brace core extension length ($L_{BRB,core}$) can be obtained from a brace manufacturer or estimated based on the number of bolts used to connect the brace to the gusset plate ($n_{BRB,bolts}$). The estimation equation is as follows:

$$L_{BRB,core} = 18.5 \text{ in} + 2 * n_{BRB,bolts} \tag{E.3}$$

The next step involves equivalent spring properties that correspond to the backbone curve of the cyclic force-displacement relationship. The backbone curve was developed using stress-strain data from cyclic testing of steel coupons (11) and consists of four segments (see Figure E-8). The four segments are specified by yield force factors (f_1 through f_4) and slopes (k_1 through k_4). The backbone curve can be correlated to a particular brace by multiplying the yield force factors by the brace yield force and determining the initial slope (k_1) using brace core section properties. Young's Modulus (E) is one such property, and it is equal to 29,000 ksi. The equations for the force factors and slopes are as follows:

$$f_1 = 1.10 \tag{E.4}$$

$$f_2 = 1.60 \tag{E.5}$$

$$f_3 = 1.95 \tag{E.6}$$

$$f_4 = 2.50 \tag{E.7}$$

$$k_1 = E * A_{brace} / L_{BRB,yield} \tag{E.8}$$

$$k_2 = k_1 * 0.128 \tag{E.9}$$

$$k_3 = k_1 * 0.035 \tag{E.10}$$

$$k_4 = k_1 * 0.006 \tag{E.11}$$

Figures E-9 through E-12 compare the hysteretic estimations (shown in blue) with actual behaviors (shown in green) of previously tested buckling-restrained braces (3).

Table E-1: Strain Level Thresholds

Level of Strain	Strain Threshold
Initial	0.005 in/in
Low	0.020 in/in
Medium	0.035 in/in
High	0.050 in/in

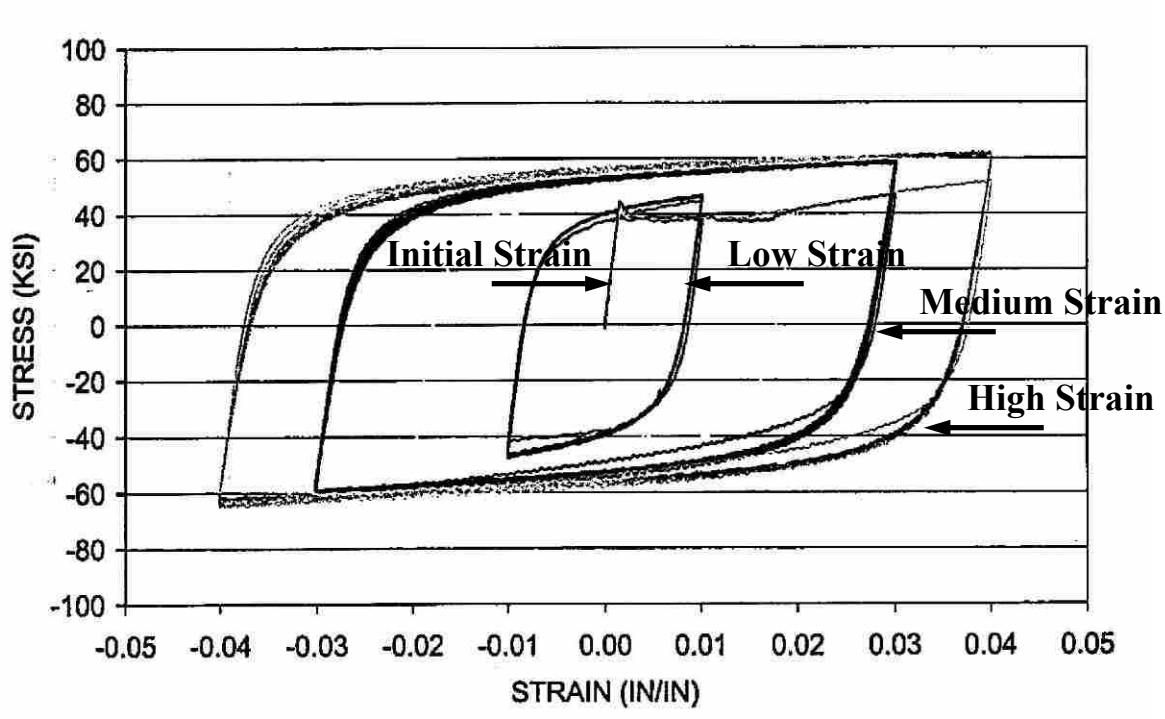

Figure E-1 Cyclic Stress-Strain Behavior of Steel D (Figure 10D) (11)

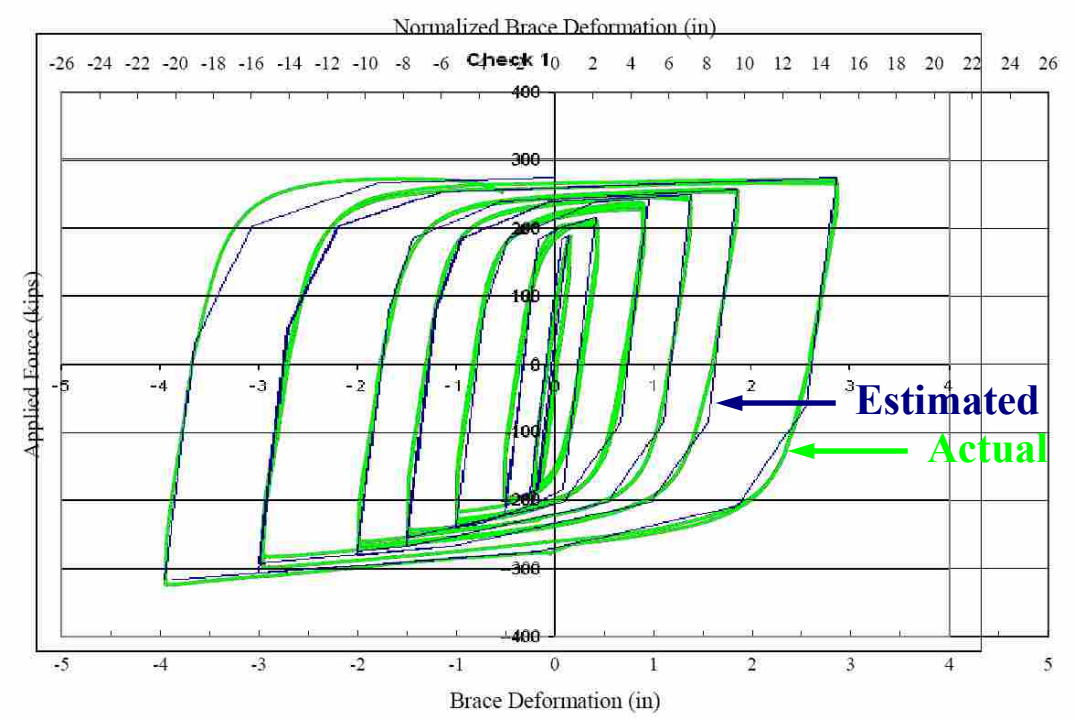

Figure E-2 Hysteretic Behavior of Specimen E1 – Strain Level Method (3)

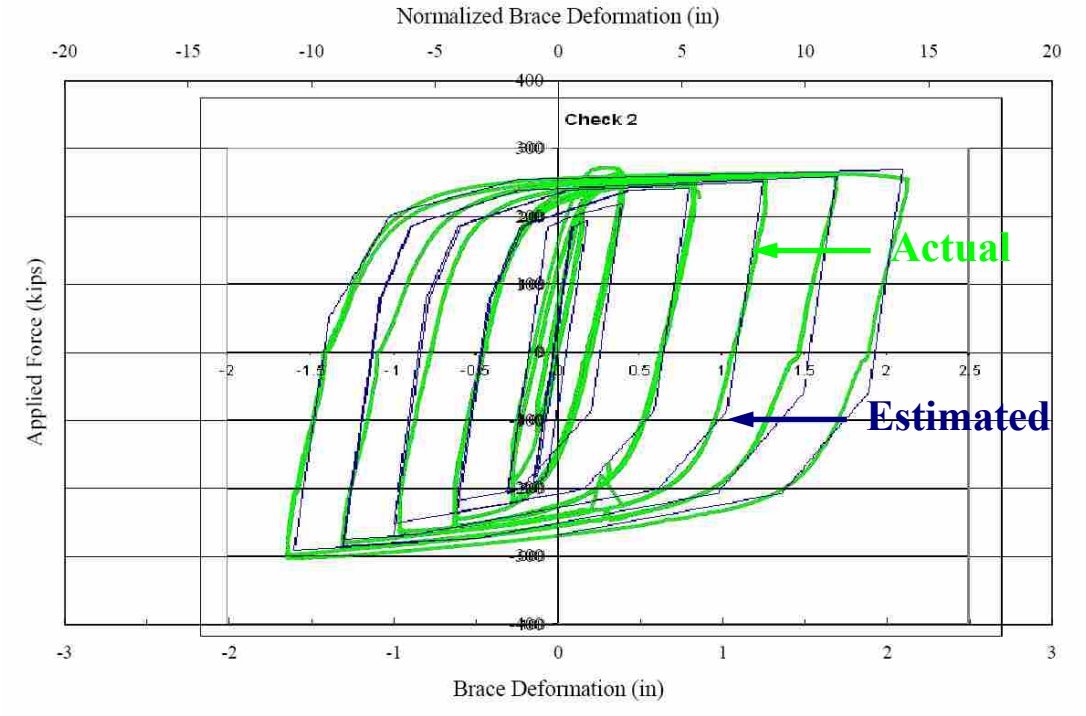

Figure E-3 Hysteretic Behavior of Specimen E2 – Strain Level Method (3)

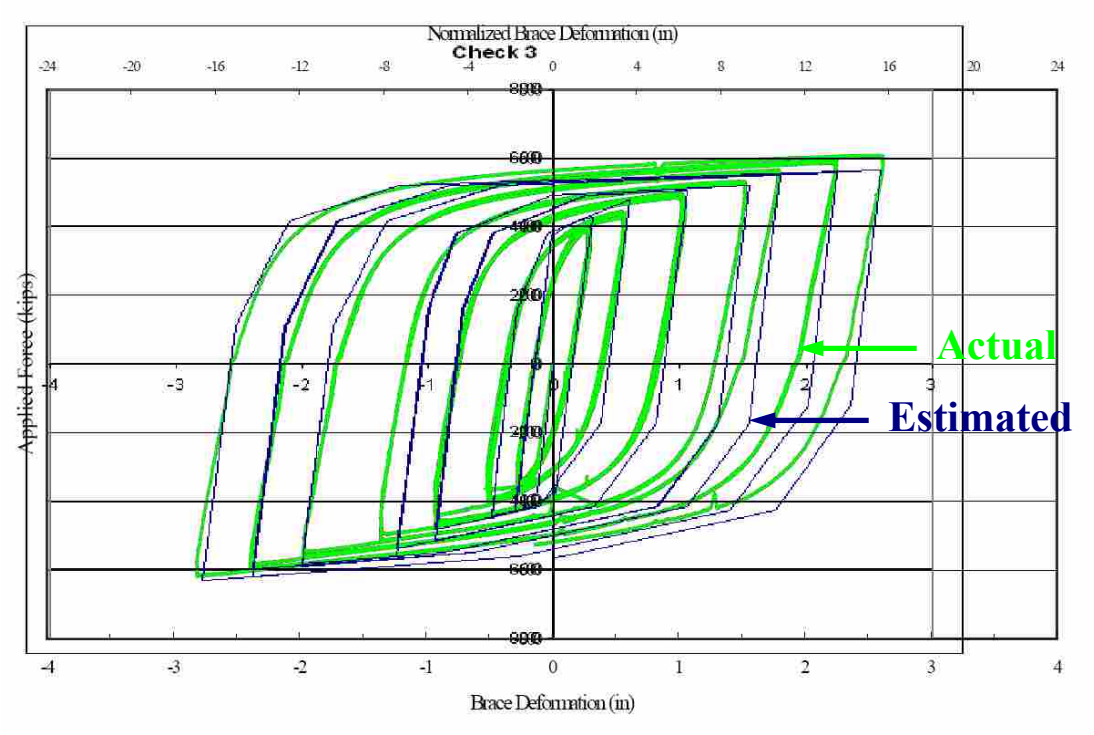

Figure E-4 Hysteretic Behavior of Specimen E3 – Strain Level Method (3)

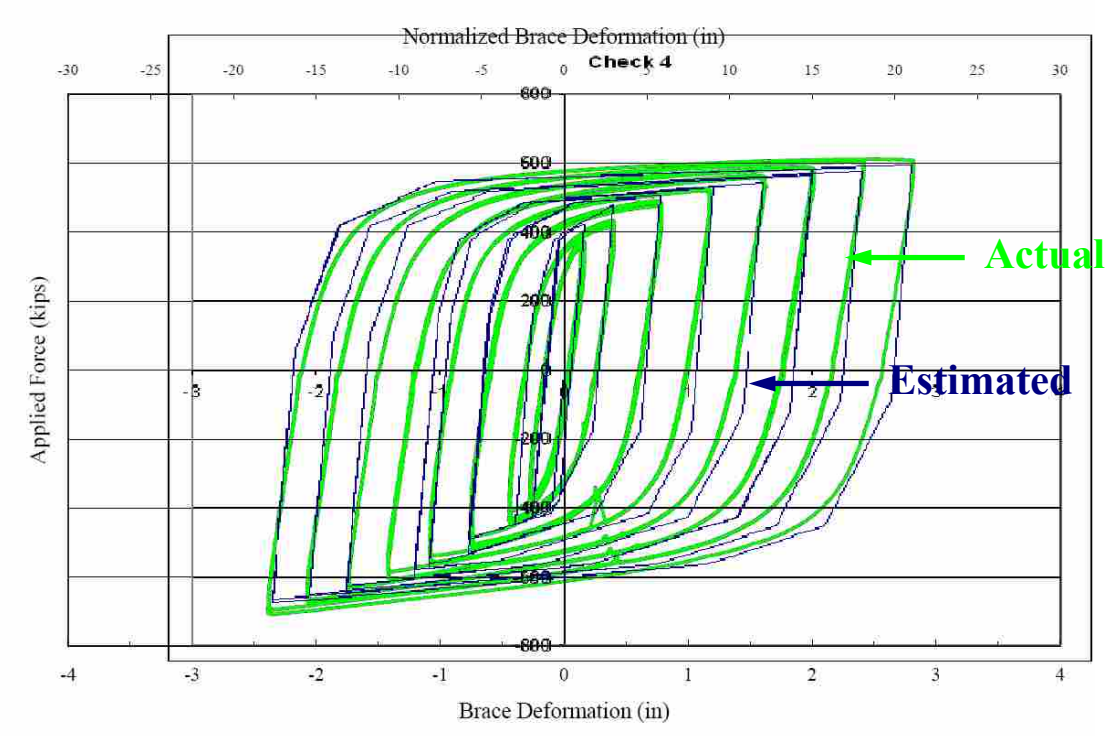

Figure E-5 Hysteretic Behavior of Specimen E4 – Strain Level Method (3)

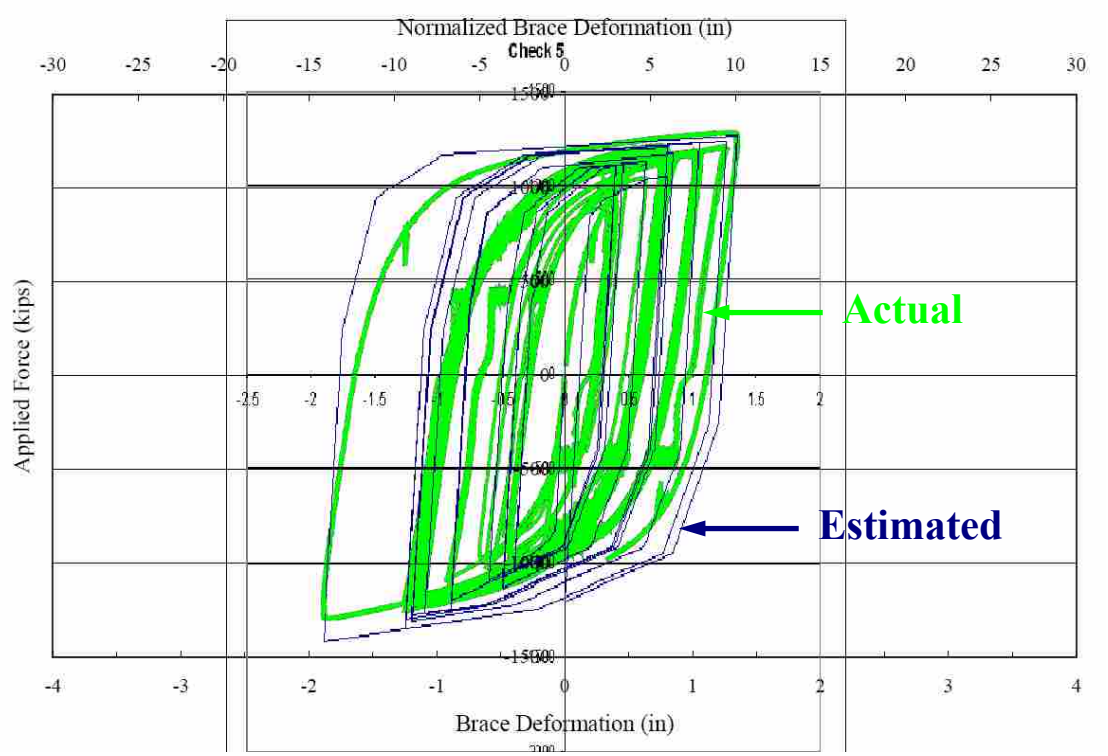

Figure E-6 Hysteretic Behavior of Specimen E5 – Strain Level Method (3)

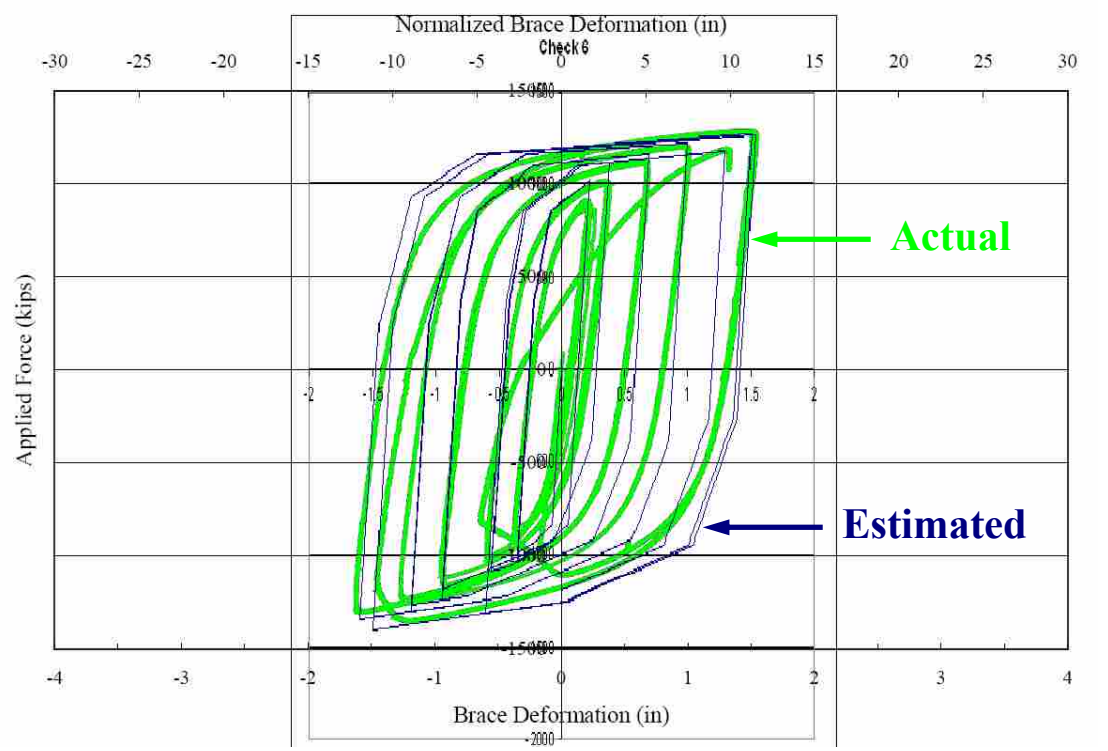

Figure E-7 Hysteretic Behavior of Specimen E6 – Strain Level Method (3)

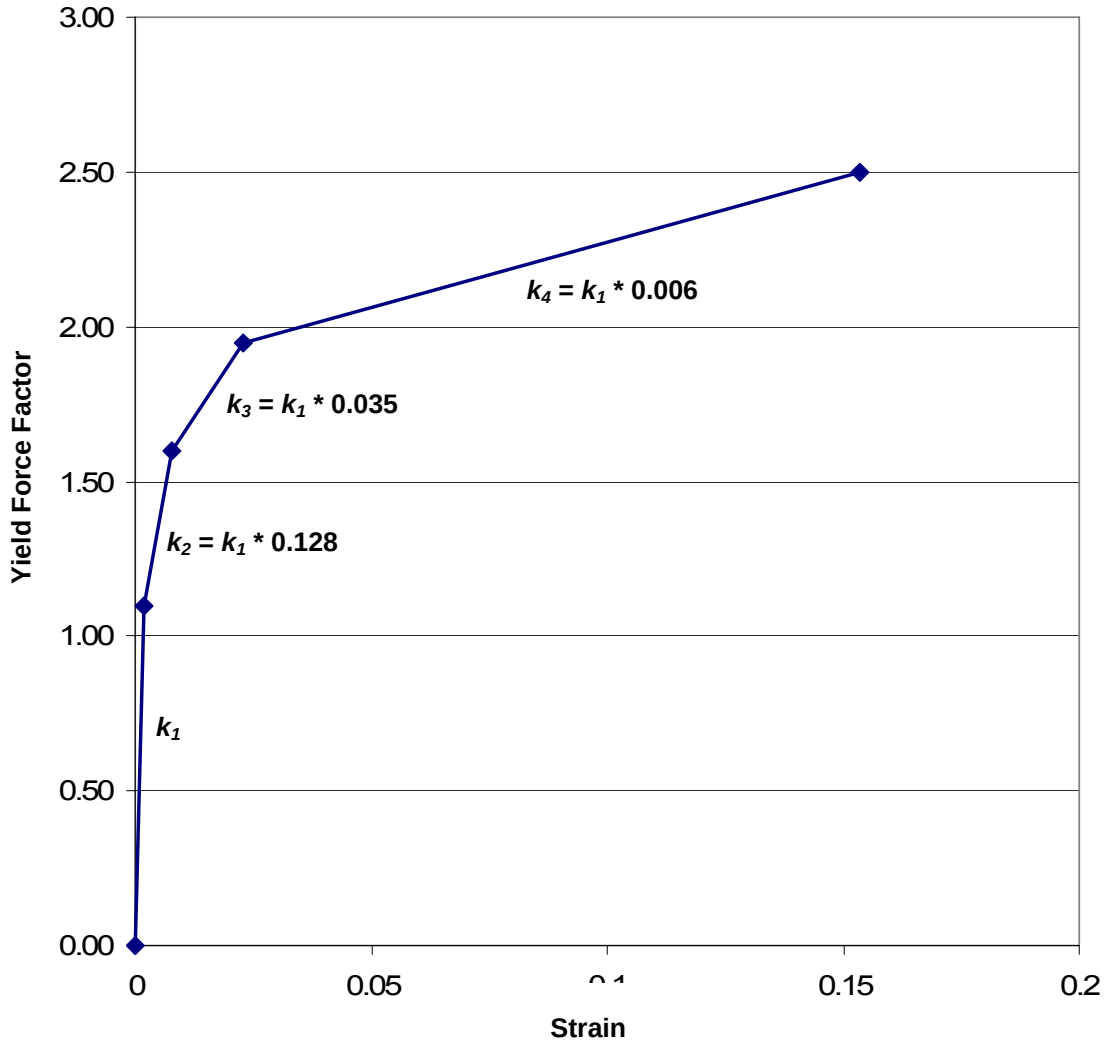

Figure E-8 Equivalent Spring Backbone Curve

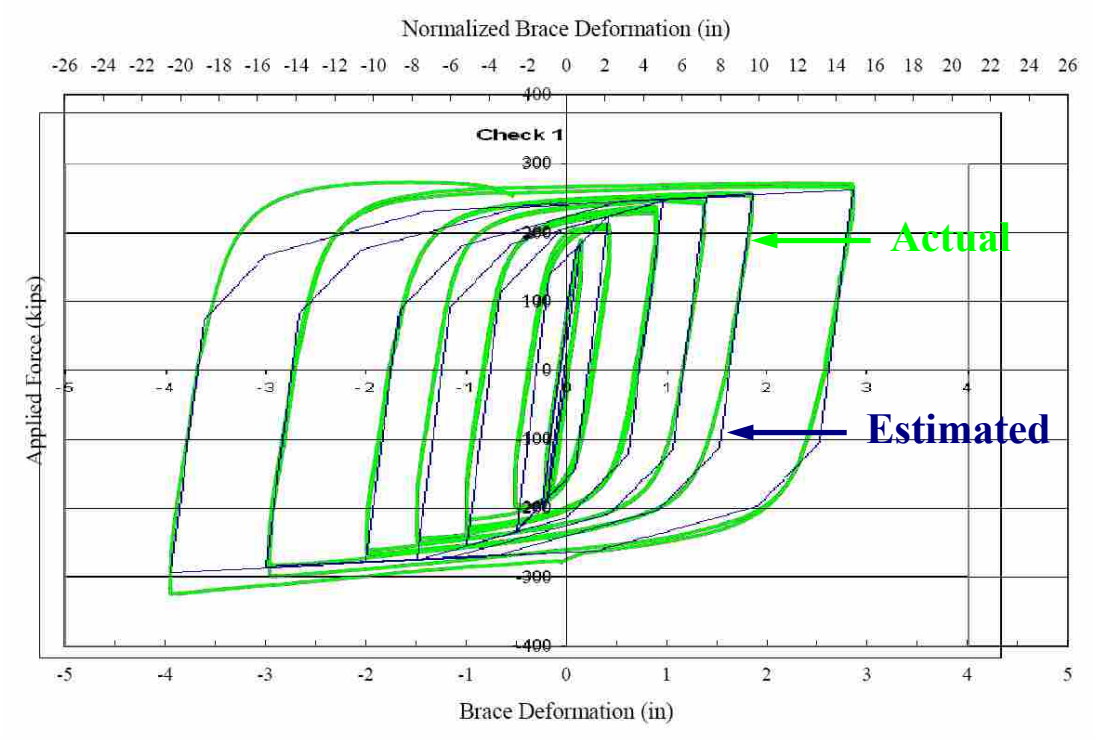

Figure E-9 Hysteretic Behavior of Specimen E1 – Spring Method (3)

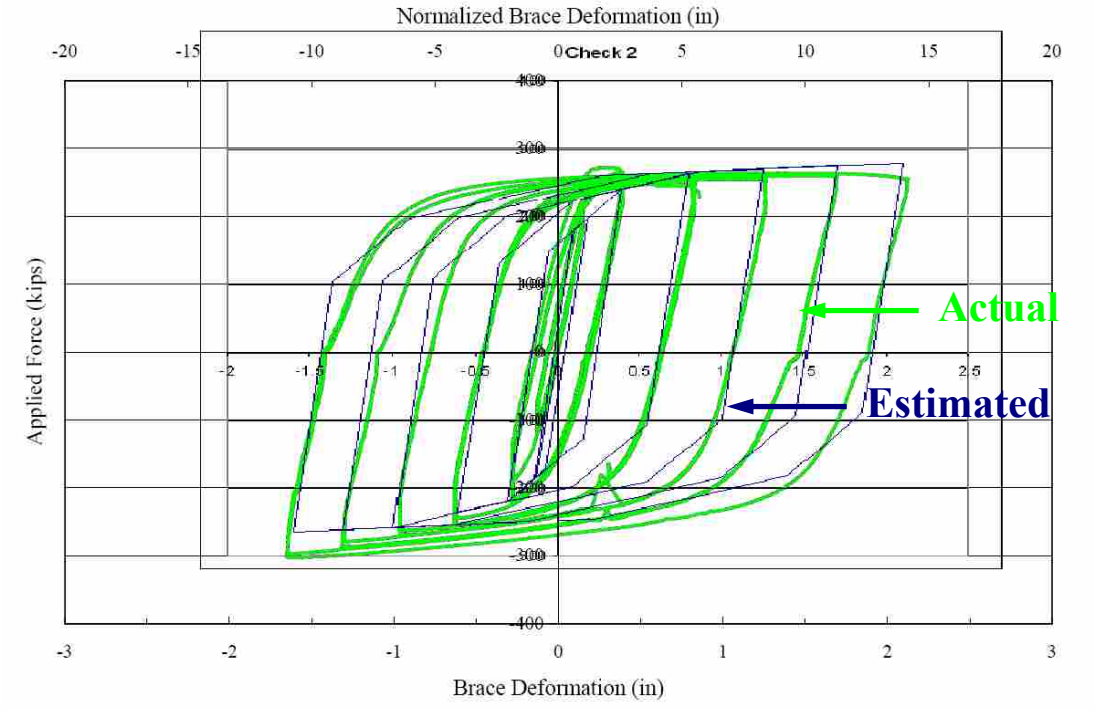

Figure E-10 Hysteretic Behavior of Specimen E2 – Spring Method (3)

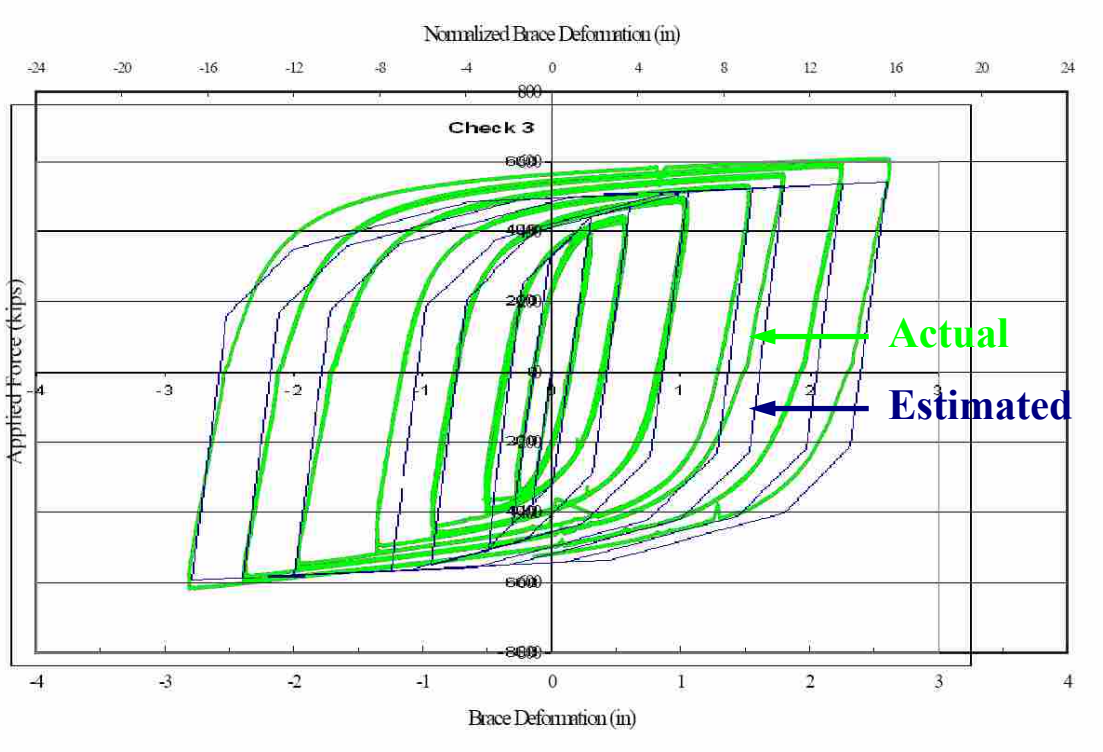

Figure E-11 Hysteretic Behavior of Specimen E3 – Spring Method (3)

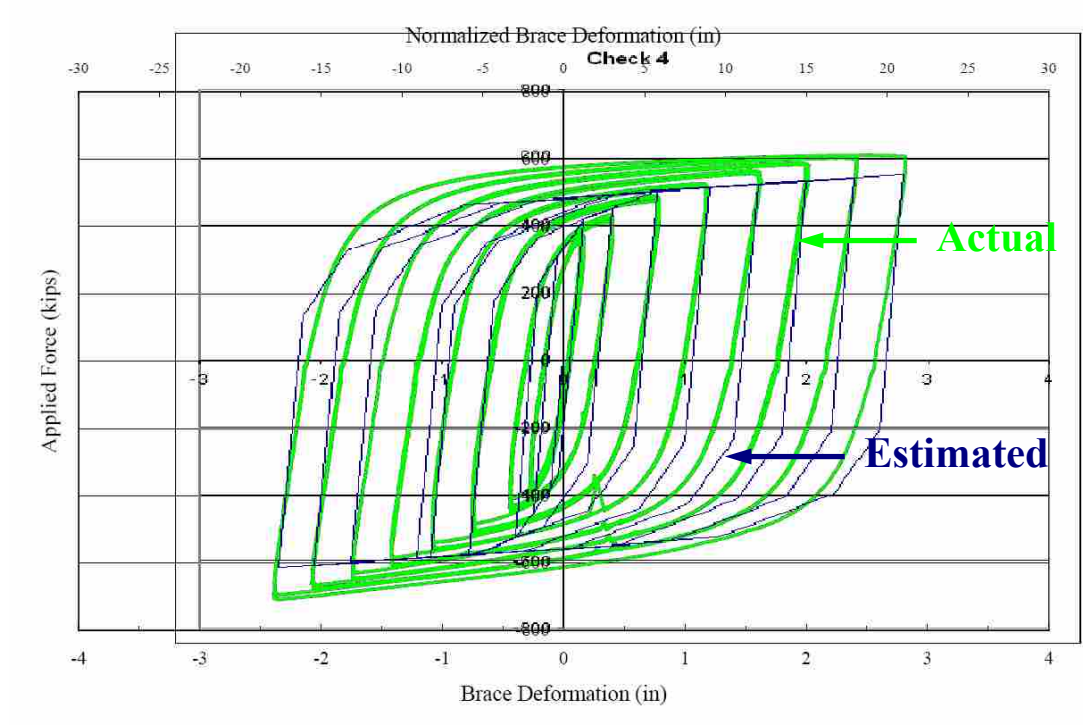

Figure E-12 Hysteretic Behavior of Specimen E4 – Spring Method (3)

Appendix F. Loading Protocol Calculations

Calculations for the loading protocols involved brace deformation values

F.1 Brace Deformation Values

The variables used in the determination of the protocol are the brace deformation values estimated to occur at the first significant yielding of the prototype BRB (Δ_{by}) and the at the point when the prototype bay is at its design story drift (Δ_{bm}) (2). The initial yielding deformation is calculated based on yield stress (F_y), yield length (L_y), and Young's Modulus of steel (E):

$$F_y = 42 \text{ ksi} \tag{F.1}$$

$$L_y = 190 \text{ in.} \tag{F.2}$$

$$E = 29{,}000 \text{ ksi} \tag{F.3}$$

$$\Delta_{by} = L_y * F_y / E = 0.275 \text{ in.} \tag{F.4}$$

The design story drift deformation (Δ_{bm}) is determined using the geometry of the prototype frame when it is experiencing an inter-story drift (δ_{drift}) of 2% (see Figure F-1):

$$\Delta_{bm} = 2.590 \text{ in.} \tag{F.5}$$

Initially, the protocol was specified in terms of Δ_{by}. Then, a shift was made, and the focus was on Δ_{bm}. Having calculated both variables, their relationship can be found,

$$\Delta_{bm} / \Delta_{by} = 2.590 / 0.275 \quad => \quad \Delta_{bm} = \Delta_{by} * 9.418 \qquad \text{(F.6)}$$

Using this relationship, all the BRB deformations were found in terms of Δ_{by} in order to have a common point of comparison between the magnitudes of all protocol cycles.

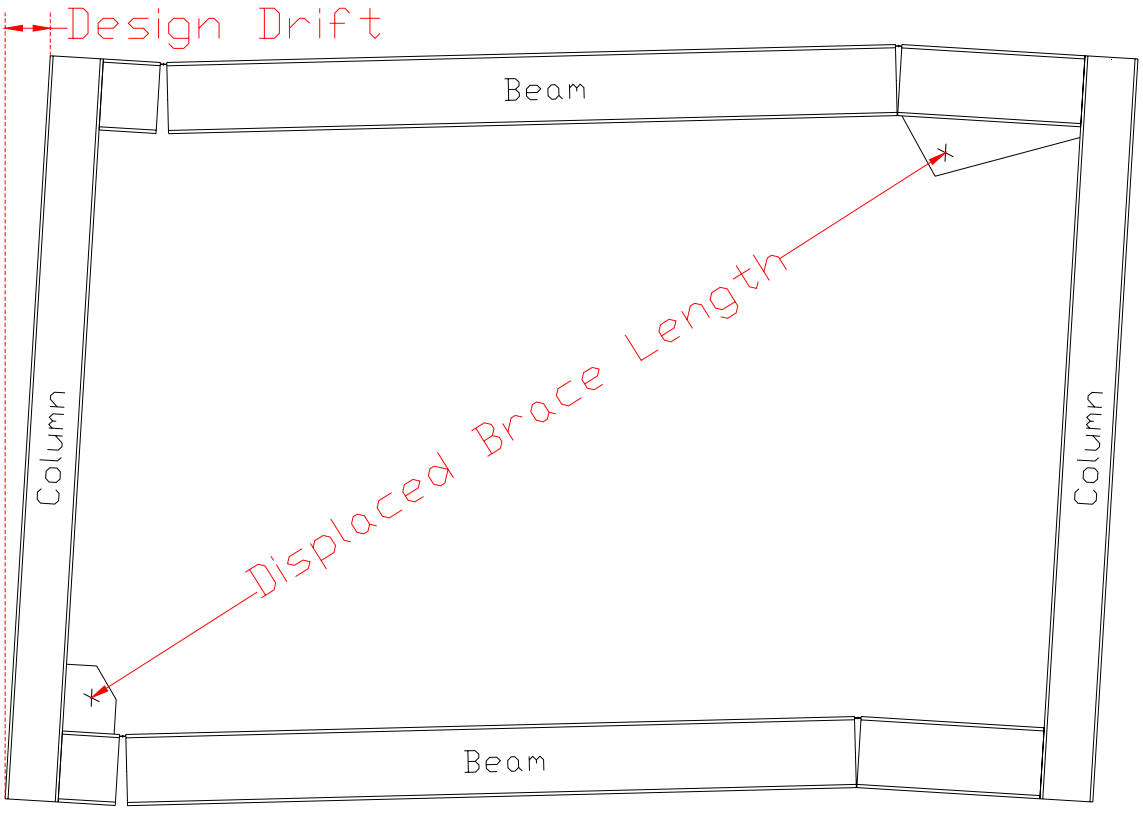

Figure F-1 Design Story Drift Deformation Geometry

Appendix G. Loading Protocols

The loading protocols are found in Table G-1 for Specimen 1 and in Table G-2 for Specimen 2.

Table G-1: Loading Protocols for Specimen 1

Half Cycle	Step	Drift	Actuator 1 Force (kip)	Actuator 2 Displacement (in.)	Loading Rate (kip/sec)	Step Time (sec)
	0	0.00%	0	0.00		
1A	1	-0.24%	200	-0.46	0.05	9.2
1B	2	0.24%	-200	0.46	0.05	18.4
2A	3	-0.24%	200	-0.46	0.05	18.4
2B	4	0.24%	-200	0.46	0.05	18.4
3A	5	-0.24%	200	-0.46	0.05	18.4
3B	6	0.24%	-200	0.46	0.05	18.4
4A	7	-0.24%	200	-0.46	0.05	18.4
4B	8	0.24%	-200	0.46	0.05	18.4
5A	9	-0.24%	200	-0.46	0.05	18.4
5B	10	0.24%	-200	0.46	0.05	18.4
6A	11	-0.24%	200	-0.46	0.05	18.4
6B	12	0.24%	-200	0.46	0.05	18.4
7A	13	-0.24%	200	-0.46	0.05	18.4
	14	-0.61%	220	-0.96	0.10	5.0
	15	-1.15%	232	-1.69	0.10	7.3
7B	16	-0.76%	-86	-0.97	0.05	14.4
	17	-0.35%	-202	-0.35	0.10	6.2
	18	0.99%	-251	1.49	0.10	18.4
8A	19	0.70%	94	0.89	0.05	12.0
	20	-0.18%	219	-0.38	0.10	12.7
	21	-1.15%	234	-1.69	0.10	13.1
8B	22	-0.75%	-86	-0.96	0.05	14.6
	23	-0.34%	-202	-0.34	0.10	6.2
	24	0.99%	-251	1.49	0.10	18.3

Table G-1 – *Continued*

Half Cycle	Step	Drift	Actuator 1 Force (kip)	Actuator 2 Displacement (in.)	Loading Rate (kip/sec)	Step Time (sec)
9A	25	0.70%	94	0.89	0.05	12.0
	26	-0.18%	219	-0.38	0.10	12.7
	27	-2.30%	261	-3.23	0.10	28.5
9B	28	-1.87%	-86	-2.44	0.05	15.8
	29	-1.46%	-202	-1.83	0.10	6.1
	30	-0.12%	-259	-0.01	0.10	18.2
	31	2.26%	-271	3.26	0.15	21.8
10A	32	1.82%	94	2.43	0.05	16.6
	33	0.95%	219	1.15	0.10	12.8
	34	-2.13%	288	-3.01	0.10	41.6
10B	35	-1.84%	-86	-2.40	0.05	12.2
	36	-1.43%	-202	-1.79	0.10	6.1
	37	-0.09%	-259	0.03	0.10	18.2
	38	2.26%	-271	3.26	0.15	21.5
11A	39	1.82%	94	2.43	0.05	16.6
	40	0.95%	219	1.15	0.10	12.8
	41	-2.13%	291	-3.01	0.10	41.6
	42	-3.47%	300	-4.76	0.15	11.7
11B	43	-3.03%	-56	-3.97	0.05	15.8
	44	-2.24%	-221	-2.85	0.10	11.2
	45	-0.61%	-276	-0.66	0.10	21.9
	46	3.39%	-284	4.85	0.15	36.7
12A	47	2.96%	64	4.04	0.05	16.2
	48	1.88%	219	2.43	0.10	16.1
	49	-1.14%	291	-1.71	0.10	41.4
	50	-3.47%	309	-4.77	0.15	20.4
12B	51	-3.01%	-56	-3.95	0.05	16.4
	52	-2.23%	-221	-2.83	0.10	11.2
	53	-0.60%	-276	-0.64	0.10	21.9
	54	3.39%	-284	4.85	0.15	36.6
13A	55	2.96%	64	4.04	0.05	16.2
	56	1.88%	219	2.43	0.10	16.1
	57	-1.14%	291	-1.71	0.10	41.4
	58	-4.64%	319	-6.26	0.15	30.3
13B	59	-4.17%	-56	-5.43	0.05	16.6
	60	-3.38%	-221	-4.32	0.10	11.1
	61	-1.73%	-276	-2.15	0.10	21.7
	62	4.49%	-297	6.43	0.15	57.2
14A	63	4.06%	64	5.60	0.05	16.6
	64	2.99%	226	3.98	0.10	16.2
	65	0.00%	298	-0.19	0.10	41.7
	66	-4.64%	331	-6.27	0.15	40.5

Table G-1 – *Continued*

Half Cycle	Step	Drift	Actuator 1 Force (kip)	Actuator 2 Displacement (in.)	Loading Rate (kip/sec)	Step Time (sec)
14B	67	-4.16%	-56	-5.42	0.05	17.0
	68	-3.37%	-221	-4.31	0.10	11.1
	69	-1.72%	-276	-2.13	0.10	21.8
	70	4.49%	-297	6.43	0.15	57.1
15A	71	4.06%	64	5.60	0.05	16.6
	72	2.99%	226	3.98	0.10	16.2
	73	0.00%	298	-0.19	0.10	41.7
	74	-5.83%	340	-7.75	0.15	50.4
15B	75	-5.33%	-56	-6.89	0.05	17.2
	76	-4.53%	-221	-5.79	0.10	11.0
	77	-2.87%	-276	-3.64	0.10	21.5
	78	5.60%	-304	8.04	0.15	77.9
16A	79	5.17%	64	7.19	0.05	17.0
	80	4.10%	226	5.55	0.10	16.4
	81	1.12%	298	1.34	0.10	42.1
	82	-5.83%	350	-7.76	0.15	60.7
16B	83	-5.32%	-56	-6.88	0.05	17.6
	84	-4.51%	-221	-5.77	0.10	11.1
	85	-2.86%	-276	-3.62	0.10	21.5
	86	5.60%	-304	8.04	0.15	77.7
17A	87	5.17%	64	7.19	0.05	17.0
	88	4.10%	226	5.55	0.10	16.4
	89	1.12%	298	1.34	0.10	42.1
	90	-7.01%	359	-9.23	0.15	70.5
17B	91	-6.52%	-32	-8.38	0.05	17.0
	92	-5.59%	-222	-7.12	0.10	12.6
	93	-3.56%	-289	-4.51	0.10	26.1
	94	6.70%	-317	9.65	0.15	94.4
18A	95	6.27%	49	8.81	0.05	16.8
	96	4.98%	239	6.81	0.10	20.0
	97	2.58%	297	3.35	0.10	34.6
	98	-7.01%	359	-9.23	0.15	83.9
18B	99	-6.52%	-32	-8.37	0.05	17.2
	100	-5.59%	-222	-7.12	0.10	12.5
	101	-3.56%	-289	-4.51	0.10	26.1
	102	6.70%	-317	9.65	0.15	94.4
19A	103	6.27%	49	8.81	0.05	16.8
	104	4.98%	239	6.81	0.10	20.0
	105	2.58%	297	3.35	0.10	34.6
	106	0.00%	314	-0.20	0.15	23.7

Table G-2: Loading Protocols for Specimen 2

Half Cycle	Step	Drift	Actuator 1 Force (kip)	Actuator 2 Displacement (in.)	Loading Rate (kip/sec)	Step Time (sec)
	0	0.00%	0	0.00		
1A	1	-0.07%	66	-0.14	0.01	14.0
1B	2	0.07%	-60	0.13	0.01	27.0
2A	3	-0.07%	66	-0.14	0.01	27.0
2B	4	0.07%	-60	0.13	0.01	27.0
3A	5	-0.07%	66	-0.14	0.01	27.0
3B	6	0.07%	-60	0.13	0.01	27.0
4A	7	-0.11%	102	-0.22	0.01	35.0
4B	8	0.11%	-96	0.20	0.01	42.0
5A	9	-0.11%	102	-0.22	0.01	42.0
5B	10	0.11%	-96	0.20	0.01	42.0
6A	11	-0.11%	102	-0.22	0.01	42.0
6B	12	0.11%	-96	0.20	0.01	42.0
7A	13	-0.22%	200	-0.44	0.02	32.0
7B	14	0.22%	-200	0.42	0.02	43.0
8A	15	-0.22%	200	-0.44	0.02	43.0
8B	16	0.22%	-200	0.42	0.02	43.0
9A	17	-0.22%	200	-0.44	0.02	43.0
9B	18	0.22%	-200	0.42	0.02	43.0
10A	19	-0.22%	200	-0.44	0.02	43.0
10B	20	0.22%	-200	0.42	0.02	43.0
11A	21	-0.22%	200	-0.44	0.02	43.0
11B	22	0.22%	-200	0.42	0.02	43.0
12A	23	-0.22%	200	-0.44	0.02	43.0
12B	24	0.22%	-200	0.42	0.02	43.0
13A	25	-0.22%	200	-0.44	0.02	43.0
	26	-1.05%	237	-1.69	0.04	31.3
13B	27	-0.69%	-86	-1.00	0.02	34.5
	28	-0.32%	-202	-0.39	0.04	15.3
	29	1.03%	-260	1.69	0.08	26.0
14A	30	0.64%	94	0.92	0.02	38.5
	31	-0.16%	219	-0.35	0.04	31.8
	32	-1.05%	242	-1.69	0.08	16.8
14B	33	-0.68%	-86	-0.99	0.02	35.0
	34	-0.31%	-202	-0.38	0.04	15.3
	35	1.03%	-260	1.69	0.08	25.9
15A	36	0.64%	94	0.92	0.02	38.5
	37	-0.16%	219	-0.35	0.04	31.8
	38	-2.11%	269	-3.28	0.08	36.6
15B	39	-1.72%	-86	-2.52	0.02	38.0
	40	-1.34%	-202	-1.91	0.04	15.3
	41	-0.11%	-259	-0.04	0.08	23.4
	42	2.05%	-273	3.29	0.12	27.8

Table G-2 – *Continued*

Half Cycle	Step	Drift	Actuator 1 Force (kip)	Actuator 2 Displacement (in.)	Loading Rate (kip/sec)	Step Time (sec)
16A	43	1.65%	94	2.49	0.02	40.0
	44	0.86%	219	1.20	0.04	32.3
	45	-2.11%	293	-3.29	0.08	56.1
16B	46	-1.69%	-86	-2.48	0.02	40.5
	47	-1.31%	-202	-1.87	0.04	15.3
	48	-0.08%	-259	0.00	0.08	23.4
	49	2.05%	-273	3.29	0.12	27.4
17A	50	1.65%	94	2.49	0.02	40.0
	51	0.86%	219	1.20	0.04	32.3
	52	-1.95%	291	-3.05	0.08	53.1
	53	-3.18%	303	-4.84	0.12	14.9
17B	54	-2.78%	-56	-4.08	0.02	38.0
	55	-2.06%	-221	-2.96	0.04	28.0
	56	-0.56%	-276	-0.71	0.08	28.1
	57	3.06%	-290	4.90	0.12	46.8
18A	58	2.67%	64	4.12	0.02	39.0
	59	1.70%	226	2.51	0.04	40.3
	60	-1.04%	298	-1.71	0.08	52.8
	61	-3.18%	316	-4.85	0.12	26.2
18B	62	-2.76%	-56	-4.05	0.02	40.0
	63	-2.04%	-221	-2.93	0.04	28.0
	64	-0.54%	-276	-0.69	0.08	28.0
	65	3.06%	-290	4.90	0.12	46.6
19A	66	2.67%	64	4.12	0.02	39.0
	67	1.70%	226	2.51	0.04	40.3
	68	-1.04%	298	-1.71	0.08	52.8
	69	-4.27%	325	-6.39	0.12	39.0
19B	70	-3.83%	-56	-5.58	0.02	40.5
	71	-3.10%	-221	-4.47	0.04	27.8
	72	-1.59%	-276	-2.24	0.08	27.9
	73	4.05%	-298	6.51	0.12	72.9
20A	74	3.67%	64	5.72	0.02	39.5
	75	2.71%	226	4.10	0.04	40.5
	76	0.00%	298	-0.15	0.08	53.1
	77	-4.27%	334	-6.40	0.12	52.1
20B	78	-3.82%	-56	-5.57	0.02	41.5
	79	-3.09%	-221	-4.45	0.04	28.0
	80	-1.57%	-276	-2.22	0.08	27.9
	81	4.05%	-298	6.51	0.12	72.8
21A	82	3.67%	64	5.72	0.02	39.5
	83	2.71%	226	4.10	0.04	40.5
	84	0.00%	298	-0.15	0.08	53.1
	85	-5.37%	343	-7.93	0.12	64.8

Table G-2 – *Continued*

Half Cycle	Step	Drift	Actuator 1 Force (kip)	Actuator 2 Displacement (in.)	Loading Rate (kip/sec)	Step Time (sec)
21B	86	-4.91%	-56	-7.09	0.02	42.0
	87	-4.16%	-221	-5.98	0.04	27.8
	88	-2.63%	-276	-3.76	0.08	27.8
	89	5.03%	-306	8.12	0.12	99.0
22A	90	4.65%	64	7.31	0.02	40.5
	91	3.70%	226	5.68	0.04	40.8
	92	1.02%	298	1.41	0.08	53.4
	93	-5.37%	352	-7.94	0.12	77.9
22B	94	-4.89%	-56	-7.07	0.02	43.5
	95	-4.16%	-221	-5.97	0.04	27.5
	96	-2.62%	-276	-3.75	0.08	27.8
	97	5.03%	-306	8.12	0.12	98.9
23A	98	4.65%	64	7.31	0.02	40.5
	99	3.70%	226	5.68	0.04	40.8
	100	1.02%	298	1.41	0.08	53.4
	101	-6.49%	361	-9.46	0.12	90.6
23B	102	-6.02%	-32	-8.63	0.02	41.5
	103	-5.16%	-222	-7.36	0.04	31.8
	104	-3.27%	-289	-4.67	0.08	33.6
	105	6.01%	-318	9.75	0.12	120.2
24A	106	5.62%	49	8.94	0.02	40.5
	107	4.48%	239	6.95	0.04	49.8
	108	2.33%	297	3.46	0.08	43.6
	109	-6.49%	362	-9.46	0.12	107.7
24B	110	-6.02%	-32	-8.63	0.02	41.5
	111	-5.16%	-222	-7.36	0.04	31.8
	112	-3.27%	-289	-4.67	0.08	33.6
	113	6.01%	-318	9.75	0.12	120.2
25A	114	5.62%	49	8.94	0.02	40.5
	115	4.48%	239	6.95	0.04	49.8
	116	2.33%	297	3.46	0.08	43.6
	117	-6.49%	362	-9.46	0.12	107.7
25B	118	-6.02%	-32	-8.63	0.02	41.5
	119	-5.16%	-222	-7.36	0.04	31.8
	120	-3.27%	-289	-4.67	0.08	33.6
	121	6.01%	-318	9.75	0.12	120.2
26A	122	5.62%	49	8.94	0.02	40.5
	123	4.48%	239	6.95	0.04	49.8
	124	2.33%	297	3.46	0.08	43.6
	125	-6.49%	362	-9.46	0.12	107.7
26B	126	-6.02%	-32	-8.63	0.02	41.5
	127	-5.16%	-222	-7.36	0.04	31.8
	128	-3.27%	-289	-4.67	0.08	33.6
	129	6.01%	-318	9.75	0.12	120.2

Table G-2 – *Continued*

Half Cycle	Step	Drift	Actuator 1 Force (kip)	Actuator 2 Displacement (in.)	Loading Rate (kip/sec)	Step Time (sec)
27A	130	5.62%	49	8.94	0.02	40.5
	131	4.48%	239	6.95	0.04	49.8
	132	2.33%	297	3.46	0.08	43.6
	133	-6.49%	362	-9.46	0.12	107.7
27B	134	-6.02%	-32	-8.63	0.02	41.5
	135	-5.16%	-222	-7.36	0.04	31.8
	136	-3.27%	-289	-4.67	0.08	33.6
	137	6.01%	-318	9.75	0.12	120.2
28A	138	5.62%	49	8.94	0.02	40.5
	139	4.48%	239	6.95	0.04	49.8
	140	2.33%	297	3.46	0.08	43.6
	141	-6.49%	362	-9.46	0.12	107.7
28B	142	-6.02%	-32	-8.63	0.02	41.5
	143	-5.16%	-222	-7.36	0.04	31.8
	144	-3.27%	-289	-4.67	0.08	33.6
	145	6.01%	-318	9.75	0.12	120.2
29A	146	5.62%	49	8.94	0.02	40.5
	147	4.48%	239	6.95	0.04	49.8
	148	2.33%	297	3.46	0.08	43.6
	149	-6.49%	362	-9.46	0.12	107.7
29B	150	-6.02%	-32	-8.63	0.02	41.5
	151	-5.16%	-222	-7.36	0.04	31.8
	152	-3.27%	-289	-4.67	0.08	33.6
	153	6.01%	-318	9.75	0.12	120.2
30A	154	5.62%	49	8.94	0.02	40.5
	155	4.48%	239	6.95	0.04	49.8
	156	2.33%	297	3.46	0.08	43.6
	157	-6.49%	362	-9.46	0.12	107.7
30B	158	-6.02%	-32	-8.63	0.02	41.5
	159	-5.16%	-222	-7.36	0.04	31.8
	160	-3.27%	-289	-4.67	0.08	33.6
	161	6.01%	-318	9.75	0.12	120.2
31A	162	5.62%	49	8.94	0.02	40.5
	163	4.48%	239	6.95	0.04	49.8
	164	2.33%	297	3.46	0.08	43.6
	165	-6.49%	362	-9.46	0.12	107.7
31B	166	-6.02%	-32	-8.63	0.02	41.5
	167	-5.16%	-222	-7.36	0.04	31.8
	168	-3.27%	-289	-4.67	0.08	33.6
	169	6.01%	-318	9.75	0.12	120.2
32A	170	5.62%	49	8.94	0.02	40.5
	171	4.48%	239	6.95	0.04	49.8
	172	2.33%	297	3.46	0.08	43.6
	173	-6.49%	362	-9.46	0.12	107.7

Table G-2 – *Continued*

Half Cycle	Step	Drift	Actuator 1 Force (kip)	Actuator 2 Displacement (in.)	Loading Rate (kip/sec)	Step Time (sec)
32B	174	-6.02%	-32	-8.63	0.02	41.5
	175	-5.16%	-222	-7.36	0.04	31.8
	176	-3.27%	-289	-4.67	0.08	33.6
	177	6.01%	-318	9.75	0.12	120.2
33A	178	5.62%	49	8.94	0.02	40.5
	179	4.48%	239	6.95	0.04	49.8
	180	2.33%	297	3.46	0.08	43.6
	181	-6.49%	362	-9.46	0.12	107.7
33B	182	-6.02%	-32	-8.63	0.02	41.5
	183	-5.16%	-222	-7.36	0.04	31.8
	184	-3.27%	-289	-4.67	0.08	33.6
	185	6.01%	-318	9.75	0.12	120.2
34A	186	5.62%	49	8.94	0.02	40.5
	187	4.48%	239	6.95	0.04	49.8
	188	2.33%	297	3.46	0.08	43.6
	189	-6.49%	362	-9.46	0.12	107.7
34B	190	-6.02%	-32	-8.63	0.02	41.5
	191	-5.16%	-222	-7.36	0.04	31.8
	192	-3.27%	-289	-4.67	0.08	33.6
	193	6.01%	-318	9.75	0.12	120.2

Appendix H. Gap Rotation Calculation Methodology

The gap rotation was estimated based on data gathered from the three string pots located on the beam web. Calculations were performed using the connection member dimensions and the string pot displacements. For the calculations, it was assumed that the axial deformation in the splice plates was insignificant when compared to the flexural deformation in the splice plates. A consistent point of hinging in the splice plates was also assumed for the calculations. Given the assumptions, a triangle is formed for each string pot (see example in Figure H-1), and the lengths of all the sides (i.e. a, b, and c) are known at all times (a is given in the data, while b and c are fixed by the geometric assumptions). Therefore, the angle of interest can be calculated using the law of cosines, which is as follows:

$$a^2 = b^2 + c^2 - 2bc*\cos(A) \quad \text{or} \quad A = \cos^{-1}\left((a^2 + b^2 - c^2) / (2bc) \right) \tag{H.1}$$

The gap rotation estimation can then be determined by subtracting the angle A from the angle corresponding to the un-displaced geometry. This methodology was performed for the three string pots along the beam web of Specimen 1 and for the three string pots along the beam web of Specimen 2. Each set of three gap rotation estimations was averaged to obtain one gap rotation per specimen per displacement.

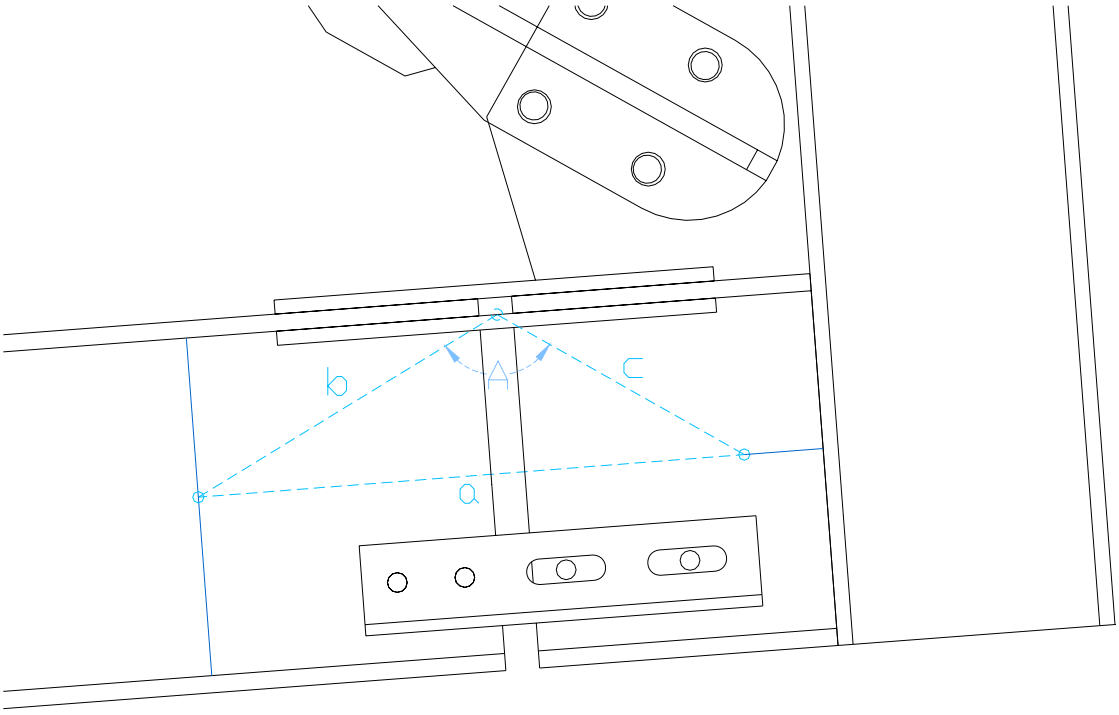

Figure H-1 Example of String Pot Triangle – Middle String Pot of Specimen 1

Appendix I. Validation of Testing

Control issues regarding the hysteretic action of the actuators are discussed and the test design assumptions are validated.

I.1 Control Issues Regarding Hysteretic Action

One control issue of concern is the hysteretic action of the actuators. For both tests, measured Actuator 2 hysteretic action matches the input while measured Actuator 1 hysteretic action does not, even though some desirable elements (e.g. obvious cycles and increasing forces) exist. The Actuator 1 hysteresis has segments that indicate the actuator displaced in the opposite direction of what would be expected. These shifts in direction occur in each half-cycle and correspond with the BRB actuator force transitions (i.e. when the applied actuator force changes from positive to negative, and vice-versa).

One factor that contributed to the unanticipated shift was bolt slippage in the gusset plate-BRB core extension assembly connection. Slippage, however, is unlikely to be the only factor, because the distance available for slippage is roughly 3/4 in. while the amount of unaccounted displacement is 1 to 2 in..

Another possible factor is the interaction between the different elements of the connection and between the specimen and self-reacting frame. The splice plates, gusset plate, beam, column, and self-reacting frame experienced different forms of deformation

when loaded in compression versus tension. In addition to the interaction between elements, there is a self-adjustment or alignment that occurs during load reversals. Therefore, it is possible that these interactions and self alignments account for the remainder of the unexpected deformation. Furthermore, Actuator 1 is programmed to respond with a pre-specified force to a continually shifting specimen. The demands that are placed on the actuator and the adjustments it needs to make are complex and have possible lag effects.

I.2 Validation of Test Design Assumptions

The development of the loading protocols and the reduction of the data were both dependent upon assumptions concerning the deformation geometry, gap rotation, hysteretic action of brace, and frame stiffness. Measurements were made and data from several instruments was gathered to check the accuracy of the assumptions.

The most important assumption was related to the gap angle. The gap closed completely in both tests, but not until the largest applied displacement cycle and then only slightly. Since the maximum opening and closing of the connection gap corresponded to maximum applied drifts, the gap design calculations appeared accurate. These results also supported the use of the gap angle as the center point of data translation between the test setup and the prototype bay.

Results indicated that the test setup connection (with regards to the angle of the gap) responded in very much the same manner as the prototype would under the same gap angle. Percent errors were very low (less than 10% in most instances) and the assumptions were considered accurate and the data was considered validated and useful.